AD-A057 267 JOHNS HOPKINS UNIV LAUREL MD APPLIED PHYSICS LAB F/G 5/2
DEVELOPMENTS IN SCIENCE AND TECHNOLOGY.(U)
1976 N00017-72-C-4401
UNCLASSIFIED APL/JHU/DST-4 NL

1 OF 2
AD
A057 267

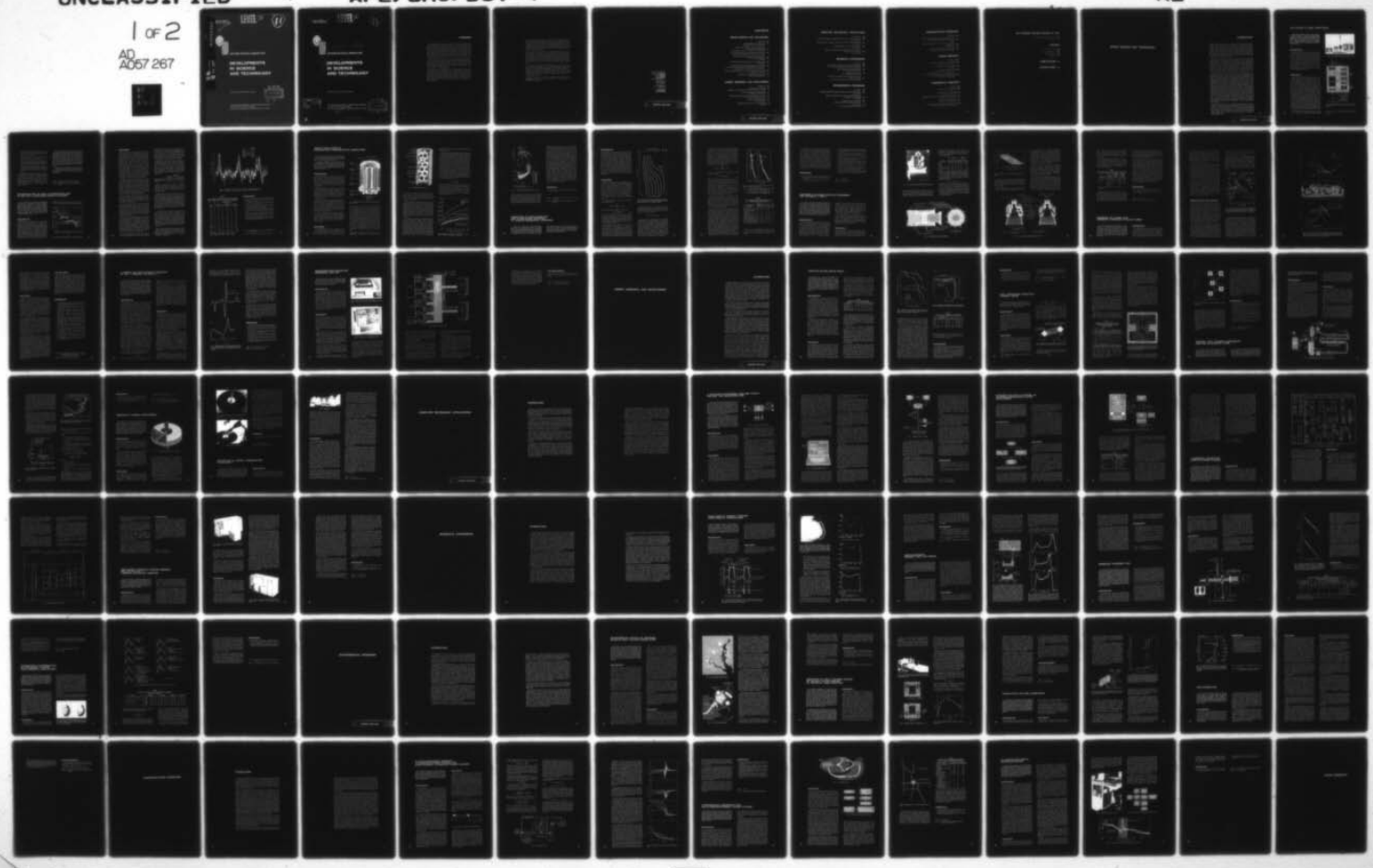

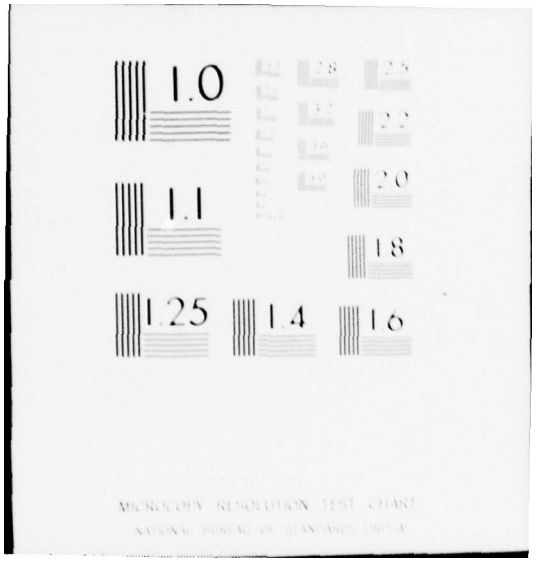
1.0
1.1
1.25
1.4
1.6
2.8
2.5
2.2
2.0
1.8
MICROCOPY RESOLUTION TEST CHART
NATIONAL BUREAU OF STANDARDS 1963-A

APL/JHU DST-4
FISCAL YEAR 1976

LEVEL III

11

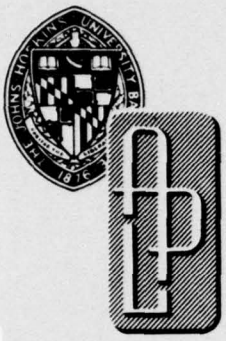

APPLIED PHYSICS LABORATORY

DEVELOPMENTS IN SCIENCE AND TECHNOLOGY

Approved for public release; distribution unlimited.

THE JOHNS HOPKINS UNIVERSITY • APPLIED PHYSICS LABORATORY
Johns Hopkins Road, Laurel, Maryland 20810

Operating under Contract N00017-72-C-4401 with the Department of the Navy

(14) APL/JHU/DST-4
FISCAL YEAR 1976

LEVEL II

(11)

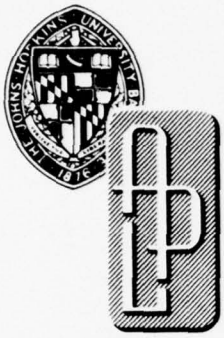

(11) 1976 (12) 134 p.

APPLIED PHYSICS LABORATORY

(6)

DEVELOPMENTS IN SCIENCE AND TECHNOLOGY

Approved for public release; distribution unlimited.

THE JOHNS HOPKINS UNIVERSITY • APPLIED PHYSICS LABORATORY
Johns Hopkins Road, Laurel, Maryland 20810

Operating under Contract N00017-72-C-4401 with the Department of the Navy

(15)

031 650

LB

FOREWORD

The Applied Physics Laboratory (APL) of The Johns Hopkins University, with field activities in Florida, Utah, New Mexico, Virginia, New Jersey, California, and Heidelberg, Germany, is located in Howard County, Maryland, midway between Baltimore and Washington. Its work is carried out under a contractual agreement between the University and the Government, with about 80% of the effort devoted to the Department of the Navy. APL employs a staff of about 2400, more than 1200 of whom are professional scientists and engineers. Their ideas are implemented and extended through a network of associate contractors from coast to coast.

The primary mission of APL is to serve the nation through the application of advanced science and technology to the solution of problems of importance in both the defense and the civil sectors. APL conducts broad programs in basic and applied research, exploratory and advanced development, component engineering, systems engineering and integration, and test and evaluation of operating systems.

The Laboratory was established in 1942 at the urgent request of the Office of Scientific Research and Development to demonstrate that science and technology could advance national security more effectively through an active partnership of military and civilian technologists than through the traditional buyer-supplier relationship. The concept was validated in less than a year when APL developed the first practical VT (variable time) fuze. This initial product proved to be a major contributor to the Allied victory in World War II.

After the war, at the request of the Secretary of the Navy, the University trustees agreed to continue the Laboratory as an important national security resource. APL quickly became a leader in guided missile and space technology as well as a contributor to fundamental knowledge in such areas as high-altitude physics, spectroscopy, flame propagation, the origin and evolution of the universe, supersonic and hypersonic aerodynamics, chemical kinetics, and magnetic resonance.

In addition to major contributions to national defense, effort is increasingly devoted to the solution of pressing problems in the civilian sector. Biomedical research and engineering, transportation, fire research, pollution of the biosphere, ocean thermal, geothermal, and flywheel energy systems, traffic control for harbors and aircraft terminals, leak detection in natural gas distribution lines, computer technology, and advanced education are a few examples of the areas to which attention has been devoted in recent years.

In its role as a University laboratory, APL performs research to advance the basic sciences underlying its technological development programs. In this area, APL has significantly contributed to Johns Hopkins' 100-year-old reputation for leadership and originality. Through unique applications of systems engineering, science, and technology to the needs of society, APL has enhanced the University's tradition of excellence while gaining worldwide recognition of its own.

This report contains a representative sample of APL technical accomplishments, primarily in the civil area. All results of these programs are fully available to the public.

CONTENTS

SPACE SCIENCE AND TECHNOLOGY

ENERGY RESEARCH AND DEVELOPMENT

COMPUTER TECHNOLOGY APPLICATIONS

BIOMEDICAL ENGINEERING

ENVIRONMENTAL PROGRAMS

TRANSPORTATION PROGRAMS

OCEAN RESEARCH

FUNDAMENTAL RESEARCH

JHU EVENING COLLEGE CENTER AT APL

PATENTS

PUBLICATIONS 136

AUTHOR INDEX 140

SPACE SCIENCE AND TECHNOLOGY

INTRODUCTION

APL's active participation in space science and technology dates back to the early years of rocketry when a group then led by Dr. James A. Van Allen used V–2 and Aerobee rockets to study cosmic rays. The discovery in 1957 by APL scientists that the position of the Russian Sputnik satellite could be tracked by observing the doppler shift of its radio signal led to the conception of a satellite navigation system based on the doppler tracking principle. The Navy Navigation Satellite System (Transit) developed by APL has provided precise, worldwide, all-weather navigational data to the Navy since 1964 and to commercial users since 1967.

APL's special capabilities in attitude stabilization and control, ultrastable oscillators, precision tracking, and other technologies, and in component and system design and development, are used in numerous space programs for NASA and DoD as well as the Navy. These capabilities were demonstrated during the past year with the design, fabrication, and successful launch of the P76–5 satellite in the incredibly short period of nine months. This spacecraft is a Transit (Oscar 15) satellite that was reconfigured by APL to carry the Wideband Signals Experiment, which is presently accumulating data on the distorting effects of the ionosphere on radio transmissions.

The space activities at APL have been supported by a small but strong and active program of basic research directed toward an understanding of the chemical and physical processes involved in the earth's atmosphere, ionosphere, and magnetosphere and in interplanetary phenomena. Some of the significant achievements include the first detection of solar cosmic rays with satellite-borne solid-state detectors, the design and construction of one of the longest-lived and most productive scientific satellites ever launched (1963–38C), the first measurement of short-period magnetohydrodynamic waves near synchronous altitude, the discovery of heavy ions (C, N, O) trapped in the earth's radiation belts, the experimental confirmation of large-scale field-aligned currents in the auroral regions, the demonstration of the effect of stratospheric pressure variations on the ionosphere, and the development of radio astronomy techniques for the prediction of geomagnetic storms that can cause disturbances to terrestrial radio transmissions. These research activities have involved collaborations with scientists from more than a dozen U.S. and international academic institutions including the University of Tokyo, the Max-Planck Institutes in Lindau and Munich, West Germany, the Norweigian Defense Research Establishment, and the Danish Meteorological Institute.

Programs representative of those completed during the past year are described in the following articles. Current programs include the launch (in August 1977) and data analysis phase of the Low Energy Particle Experiment (described in the following) on the Voyager spacecraft, which will travel to Jupiter and Saturn, and the design and fabrication of the MAGSAT satellite, which will provide the most accurate mapping ever attempted of the geomagnetic field.

THE AN/SRN–19 GOES OPERATIONAL

The AN/SRN–19 Radio Navigation Set was designed to meet the need for a low-cost, simplified satellite navigation set for use on Navy Antisubmarine (ASW) surface ships. Several Navy evaluations have shown that in accuracy it exceeds 0.1 nmi rms at dockside and in reliability 2000 hours mean time between failures. It will be used as an operational unit aboard U.S. Navy ships.

BACKGROUND

The SRN–19 Radio Navigation Set has successfully completed an Operational Evaluation aboard a Navy destroyer, the USS *Forrest Sherman*, and a Fleet Evaluation on a submarine, the USS *Waboo*. It has demonstrated its usefulness as an accurate, reliable satellite navigation set that continuously displays ship's dead-reckoning position using automatic inputs of ship's course and speed. The dead-reckoning position is periodically updated by satellite navigation fixes. The set also provides a tape cassette recording of all ship's dead-reckoning positions and satellite fixes for playback at a Reconstruct Facility.

DISCUSSION

Figure 1 shows the SRN–19 with its antenna/preamplifier, printer, and remote display. The set consists of a 400–MHz receiver, a 5–MHz oscillator, a data processor (8K, 16–bit read-only memory), power supplies, a cassette recorder, a keyboard, a display, and two synchro-to-digital units (see Fig. 2). Ship's position is continuously displayed and updated every five seconds. The ship's heading and speed with respect to the water are obtained automatically from the Mk 19 gyrocompass and the electromagnetic underwater log. When the receiver locks onto a satellite signal, the program recognizes the beginning of a two-minute data transmission interval, collects and majority-votes the satellite message data, and computes a satellite fix, provided the following conditions are met: (a) the satellite elevation at closest approach is between 10 and 80°, and (b) the fix computation converges in five or fewer iterations and the total correction is less than 30 nmi. If these conditions are not met, the operator may enter the fix manually in the data processor to update the dead-reckoning position.

The AN/SRN–19 Operational Evaluation report from *Forrest Sherman* recommended this navigation set for Navy use. The following key results were reported:

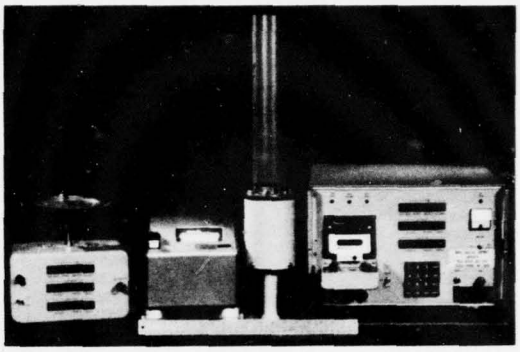

Fig. 1 The AN/SRN–19 Radio Navigation Set.

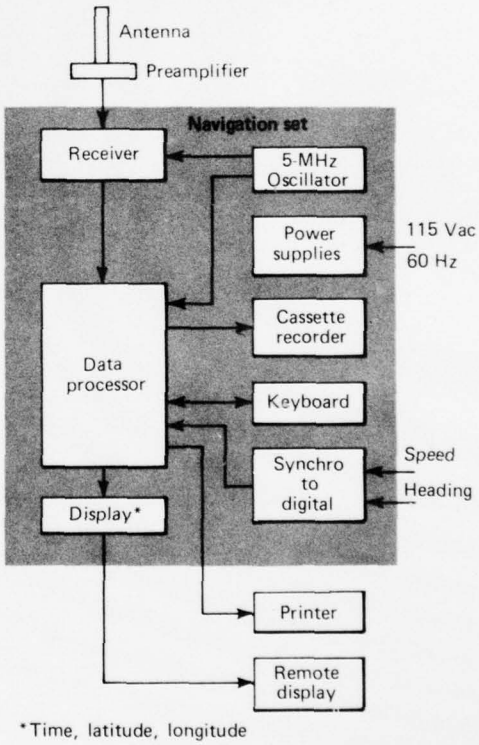

Fig. 2 Block diagram of the AN/SRN–19 Radio Navigation Set.

1. Navigation fixes in port showed an average error of 95 yards; 94% of the fixes were within the 0.1-nmi specification.
2. SRN-19 fixes under way were more accurate than loran, omega, and celestial fixes.
3. Successful navigation fixes were achieved in 90% of the eligible opportunities. No degradation due to adverse weather was observed.
4. No failures occurred in 193 days of continuous operation. The mean time between failures was greater than 2100 hours with a 90% confidence level.

The SRN-19 was installed on *Wahoo* for evaluation during the period July 1975 through September 1976. The set was matched successfully to the submarine's UHF and periscope antennas. The navigator reported good at-sea accuracy (better than 0.2 nmi) and high reliability. His recommendations for time-ordered satellite alerts and a lighted keyboard are being implemented.

To meet an urgent requirement by the Naval Tactical Support Activity, ten SRN-19 sets were fabricated and delivered by APL during the period June to September 1976. These sets are being used aboard Navy ships during ASW operations to record ship's position on a tape cassette. The tape cassettes will be sent to a Reconstruct Facility for use in plotting each ship's track. Twenty more SRN-19's are being fabricated by commercial contractors under an APL subcontract.

A specification for the SRN-19 has been prepared. It is intended that this specification and APL drawings will be used to procure production models of the SRN-19.

Authors: *R. Bauer, R. Finneran, and D. Mitchell*

Support: *NAVELEX and Naval Tactical Support Activity*

IMPLEMENTATION OF WGS–72 GEOPOTENTIAL SET IN THE NAVY NAVIGATION SATELLITE SYSTEM

On 18 December 1975, the WGS–72 geopotential coefficient set was implemented in the Orbit Improvement Program (OIP) used by the Navy Navigation Satellite System (NNSS). To complement the improved accuracy attainable with these coefficients, additional perturbation force models were included and the program was renovated to reduce computation noise to less than 1 m. As a result of these changes, worldwide satellite navigation precision was improved by a factor of two.

BACKGROUND

OIP has been in operation for 14 years without major revision. The accuracy has been improved over the years by the inclusion of more and better force models and, in particular, by larger geopotential coefficient sets. Figure 1 (Ref. 1) shows this improvement in accuracy for Transit; it is primarily a history of geodesy improvement. The invention of the disturbance compensation system (DISCOS) introduced a new era in satellite trajectory computation by eliminating drag, a major error source. The precision environment produced by the WGS–72 coefficient set and DISCOS necessitated a program review. Such a review had not been performed since OIP's implementation.

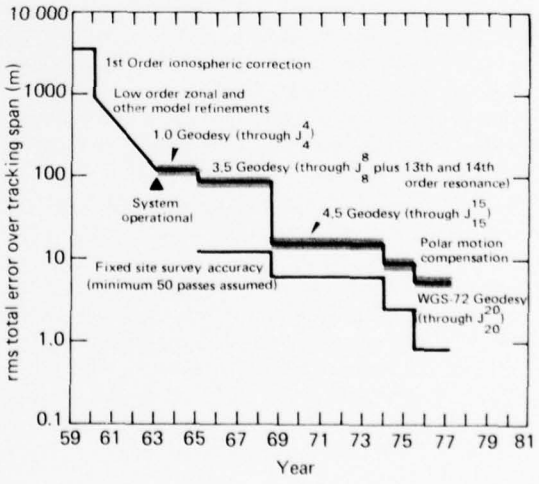

Fig. 1 History of improvement in accuracy of Transit.

DISCUSSION

During the past 10 years, there have been appreciable improvements in the mathematical models of the earth's gravity field, the geopotential. The models are a formalization of the improved knowledge of the geopotential that has accrued from intensive satellite-geodetic studies. At least two models are of comparable accuracy: the WGS–72 (Ref. 2) and one of the GEM series (Ref. 3). It was clear from background studies that we could improve the Transit System appreciably by replacing the APL 4.5 model (circa 1966) with one of the newer geopotential models. The WGS–72 model was chosen because it was slightly better for our purposes than the others and, more importantly, was designated as the standard geopotential coefficient set for use by DoD. This point is important in enforcing consistency among the diverse inertial navigation systems used by DoD.

A satellite's orbit can be determined by comparing a theoretically generated model of the doppler signals that would be received at several earth-fixed stations to the actual signals received. The quality of the fit depends on the preciseness of both the measurements and the modeling. The measurements have traditionally had a precision of 1 to 5 m, far better than our ability to model the satellite's motion. The NNSS orbit determination program includes models for all forces that perturb the satellite significantly.

What is significant depends on the type of perturbation. If the effect is secular, anything that accumulates to 50 m or more in a week should be taken into consideration. Orbital frequency perturbations should be modeled to better than 1 m.

The forces that perturb the satellite include the gravitational attractions of the earth, sun, and moon; amospheric drag; solar radiation; and a pseudo force to account for the precession and nutation of the equinoxes. Forces to account for the sun- and moon-induced earth body (not ocean) tides have been added to this force array, and the solar radiation force model has been altered (Ref. 4).

The Transit Improvement Program (TIP) satellites are being built with a DISCOS (Ref. 5) aboard to remove all perturbations sensed along the direction of the satellite velocity vector (along track). The primary cause of perturbation is atmospheric drag but a component of the force resulting from solar radiation is also included. When DISCOS is operating, the atmospheric drag model is not included in the satellite motion model. In addition, the along-track component of the radiation force must be turned off.

Drag is unpredictable and is the major source of error in satellite ephemeris predictions. Since predicted ephemerides are used in navigation (the satellite memory must be loaded with its future ephemerides to be transmitted to the user), the use of DISCOS has two important effects. First, longer prediction spans eventually will require more stringent precision criteria. Second, DISCOS can have biases, and a model had to be implemented to determine and remove them.

Whenever the operational program is changed, a thorough checking procedure is undertaken. This normally involves processing the data from several satellite arcs with the new version of the program (WGS–72) and comparing the results with those from the previous program (APL 4.5) using the same data. The WGS–72 orbit-fitting results are significantly better than those obtained with APL 4.5, as shown below.

	OIP–II	
	WGS–72	APL 4.5
Orbit determination	6 to 8 m	14 to 16 m
Prediction	6 to 10 m	14 to 17 m

A range is given because the results are satellite-dependent. The prediction results are for a span of time when solar activity (and hence drag) is near a minimum, and therefore the prediction shows very little degradation.

Satellite ephemeris comparisons (Ref. 6) show that satellite positions for the same time varied by larger amounts than anticipated and were geographically correlated. (Although peak ephemeris differences reached 90 m, since they are geographically correlated they do not persist long enough to affect survey results a like amount, as can be seen in Table 1.) This unanticipated development provoked an investigation. Once satisfied that the results were valid, we proceeded to consider their importance.

Using satellite data, a surveyor locates his position relative to the satellite's trajectory and hence to the earth's surface. If the trajectory is different, so will be his determined position. The final surveyed position is determined by taking an average over the satellite passes that come into view. Since the ephemeris differences were correlated with geographic position, surveyed position designations changed by varying amounts, depending on their general geographic locations (Ref. 6).

Figure 2 shows the along-track satellite position differences versus time referenced to (starting at) a fixed subtrack. Table 1 shows the position shifts of selected TRANET and OPNET sites due to the change in geopotential coefficient sets.

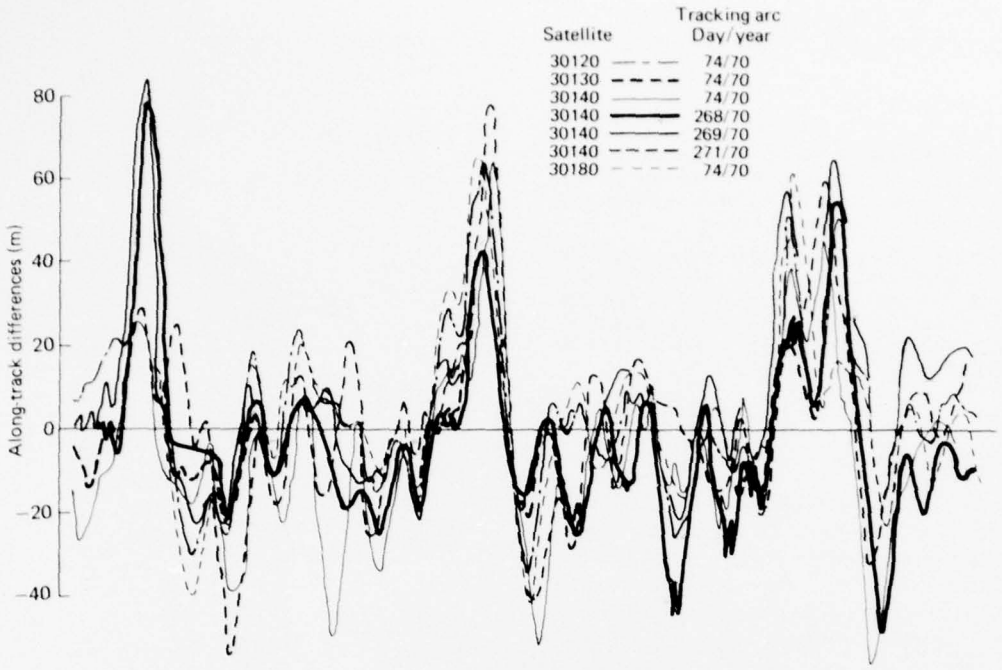

Fig. 2. Along-track differences due to geodesy change (APL 4.5 to WGS–72) resolved to same geographic location for various satellite arcs.

TABLE 1

OIP ABSOLUTE MEAN NAVIGATED POSITION SHIFT USING WGS–72 AND APL 4.5 GEODESIES

	Position Shift* (m)		
Station	Latitude	Longitude	Radius
008	0.3	1.5	−5.8
013	4.1	−2.1	0.8
014	2.5	−4.7	0.6
018	0.7	−1.7	2.9
019	2.4	3.7	−7.7
103	4.9	4.1	0.8
106	2.9	−4.7	1.4
111	1.8	−11.0	1.4
117	5.4	−9.0	−1.7
311	2.1	−7.7	−1.5
321	4.5	−0.4	4.4
330	3.4	−3.0	−0.1
340	6.8	−3.5	−5.5
Mean	3.20	−2.95	−0.79
σ	3.68	5.31	3.53
σ_{mean}	1.81	4.42	3.44

* Position shift = $\overline{NAV}_{WGS} - \overline{NAV}_{4.5} + \Delta STA$
ΔSTA = NWL10D − APL 4.5 station coordinates

REFERENCES

1. R. B. Kershner, "The Doppler Concept and the Operational Navy Navigation Satellite System," presented at the International Geodetic Symposium on Satellite Doppler Positioning, Las Cruces, NM, 12–14 October 1976.
2. T. O. Seppelin, "The Department of Defense World Geodetic System 1972," *The Canadian Surveyor*, **28**, No. 5, Ottawa, Canada, December 1974, pp. 496–506.
3. F. J. Lerch, J. E. Brownd, J. A. Richardson, and J. S. Reece, "Gravitational Models GEM–5 and GEM–6, 1974," *The National Geodetic Satellite Program Final Report*, American Geophysical Union, Washington, DC, August 1975.
4. H. D. Black et al., "The *Transit* System, 1975," presented at the 56th Annual Meeting of the American Geophysical Union, 16–20 June 1975 (also published as APL/JHU TG 1305, December 1976).
5. Staff of the Space Department, APL/JHU, and the Staff of the Guidance and Control Laboratory, Stanford University, "A Satellite Freed of All but Gravitational Forces: TRIAD I," *J. Spacecr. Rockets*, **11**, No. 9, 1974, pp. 637–644.
6. B. B. Holland, A. Eisner, and S. M. Yionoulis, "The Effect of WGS–72 Geopotential on NNSS Station Surveys," presented at the Fall Annual Meeting of the American Geophysical Union, San Francisco, CA, 6–10 December 1976.

Authors: *B. B. Holland, A. Eisner, S. M. Yionoulis, and H. D. Black*

Support: *Strategic Systems Projects Office, SP–243*

SAFETY EVALUATION OF RADIOISOTOPE THERMOELECTRIC GENERATORS

APL has evaluated the ability of the fuel-containment member of radioisotope thermoelectric generators (RTG) on board spacecraft to survive atmospheric reentry in the event of a launch failure.

To aid these evaluations, unique procedures have been developed to analyze structures with components that initially are not in contact, and to extrapolate the limited data on low-temperature interface conductance to the high-temperature condition encountered during reentry.

BACKGROUND

Radioactive materials are sometimes used to provide electric power to spacecraft. The heat generated in RTG's by the decay of radioisotopes is passed through thermoelectric material to produce electric power. The radioactive materials are contained within capsules that are designed to survive accidents during the launch of the spacecraft.

Presidential approval is required for each launch that involves radioactive materials. In addition, an extensive Safety Evaluation Report is prepared by the Energy Research and Development Administration (ERDA), the Air Force, and NASA to evaluate the probabilities of occurrence and the consequences of a variety of accidents.

The Safety Branch of the Nuclear Research and Applications Division of ERDA has asked APL to provide advice on and independent evaluations of the reentry capability of radioisotope fuel capsules in the event of inadvertent atmospheric reentry. The assignment includes serving on the Interagency Nuclear Safety Review Panel, the organization that prepares the Safety Evaluation Report.

Currently, the Multi-Hundred Watt RTG (MHW/RTG) is being reviewed for its intended application on the Voyager spacecraft. Each of the three MHW/RTG's for this mission is designed to provide approximately 130 W of electric power at the end of a four-year flight.

DISCUSSION

The MHW/RTG (Fig. 1) has a length of about 24 in. and a diameter of about 15 in. The primary reentry capsule is the portion of the RTG known as the heat source. Figure 2 is a cutaway view of the

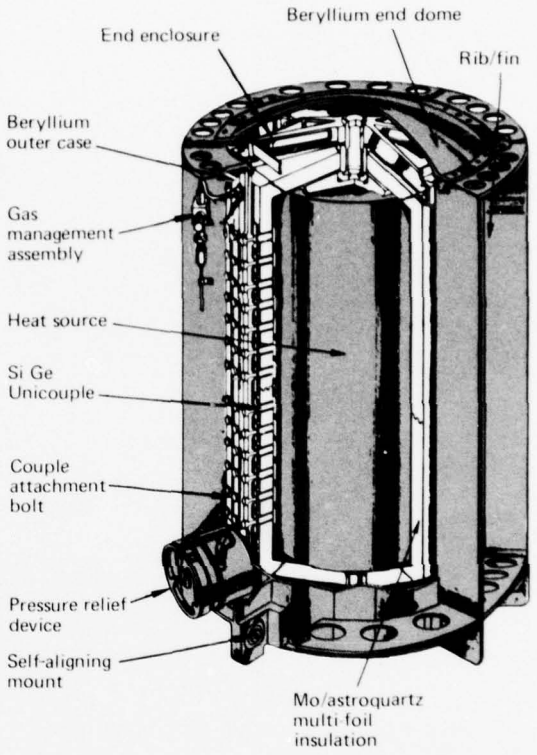

Fig. 1 Multi-Hundred Watt Radioisotope Thermoelectric Generator.

interior of the heat source. The basic cylindrical shell (the aeroshell) of the heat source is approximately 7 in. in diameter and 17 in. long and is made of fine-grained bulk graphite. Two factors that determine the reentry capability of the heat source are the ability of the aeroshell to resist the thermal and mechanical loads that result from reentry and its ability to survive the thermal ablation or burning that occurs during reentry. A carbon-based ablation sleeve over the graphite aeroshell gives added protection against these potential modes of failure. A third factor that must be evaluated is the temperature during reentry of the metallic parts within the heat source that are subject to melting; in the MHW heat source, the critical component is the iridium post-impact containment shell.

Evaluations by APL of an earlier version of the MHW/RTG source had led to the conclusion that

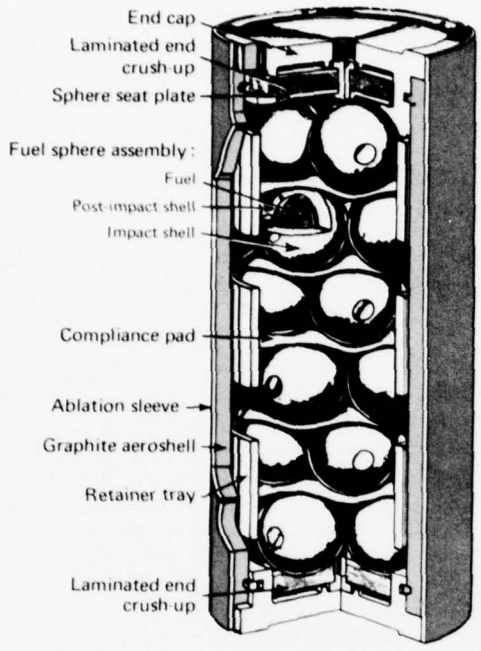

Fig. 2 MHW/RTG heat source.

the protection from ablation and the thermal response of the iridium were adequate. Therefore, evaluation of the current heat source has concentrated largely on the ability of the aeroshell to withstand the thermal and mechanical reentry loads.

Severe temperature gradients induced in the aeroshell during reentry can cause deformations known as thermal strains. The estimation of the temperature range begins with a definition of the convective and radiative thermal environment imposed on the ablation sleeve as the body enters the atmosphere. Heat is transferred through the ablation sleeve, across the interface that separates the sleeve from the aeroshell, through the graphite aeroshell wall, and into the retainer tray.

The temperature distribution depends on the heat transferred through the interface with the ablation sleeve and the interface with the retainer tray. Recent analyses have given special attention to these interfaces. A procedure has been developed to extrapolate the limited low-temperature thermal conductance data for the interface to the high-temperature conditions encountered during reentry. In addition, a previously unavailable, unique procedure has been developed that permits the analysis of structures with components that initially are not in contact, such as the region between the inner surface of the aeroshell wall and the retainer tray.

Initial attempts to extrapolate experimental thermal conductance data using both classic theory and empirical correlations developed for other materials were not successful. The classic theory requires baseline data that reflect perfect contact. The available empirical correlations were too restricted in terms of temperature range and material combinations. The chosen procedure was based on the observation that interface conductance should be enhanced by having "soft" materials that can come into more intimate contact under loading that can "hard" materials. Thus, the thermal conductance should be inversely proportional to the Young's modulus. Also, according to classic contact theory, the contact conductance should be proportional to the harmonic mean thermal conductivity of the materials. The relationship derived for the interface conductance, G, is

$$G_t \sim G_b \frac{K_t}{K_b} \frac{E_b}{E_t},$$

where K is the harmonic thermal conductivity of the material combination, E is the Young's modulus of the softer material, and the subscripts b and t represent baseline and elevated temperature, respectively. In Fig. 3, the results of the procedure are compared with the limited data available for the aeroshell and ablation sleeve material.

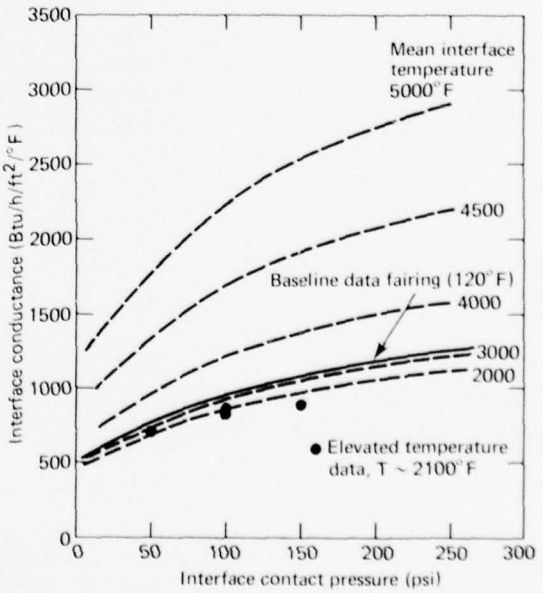

Fig. 3 Interface conductance extrapolation based on thermal conductivity and Young's modulus.

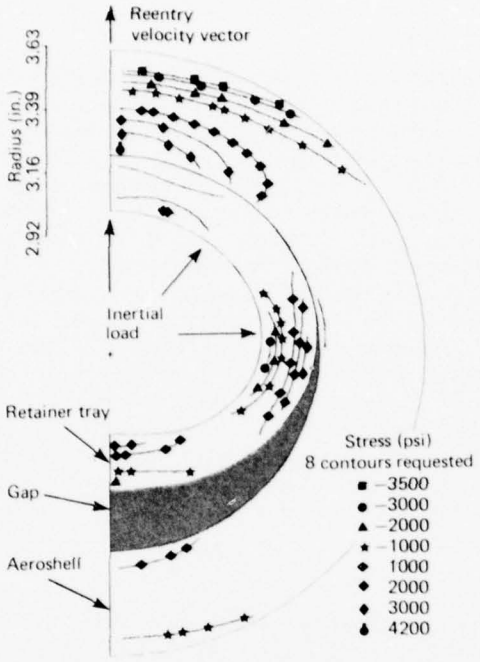

Fig. 4 Contours of hoop stress for side-on reentry.

The unique procedures that have been developed permit the analysis of structures with gaps between components. Under loading, these gaps may be closed and contact made. Although the procedure is general and may be applied to any structure that can be represented by finite elements, the present application is to the deformation of the retainer tray under inertial load and the subsequent contact of the tray with the interior wall of the aeroshell. This contact provides a thermal path of the nature described above. The unique feature of the stress analysis procedure is an iterative process that relaxes the stiffness of special interfacial gap elements to bring neighboring boundaries together. The stiffness of gap elements that do not "close" is reduced to zero so as not to impede the relative motion of the components. As neighboring boundaries approach each other and come into contact, the "gap" modulus becomes stiff enough that no further deformation of the gap is permitted. The procedure has been adapted to a conventional finite-element stress-analysis procedure, SAAS III, using a stress invariance procedure (Ref. 1). Figure 4 shows the deformed retainer ring and aeroshell under inertial loading of the retainer tray from the interior components (not shown). Prior to the loading, both the retainer tray and the aeroshell had cylindrical shapes and were separated by a uniform gap. After deformation, the cylindrical structures are in contact over a region of nearly a 90° half-angle.

REFERENCE

1. J. T. Stadter and R. O. Weiss, *Stress Analysis of Disconnected Structures in Contact through Finite Element Gaps*, APL/JHU ANSP-M-13, July 1976.

Authors: *J. C. Hagan, D. W. Conn, R. O. Weiss, and J. T. Stadter*

Support: *ERDA, Division of Nuclear Research and Applications*

PREDICTION OF EARTH-SATELLITE RAIN ATTENUATION STATISTICS AT VARIOUS GEOGRAPHIC LOCATIONS

A method for predicting rain attenuation statistics associated with earth-satellite radio transmission paths in various geographic regions using rain gauge data at these locations has been devised. Comparison with measured data shows good overall correlation. This method could result in significant cost savings by establishing design criteria associated with transmitter power, receiver sensitivity, and space diversity for ground terminals at remote sites, avoiding the need for the experimental determination of attenuation statistics at each location.

BACKGROUND

Measurements of rain attenuation statistics along earth-satellite paths cannot be made for every ground terminal location. Such an undertaking would be too costly, cumbersome, and time consuming. Therefore, it is essential that methods be found for predicting the statistics in some regions. A method is described here for predicting slant path attenuation statistics at arbitrary locations for various frequencies and path elevation angles. The method involves the use of median rain-intensity/altitude profiles measured with radar as well as long-term point rain-rate data and assumed or measured drop-size distributions. In addition, the contribution to attenuation resulting from liquid water in a cloud, exclusive of rain, is also considered.

DISCUSSION

During the summer of 1973, the rain reflectivity environment was monitored routinely at Wallops Island, Virginia, using a high-resolution (0.4° beamwidth, 1-μs pulsewidth) S-band radar (2.84 GHz) (Ref. 1). The reflectivity factor, Z, which characterizes the intensity of rain, is a convenient parameter that can be measured by radar. Its units are mm^6/m^3 or dBZ (i.e., 10 log Z) (see, for example, Ref. 2). Peak reflectivity factors at a series of altitudes, h, were determined, and Z–h profiles were established (Fig. 1).

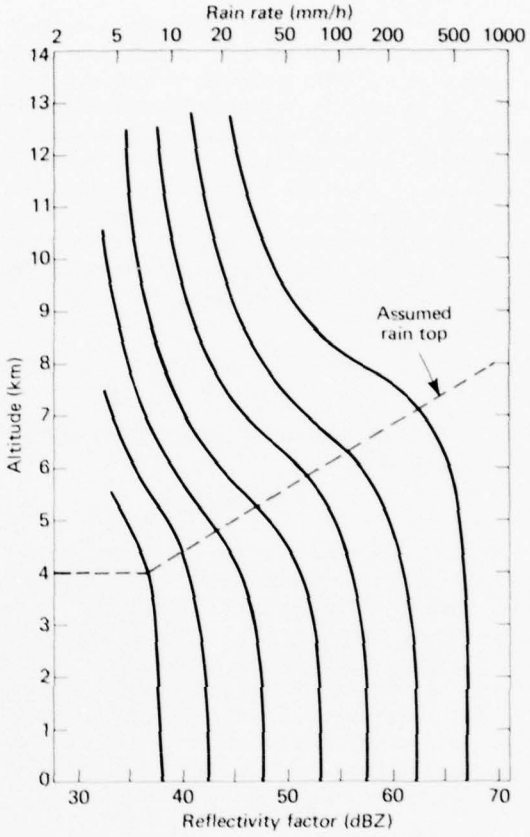

Fig. 1 Reflectivity factor versus altitude for various rain intensity categories. Lower abscissa scale shows dBZ and upper shows rain rate, assuming $Z = 200R^{1.6}$.

The vertical attenuation, A_R (90°), for each profile was computed using

$$A_R(90°) = \int_0^{h_m} k\, dh \quad \text{(dB)} \tag{1}$$

where the attenuation coefficient, k, is given by

$$k = aZ^b \text{ (dB/km)} \tag{2}$$

and Z is given in mm^6/m^3. The parameters, a and b, for a particular frequency may be derived using a measured or assumed drop-size distribution. In Eq. 1, h_m represents the height to the dashed line of Fig. 1, and the subscript R denotes the ground rain rate derived from the ground Z level.

We calculated for each frequency a system of vertical attenuations corresponding to a sequence of ground R levels. We then correlated these levels with the probabilities of exceeding the rain rate at the locations in question, measured using long-term rain gauge data. A one-to-one correspondence was obtained between the vertical attenuation and the probability of exceeding the corresponding ground rain rate. These probabilities are assumed to be the same as the corresponding probabilities of exceeding the vertical attenuations themselves. The conversion to other path angles, θ, is arrived at using

$$A_R(\theta) = A_R(90°) \csc \theta \ . \tag{3}$$

Approximation 3 has been shown to be applicable with good accuracy at elevation angles from 20 to 90° for a series of fixed probabilities and at frequencies from 13 to 100 GHz (Ref. 3). (The applicability of approximation 3 at elevation angles less than 20° has yet to be established.) It should be stressed that it represents a statistical expression rather than a deterministic one since a probability is assigned to each attenuation level, $A_R(90°)$. Hence, although the rain medium may be highly nonuniform on a case-by-case basis statistically, uniformity may be assigned to it.

In order to account for the contribution to attenuation resulting from liquid water in the cloud itself exclusive of rain, the model of Wexler and Atlas (Ref. 4) was used. It is representative of widespread summer rain for temperate latitudes and is based on a calculation that establishes the balance between the production of clouds due to updraft and their depletion due to precipitation. The model gives profiles of cloud liquid water content and height for the given ground rain rates. For each profile, the vertical cloud attenuation may be calculated using

$$A_c\,(90°) = \int_0^{h_c} k_c\,dh \quad (\mathrm{dB})\,. \tag{4}$$

In Eq. 4, k_c, the attenuation coefficient due to water clouds, is given by

$$k_c = KM_c\ (\mathrm{dB/km}) \tag{5}$$

where M_c is the cloud's liquid-water content (g/m^3) and K ($dB/km/g/m^3$) is tabulated by Gunn and East (Ref. 5) for temperatures ranging from -8 to $+20°$ C and frequencies from 3 to 33 GHz. The cloud height, h_c, is approximately 5.5 km ($-7°$ C). Above this, the temperature of the liquid water is assumed to fall rapidly to zero. Although the cloud base extends to low altitudes, the corresponding amounts of liquid water there are sufficiently small so as to contribute negligibly to attenuation.

The total zenith attenuation resulting from both rain and clouds is given by the sum of Eqs. 1 and 4 where a given ground rain rate defines each contribution. The exceedance probabilities associated with these ground rain rates are associated subsequently with the total attenuation, and the csc θ approximation given by Eq. 3 is applied to yield the fade statistics for the resultant slant path.

Two examples in Fig. 2 show predicted distributions that were tested against experimental results. The solid and dashed curves represent the measured and predicted distributions, respectively. The measured and predicted results of eight cases investigated to date are compared in Table 1. The average ratios of the probabilities corresponding to the measured and predicted curves are listed in the third column. These values were obtained by dividing the larger probability, P_1, by the smaller one, P_2, for each of a series of fixed attenuation levels over the range of fades, and then taking their average. This gives a measure of the relative uncertainty in the predicted curves. Also shown are the rms values of these ratios about the corresponding average levels and the average differences in attenuation level between the measured and predicted curves. For this case, the smaller attenuation, A_2, was subtracted from the larger one, A_1, for a series of fixed probabilities, and the average and the rms were determined (last column of the table).

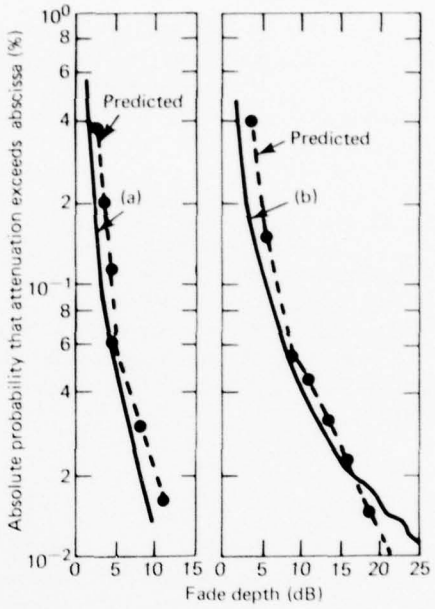

Fig. 2 Comparison of measured and predicted fade statistics at 13 and 18 GHz (Ref. 10).

(a) $f = 13$ GHz, COMSAT, ATS–F, July 1974 - May 1975, 4112 hours, $\theta = 35.8$, Cambridge, MA

(b) $f = 18$ GHz, COMSAT, ATS–F, July 1974 - May 1975, 2730 hours, $\theta = 35.8$, Cambridge, MA

TABLE 1

COMPARISON BETWEEN MEASURED AND PREDICTED FADE CURVES

Fade Distribution Location	Frequency (GHz)	P_1/P_2 Av.	P_1/P_2 rms	$A_1 - A_2$ Av.	$A_1 - A_2$ rms
Austin, TX (Ref. 7)	30	1.3	0.2	3.3	0.8
Clarksburg, MD (Ref. 8)	15.3	1.3	0.1	1.1	0.7
Slough, Bucks, England (Ref. 9)	19	1.5	0.3	0.9	0.75
Slough, Bucks, England (Ref. 9)	37	1.9	0.2	2.0	0.5
Cambridge, MA (Ref. 10)	13	1.3	0.2	0.6	0.5
Cambridge, MA (Ref. 10)	18	1.3	0.4	1.3	0.7
Fayetteville, NC (Ref. 10)	13	1.6	0.4	1.8	1.6
Fayetteville, NC (Ref. 10)	18	1.3	0.1	2.2	1.0
Overall (eight stations)		1.4		1.7	

In view of the many varied assumptions and recognizing that we are comparing probability distributions on an absolute scale, the overall correlation of the prediction method is remarkably good. Of course, more checks should be made before a final assessment of the method is possible. Unfortunately, long-term fade data at fixed path angles accompanied by instantaneous point rain rate data are either sparse or nonexistent. However, the proposed method may be tested in the future at various locations by analyzing the 19.04 and 28.56 GHz beacon signals from the recently launched geosynchronous COMSTAR satellites, which should be operational for the next several years (Ref. 6).

REFERENCES

1. T. G. Konrad and R. A. Kropfli, *Radar Derived Spatial Statistics of Summer Rain, Data Reduction and Analysis*, II, NASA CR-2592, prepared by APL/JHU under NASA/DoD Agreement S-70248AG, 1975.
2. L. J. Battan, *Radar Observation of the Atmosphere*, The University of Chicago Press, Chicago, p. 84.
3. J. Goldhirsh, "Prediction Methods for Rain Attenuation Statistics at Variable Path Angles and Carrier Frequencies between 13 and 100 GHz," *IEEE Trans. Antennas Propag.*, **AP-23**, No. 6, 1975, pp. 786–791.
4. R. Wexler and D. Atlas, "Moisture Supply and Growth of Stratiform Precipitation," *J. Meteorol.*, **15**, 1958, pp. 531–538.
5. K. L. S. Gunn and T. W. R. East, "The Microwave Properties of Precipitation Particles," *Q. J. R. Meteorol. Soc.*, **80**, 1954, pp. 522–545.
6. D. C. Cox, "Design of the Bell Laboratories 19 and 28 GHz Satellite Beacon Propagation Experiment," *ICC 1974 Conference Record*, 17–19 June 1974, pp. 27E-1 to 27E-5.
7. W. J. Vogel, A. W. Stratton, B. M. Fannin, and N. K. Wagner, *ATS-6 Attenuation and Diversity Measurements at 20 and 30 GHz*, NASA TN-D-8197 (*20- and 30-GHz Millimeter Wave Experiment with the ATS-6 Satellite*, L. J. Ippolito (Ed.), NASA/GSFC), 1970, pp. 11–32.
8. H. D. Craft, "Attenuation Statistics at 15.3 GHz for Clarksburg, Md.," *COMSAT Tech. Rev.*, **1**, 1971, pp. 221–225.
9. P. O. Davies, "Radiometer Measurements of Atmospheric Attenuation at 19 and 37 GHz Along Sun-Earth Paths," *Proc. Inst. Electr. Eng.*, **120**, No. 2, 1973, pp. 159–164.
10. G. Hyde, *Data Analysis Report—Part 1 for ATS-F COMSAT Millimeter Wave Propagation Experiment*, prepared by COMSAT Laboratories, Clarksburg, MD, for NASA/GSFC under Contract NAS5-21616.

Author: J. Goldhirsh

Support: NASA S50748A

LOW-ENERGY CHARGED PARTICLE EXPERIMENT FOR VOYAGERS 1 AND 2

A Low-Energy Charged Particle Experiment that has been designed, constructed, and tested at APL will be carried by the Voyager spacecraft to explore the outer planets. The instrument will provide the first measurement of the energy and spatial distributions and intensities of electrons, protons, and heavier nuclei in the interplanetary medium and near Jupiter, Saturn, Uranus, and possibly Neptune as well as the satellites of these two planets. The principal investigator for the instrument is S. M. Krimigis of APL.

BACKGROUND

The Low-Energy Charged Particle Experiment (Fig. 1) will be launched on two Voyager spacecraft in August and September 1977. The experiment has been designed to perform particle measurements in the intense radiation belts of the Jovian, Saturnian, and Uranian environments and to provide detailed spectral analysis of both solar and galactic particles in interplanetary space. These objectives are met by a single instrument that uses 23 solid-state detectors configured in two distinct detector subsystems. One subsystem is optimized for interplanetary and interstellar measurements. The other is optimized for the specific particle species, energies, and intensities expected near the planets. Angular distributions in the ecliptic plane and pitch angle distributions are obtained using an eight-sector scanning motor.

Over 30 000 solder joints bond nearly 6000 components within the instrument. Because of the complexity of the experiment, the circuitry is based on the use of 14 different types of 261 custom-designed hybrids for amplification, discrimination, timing, pulse height analysis, and data functions.

DISCUSSION

INTERPLANETARY/INTERSTELLAR MEASUREMENTS. The interplanetary/interstellar particle measurement subsystem is based on a bidirectional telescope consisting of seven silicon surface barrier detectors. The

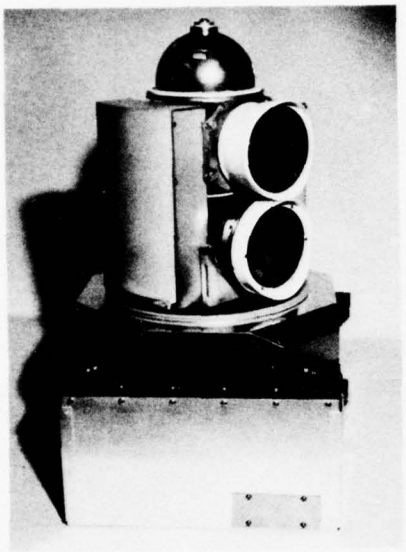

Fig. 1 The Low-Energy Charged Particle Experiment.

Low-Energy Particle Telescope (LEPT) is shown in Fig. 2. The telescope consists of two multi-$dE/dx \times E$ detector systems (D1 to D5) placed back to back and utilizes a common-element, cylindrical, lithium-drifted silicon detector shield (AC1 to AC8). Detectors in the LEPT vary in thickness between 2.0 μm and 2.5 mm. The particle types and nominal energy passbands are listed below.

Particle	Enter D1 First (MeV/nucleon)	Enter D5 First (MeV/nucleon)
protons	0.35 – 20	3.0 – >170
alphas	0.07 – 21	3.0 – >64
(light, e.g., Be)	0.12 – 33	4.0 – 21
(medium, e.g., N)	0.05 – 40	6.3 – 200
$Z \geq 19$	0.06 – 74	8.6 – >1000

The interplanetary/interstellar subsystem makes use of two basic particle-identification and energy-measurement techniques. The first is the conventional range-energy technique. The second (Ref. 1) relies on forming the product

$$P = a\ \Delta E_1\ \Delta E_2{}^b,$$

where ΔE_1 and ΔE_2 are the energies deposited in detectors 1 and 2 and a and b are constants. The product, P, is unique for each particle type and has a relatively constant slope on a log-log scale over a large range of particle energy. Appropriate P discriminator levels (which, when plotted, P is a constant) as well as energy discriminators are then used to distinguish particle types (Fig. 3).

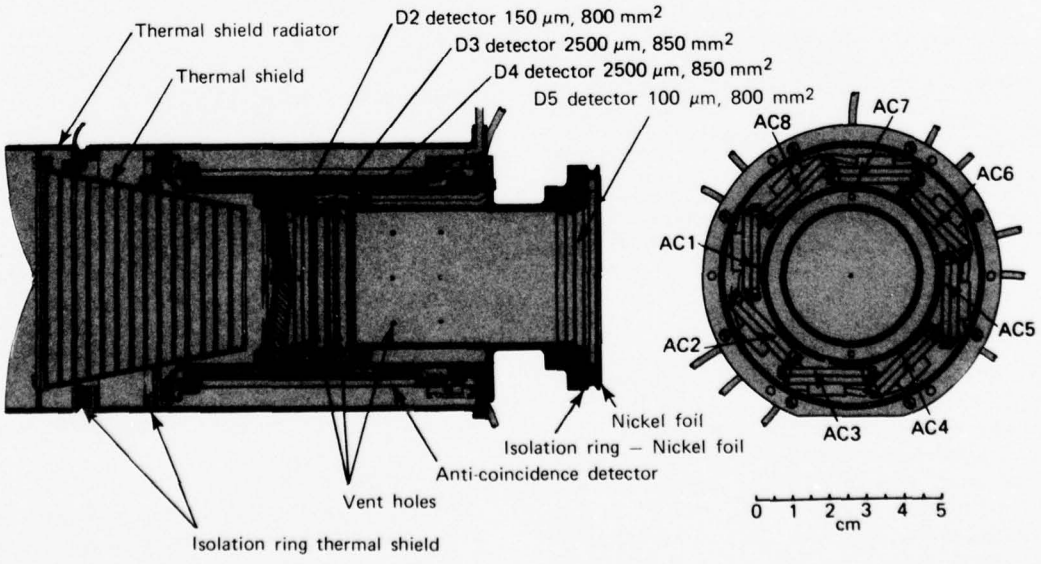

Fig. 2 The Low-Energy Particle Telescope.

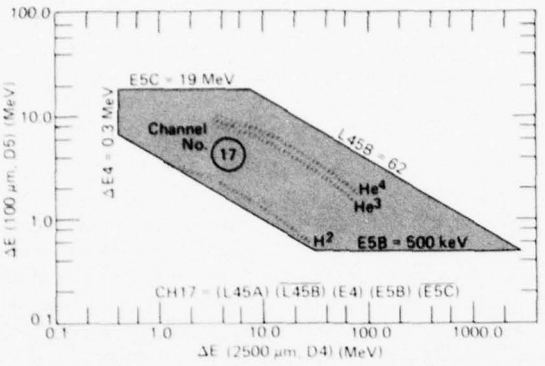

Fig. 3 Energy loss in 100– to 2500–μm detectors of LEPT.

The large range of particles and energies measured by this subsystem require the use of logarithmic pulse amplifiers. The amplifiers combined with pulse summing amplifiers form the product P in a straightforward manner.

Other significant features of this subsystem include a dual, 256–channel, pulse-height analyzer for precision energy determination, a 64–channel digital data system that uses 24 to 12 bit logarithmic compression to better utilize data rates, a priority selection scheme to ensure that rare particle types are observed, and a 120–channel analog data commutator for instrument calibration (Ref. 2) and housekeeping data. The instrument also contains power conversion, power switching, and a command subsystem for flexibility and reliability by means of redundancy.

NEAR-PLANET MEASUREMENTS. The near-planet subsystem is primarily a magnetospheric instrument designed to investigate a large variety of moderately and highly abundant particles. The detector arrangement (Fig. 4) is called the Low Energy Magnetospheric Particle Analyzer (LEMPA). LEMPA uses two primary identification methods.

In the first, low- and medium-energy electrons are deflected into total energy detectors (beta and gamma) via a sintered cobalt-samarium rare earth magnet. The more massive protons and ions pass through the magnet's field and strike the total energy detector, alpha. The low-noise alpha and beta channels allow measurement of electron and proton energies as low as 12 keV. As particle intensities increase and simple pulse counting becomes difficult, the alpha and beta

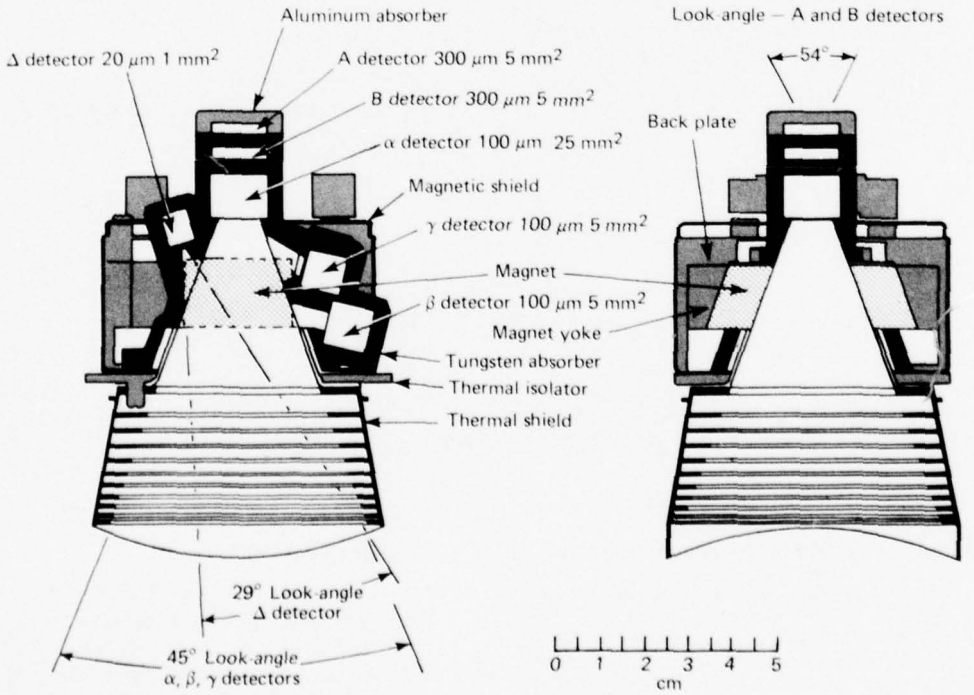

Fig. 4 Low-energy magnetospheric particle analyzer.

detector currents are monitored, thus extending the useful range of intensity measurements. The pulse widths of the alpha and beta amplifiers are approximately 1.5 μs from the beginning of the pulse to its zero crossing.

The second identification method uses a combination of shielding and energy loss to restrict the response of detectors A and B to high-energy particles. The A–B detector system is also arranged as a telescope. The particles detected by the LEMPA telescope are indicated in Table 1.

TABLE 1

PARTICLES DETECTED BY LEMPA TELESCOPE

Detector	Particle Type	Medium Intensity MeV	High Intensity MeV
β, β', γ (A, B)	electron	0.01 – 1.5	($\geq$1, $\geq$10)
α (A, B)	proton	0.015 – 4.0	(20 – 180)
α	alpha	1.0 – 4.0 *	—
δ, δ'	$Z \geq 1$, $Z \geq 2$, $Z \geq 3$	—	3.0 – $\approx$5*

* MeV/nuc

High-energy electrons will be abundant near the planets and heavy shielding is necessary to prevent their contaminating the low-energy detectors. About one pound of tungsten is used for this purpose. The high intensities of radiation trapped in the Jovian and (probably in the) Saturnian magnetic fields necessitate the use of extremely fast pulse circuitry in several channels to prevent pulse pile-up effects and saturation. Special hybrid amplifiers and discriminators were developed to handle counting rates in excess of 25 million particles per second.

PITCH ANGLE DISTRIBUTION. The attitude of the Voyager spacecraft is very nearly fixed in inertial space except during occasional maneuvers. Therefore, measurements of particle angular distributions require a rotating platform. The platform is driven by a step motor through eight 45° sectors. The sector rate is once every 24 seconds during planetary encounter, once every six seconds during Io (a Jovian moon) encounter, and once every six minutes in the interplanetary medium. Pitch-angle distributions are obtained by two additional detectors placed in a cone/dome combination in which the cone sets the azimuth view angle and holes cut in the dome set the elevation view angles. Thus, a single mechanism is used to obtain pitch-angle distributions in two planes.

REFERENCES

1. J. B. A. England, "A Fast Analogue Particle Identification System," *Nucl. Instrum. Methods*, **106**, 1973, pp. 45–59.
2. D. P. Peletier, "A Closed Loop Threshold Calibrator for Pulse Height Discriminators," *IEEE Trans. Nucl. Sci.*, **NS-22**, No. 1, February 1975, pp. 592–594.

Author: D. P. Peletier

Support: NASA Planetary Programs Office

EMISSIONS OF PLASMA AND ENERGETIC PARTICLES IN SOLAR FLARES

Plasma and energetic-particle data acquired by detectors on many deep-space spacecraft in orbits around the sun have been used to carry out multiple-site interplanetary space "meteorology" of solar flare disturbances. The principal conclusion of this study is that the solar magnetic fields strongly control the emission of flare particles. This fact significantly improves our ability to predict terrestrial effects of solar flares.

BACKGROUND

A well-established fact of plasma physics is that a moving plasma carries a magnetic field along with it as if the field lines were "frozen in" the plasma. Therefore, if we know where the interplanetary plasma (called the solar wind) was emitted from the sun, we also know the point of origin of the coronal

field line that the plasma carried out into interplanetary space. It has also been demonstrated that energetic particles are constrained to gyrate around interplanetary field lines although they are free to move along them (Ref. 1). Therefore, the place on the sun where the plasma (and field line) originated must also be the origin of the energetic particles measured at the same time by a spacecraft.

Time-intensity profiles observed by spacecraft in the interplanetary medium are difficult to interpret. They show the intermixed effects of temporal and spatial variations because the high coronal spacecraft-connection longitude of the interplanetary magnetic field lines changes continuously due to the rotation of the sun (Ref. 1). Superimposed on the continuous change are irregular changes of the connection longitude due to variations in the velocity of the solar wind. However, when a solar wind stream decays, the decrease in its velocity tends to move the connection longitude westward, thereby canceling the effect of the sun's rotation. The spacecraft is then connected to the same heliolongitude for some time and observes the temporal change at that heliolongitude. On the other hand, when the solar wind increases strongly, the connection longitude rapidly shifts eastward. Then we observe the particle intensity over about 30° of heliolongitude in a very short time so that we sample primarily the longitudinal gradient.

OBSERVATIONS AND ANALYSIS

The clearest separation of temporal and spatial variations is provided by simultaneous measurements by several spacecraft at different heliolongitudes. The first four months of 1969 is perhaps one of the most fruitful time periods for such a study: numerous particle flares with intense fluxes were observed by five spacecraft, Pioneers 6 through 9 and Explorer 34, distributed more or less uniformly over more than 180° around the sun, with good coverage of particle flux data and solar wind plasma measurements. This period provides a unique opportunity to study the interrelationship between the emission longitude profiles of energetic protons and solar wind plasma.

An analysis of the 10 April 1969 event will be given as an example of the multispacecraft technique. The event was previously studied by McCracken et al. (Ref. 2) and Keath et al. (Ref. 3) who have already pointed out the existence of unusual spatial gradients in the energetic particle fluxes. Their work is carried further here by adding the proton data of Explorer 34 and solar wind plasma data from the five spacecraft. Thus, we can use the new techniques of mapping the observed particle fluxes and solar wind velocities back to the sun and study the coronal control of plasma and energetic particle emission (Ref. 4).

Figure 1 shows the 7.5 to 45 MeV proton fluxes observed by the University of Texas, Dallas, detectors on Pioneers 6 through 9 and the >10 MeV proton fluxes observed by the APL detector on Explorer 34, together with the locations of the five spacecraft in the ecliptic as seen from the north. Data points from Pioneers 6 through 9 are taken from Ref. 2; in addition, some unpublished Pioneer 8 and 9 data were used.

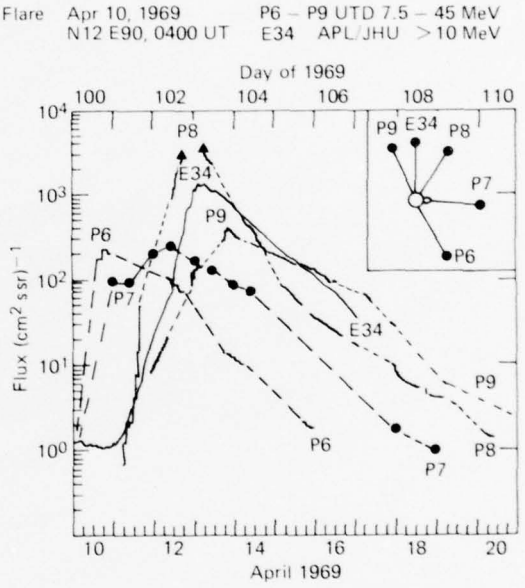

Fig. 1 Energetic particle fluxes for the 10 April 1969 event observed by Pioneers 6 through 9 and Explorer 34. The insert shows spacecraft positions in the ecliptic as seen from the north; the bubble indicates the flare site.

The method used to separate spatial from temporal variations and to deduce the coronal gradients as a function of time is straightforward. All the particle fluxes are mapped back to the high corona using the two approximations of nonaccelerating radial solar wind transport with frozen-in magnetic field lines (Refs. 5 and 6) and of relatively small gradients of particle intensity along individual interplanetary field lines (Ref. 7). The particle intensities are connected at the same time of observation, giving the instantaneous coronal emission profile. This is done for the labeled times for particle fluxes (Fig. 2, bottom) and for solar wind velocities (Fig. 2, top). It is then pos-

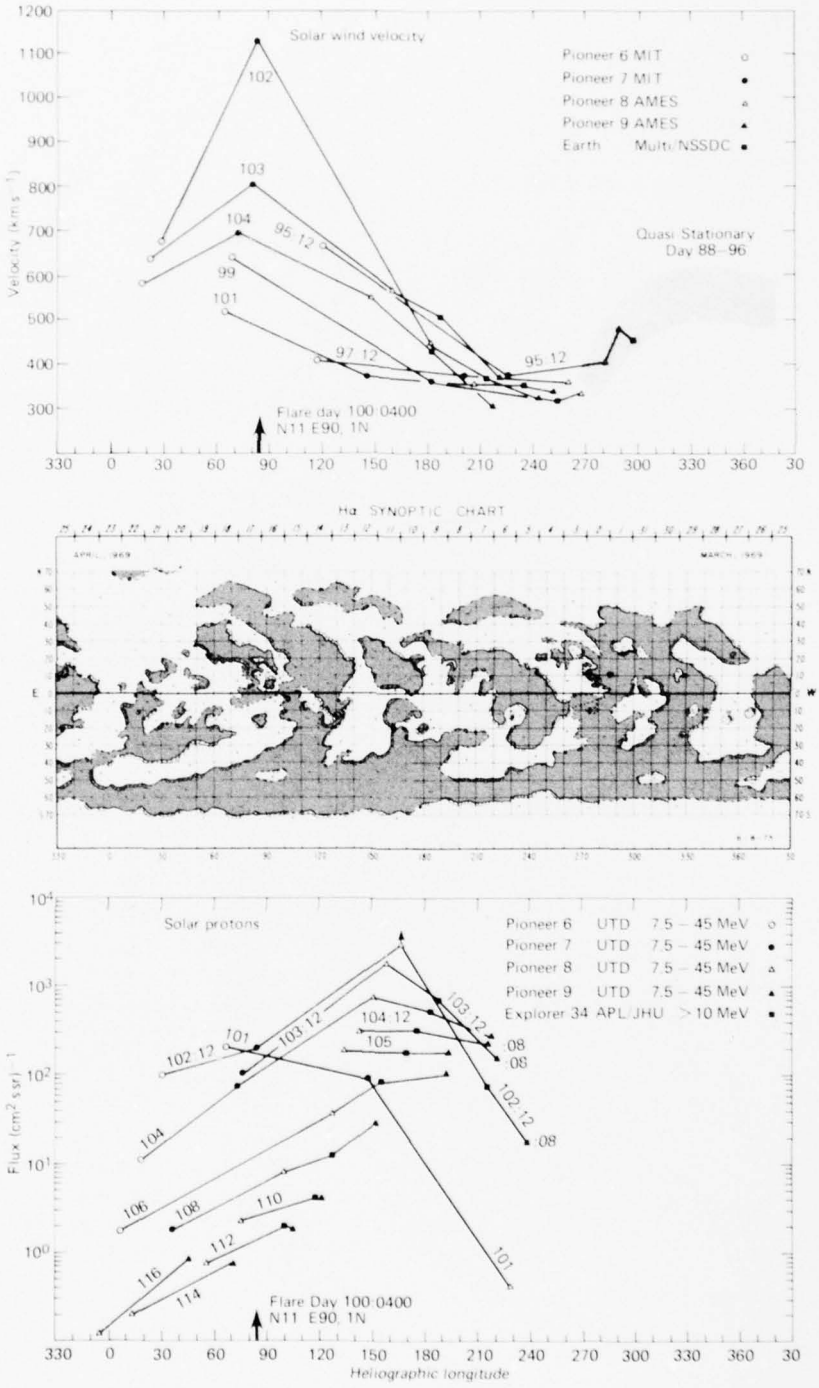

Fig. 2 Coronal solar wind velocity emission profiles (upper panel), Hα synoptic chart (center panel), and coronal particle flux emission profiles (lower panel). Numbers on the emission profiles give the time of the observations (days:hours). Rotation 1546, April 1969.

sible to study the temporal development of the coronal emission profiles, to compare the emission profiles of particle fluxes and solar wind plasma, and, finally, to compare the emission profiles with the global chromospheric magnetic polarity structure visible on the Hα synoptic chart (Fig. 2, center). The Hα chart is constructed from absorption features in solar photographs taken in the red line of hydrogen. These features (the lines on the chart) mark the boundaries between magnetic fields out of (+) or into (−) the sun. Also indicated in Fig. 2 is the heliographic longitude of the flare location.

DISCUSSION

On day 101 (11 April) the peak particle flux is at Pioneer 6, connected closest to the flare longitude. The flux is somewhat lower at Pioneer 7, while Pioneer 8, Explorer 34, and Pioneer 9 are still at the background level. This is consistent with the idea that the peak flux at the flare site is decreasing gradually with time and also with distance from the flare. However, on day 102 (12 April) the peak flux is at 170°, more than one order of magnitude above the flux that is observed to be enhanced up to day 114, 14 days after the flare. Then the fluxes finally fall below the detector's background level.

A most unexpected result is found by comparing the coronal emission profiles of the energetic particles with the heliolongitude emission profiles of the solar wind velocity (Fig. 2, top). The flare-associated solar wind plasma preferentially escapes over the flare site near 85°. However, although the particles also preferentially escape over the flare site initially, they eventually peak almost 100° to the west of it. The emission profile of the particles evidently is controlled by coronal structure remote from the flare site, whereas that of the plasma is not.

The low coronal magnetic structure revealed in the Hα synoptic chart shows that the active region where the flare occurred extends more than 50° in azimuth and has strong magnetic fields indicative of closed-loop structures. Such loops of strong fields may have inhibited the initial release of particles over the flare site. On the other hand, the peak emission of particles from day 102 on at a heliographic longitude of 170° is associated with a region of weak magnetic fields; this region appears on the Hα map as a negative island extending from 150 to 180°. The weak fields indicate high-lying loop structures with perhaps a greater fraction of open field lines, which would facilitate the escape of energetic particles out to interplanetary field lines.

FUTURE WORK

We are now systematically investigating solar flare plasma and energetic particle events that occurred over the last solar cycle, beginning in 1964 (Ref. 8). We will concentrate on disturbances that had "good coverage" by the network of deep-space probes, such as the April 1969 period discussed here. As we identify characteristic coronal magnetic structures that control the arrival of the solar plasma and energetic particles at earth, we will incorporate these coronal magnetic "signatures" into the prediction algorithms for geomagnetic storms and ionospheric disturbances that we have developed over the past five years (Refs. 9 to 11).

REFERENCES

1. E. C. Roelof and S. M. Krimigis, "Analysis and Synthesis of Coronal and Interplanetary Energetic Particle, Plasma and Magnetic Field Observations Over Three Solar Rotations," *J. Geophys. Res.*, **78**, 1973, pp. 5375–5410.
2. K. G. McCracken, U. R. Rao, R. P. Bukata, and E. P. Keath, "The Decay Phase of Solar Flare Events," *Solar Phys.*, **18**, 1971, pp. 100–132.
3. E. P. Keath, R. P. Bukata, K. G. McCracken, and U. R. Rao, "The Anomalous Distribution in Heliocentric Longitude of Solar Injected Cosmic Radiation," *Solar Phys.*, **18**, 1971, pp. 503–509.
4. R. E. Gold, E. P. Keath, E. C. Roelof, and R. Reinhard, "Coronal Structure of the April 10, 1969 Solar Flare Particle Event," *Proceedings of the 15th International Cosmic Ray Conference*, 1977.
5. J. T. Nolte and E. C. Roelof, "Large-Scale Structure of the Interplanetary Medium I: High Coronal Source Longitude of the Quiet-Time Solar Wind," *Solar Phys.*, **33**, 1973a, pp. 241–257.
6. J. T. Nolte and E. C. Roelof, "Large-Scale Structure of the Interplanetary Medium II: Evolving Magnetic Configurations Deduced from Multi-Spacecraft Observations," *Solar Phys.* **33**, 1973b, pp. 483–504.
7. E. C. Roelof, "Solar Particle Emission," *Proceedings of the International Symposium of Solar-Terrestrial Physics (Boulder)*, **1**, D. J. Williams (Ed.), American Geophysical Union, 1976, pp. 214–231.
8. J. T. Nolte and E. C. Roelof, "Solar Wind, Energetic Particles and Coronal Magnetic Structure: The First Year of Solar Cycle 20," *J. Geophys. Res.*, **82**, 1977.
9. R. E. Gold and E. C. Roelof, "A Prediction Technique for Low Energy Solar Proton Fluxes near 1AU," *Space Res.*, **XVI**, 1976, pp. 791–796.
10. E. C. Roelof and R. E. Gold, *Prediction of Solar Energetic Particle Event Histories Using Real-Time Particle and Solar Wind Measurements*, Air Force Geophysics Laboratory, AFGL-TR-76-0136, 1976.
11. E. C. Roelof, R. E. Gold, and E. P. Keath, "Evaluation of a Prediction Technique for Low Energy Solar Particle Events," *Space Res.*, **XVII**, 1977, p. 545–551.

Authors: *E. C. Roelof, R. E. Gold, and E. P. Keath (APL), and R. Reinhard (European Centre for Space Research and Technology)*

Support: *Air Force Geophysics Laboratory*

g–TENSOR AND SPIN DOUBLING CONSTANT IN THE $^2\Sigma$ RADICALS CN AND C_2H

The electronic magnetic moments of the cyanogen (CN) and ethynyl (C_2H) radicals have been determined by analysis of high-resolution electron spin resonance (ESR) spectra of these radicals in argon (Ar) and krypton (Kr) matrices at 4 K. The results support a predicted relationship between the electronic magnetic moment and the magnetic field produced by molecular rotation (spin-doubling interaction). The results also resolve a serious discrepancy between the nitrogen hyperfine splittings of the CN radical obtained from its ESR spectrum and from its interstellar microwave emissions.

BACKGROUND

Many of the radicals studied and characterized by the free-radicals research program at APL have been detected recently in interstellar space by radio astronomers at other laboratories. Two especially interesting examples are the CN and C_2H radicals. These species are so reactive that, prior to the interstellar observations (Refs. 1 and 2), the only information about their magnetic fine and hyperfine structure came from ESR studies (at APL and elsewhere) of the radicals trapped in inert gas matrices at 4 K (Refs. 3 and 4). The matrix ESR data were useful in establishing the identity of the radicals from their interstellar emissions, which correspond to transitions from the first excited rotational state to the ground state.

However, attempts at more detailed comparisons of the available ESR data with magnetic fine structure in the microwave emissions indicated a need for more precise ESR measurements. Also needed was a consideration of possible changes in the magnetic parameters of the isolated radicals resulting from interactions between the radical and the host matrix and or averaging of the isolated radical parameters over some rotational motion of the radicals in the matrix. Of particular interest was the fact that the CN and C_2H radicals provide an especially stringent test of an important predicted relationship between the electronic magnetic moment of a radical (which is readily measured by terrestrial ESR experiments) and the spin-doubling splitting of the microwave rotational lines.

If the electron magnetic moment is written as $\mu_s = g\mu_\beta S$, where μ_β is the Bohr magneton and S is the electron spin, this relationship is (Ref. 5)

$$\gamma = -2B_0(g_\perp - g_e) \qquad (1)$$

where γ and B_0 are the spin-doubling and rotational constants, $g_\perp$ is the electron g factor in a direction perpendicular to the molecular axis (direction of the rotation axis), and $g_e = 2.00232$ is the free-spin g value. The physical origin of Eq. 1 is as follows: $g_\perp$ usually differs slightly from g_e because perturbation of the orbital motion of the electrons within the radical by the magnetic field, H, results in a small orbital contribution to μ_s. Similarly, the perturbation of the electron orbital motions by molecular rotation creates a magnetic field whose interaction with μ_s splits each rotational line into a doublet. The connection between these effects, embodied in Eq. 1, is provided by Larmor's theorem, which states that under fairly general conditions the magnetic interaction $H\mu_s$ may be represented by a rotating coordinate system or, physically, a rotating molecule at the rotation frequency $\omega = \mu_s H$.

DISCUSSION

The electronic magnetic moment of a radical is determined from the ESR spectrum by the relationship $\nu = g\mu_\beta H$, where ν is the microwave frequency and H is the magnetic field strength at which the ESR line appears. In order to make the most accurate measurements, several improvements were made in the automatic frequency control loop that stabilizes the microwave frequency of the ESR spectrometer. Also, the proton magnetometer, which measures H, was calibrated using the precisely known g factor of the hydrogen atom in Ar and Kr matrices.

Matrix perturbations were found to affect the g values of C_2H but not those of CN. The observed differences between the g values of C_2H in Ar and Kr, combined with the theory of matrix shifts of g, indicated that the Ar value, $g_\perp = 2.00288$, should be close to but slightly less than the isolated radical value. Use of this value in Eq. 1 gave $\gamma = -48.9$ MHz as compared to the observed value of -62.3 MHz (Ref. 2). Estimates of the matrix shifts of $g_\perp$ for C_2H, obtained by assuming that the shifts are proportional to the known matrix shifts of the hydrogen atom, gave even better agreement: $g_\perp = 2.00309$ and $\gamma = -67.3$ MHz (Ref. 6).

Even though there were no matrix shifts of g, the CN case was more complex because the ESR spectrum of this radical in Ar at 4 K was inconsistent with the spectrum of an axially symmetric radical. In this spec-

trum (Fig. 1), let us momentarily ignore the outer lines of the triplet shown in Fig. 1a, which are due to the nitrogen hyperfine splitting, and concentrate on the expanded trace of the centerline in Fig. 1b. The

Fig. 1 ESR spectrum of CN in an Ar matrix at 4 K. (a) Complete spectrum. (b) Expanded trace of the centerline. H_e denotes the resonant field of a free electron spin.

complex shape of this line has two distinct peaks at its outer limits and an interior shoulder, denoted g_1, g_3, and g_2, respectively. In a polycrystalline matrix, this line represents a superposition of spectra for all possible orientations of the radical with respect to the external magnetic field. The distinct features correspond to radicals that are oriented so that the magnetic field is parallel to a principal axis of the electron magnetic moment or g factor tensor. Since there are three, rather than two, distinct features, CN in Ar cannot be an axially symmetric system but has three distinct g values: $g_1 = 2.00165$, $g_2 = 2.00067$, and $g_3 = 2.00036$ (Ref. 6).

The nonaxial symmetry indicates that CN undergoes a complex motion in the Ar matrix resulting in an observed nonaxial g tensor that is the motional average of the axially symmetric free molecule g tensor. A model of the motion gave $g_1 = 2.00028$ (Ref. 6). Use of this value in Eq. 1 gave $\gamma = 234$ MHz, in excellent agreement with the observed value of 217 MHz (Ref. 1).

Furthermore, using this model and the nitrogen hyperfine constants of free CN, obtained from the interstellar microwave data, to compute the motionally averaged nitrogen hyperfine splitting gave a predicted hyperfine splitting of 27.9 MHz for CN in Ar. This value is in excellent agreement with the observed splitting of 28.0 MHz, whereas in the absence of motional corrections the value disagreed with the interstellar CN data (Ref. 6).

REFERENCES

1. A. A. Penzias, R. W. Wilson, and K. B. Jefferts, "Hyperfine Structure of the CN Radical Determined from Astronomical Observations," *Phys. Res. Lett.*, **32**, No. 13, 1974, pp. 701–703.
2. K. D. Tucker, M. L. Kutner, and P. Thaddeus, "The Ethynyl Radical, C_2H—A New Interstellar Molecule," *Astrophys. Lett.*, **193**, 1974, p. L115.
3. E. L. Cochran, F. J. Adrian, and V. A. Bowers, "ESR Detection of Cyanogen and Methylene Imino Free Radicals," *J. Chem. Phys.*, **36**, No. 7, 1962, pp. 1938–1942.
4. E. L. Cochran, F. J. Adrian, and V. A. Bowers, "ESR Study of Ethynyl and Vinyl Free Radicals," *J. Chem. Phys.*, **40**, No. 1, 1964, pp. 213–220.
5. R. F. Curl, Jr., "The Relationship between Electron Spin Rotation Coupling Constants and g-Tensor Components," *Mol. Phys.*, **9**, 1965, pp. 585–597.
6. F. J. Adrian and V. A. Bowers, "g-Tensor and Spin Doubling Constant in the $^2\Sigma$ Molecules CN and C_2H," *Chem. Phys. Lett.*, **41**, August, 1976, pp. 517–520.

Authors: F. J. Adrian and V. A. Bowers

Support: Indirectly Funded R&D

MICROCOMPUTER-CONTROLLED CARTRIDGE TAPE UNIT

The advent of microprocessor technology has made practical the design of compact, software-adaptable equipment. The cartridge tape unit (CTU) is one of APL's first applications of microprocessor technology to culminate in operational hardware.

BACKGROUND

In 1972, APL developed a data collection and recording (DC&R) system to retrieve data at remote installations. It was designed to operate reliably, virtually hands-off, for extended periods of time. One of the major components of the system was a nine-track, IBM-compatible, synchronous tape drive. This type of drive is highly complex and requires routine maintenance to ensure reliable operation. Four years of experience with the DC&R system indicated that the recorder was not meeting the reliability requirements of the system and an effort was begun in 1976 to develop a replacement for it.

DISCUSSION

A relatively new type of recording system was chosen as a replacement. It employs a 3M tape cartridge with take-up reels and an elastomeric drive belt that eliminates the need for reel servo control. This approach dramatically reduces the mechanics and the circuit components needed to control tape motion. Several manufacturers produce digital cartridge drive units that are compatible with the 3M tape data cartridge.

The CTU (Figs. 1 and 2) was developed as a plug-in replacement for the recorder being used in the DC&R system. The decision was made at the onset of the task to develop the CTU around a microprocessor controller. The Motorola M6800 system was chosen because of a large family of supporting input/output (I/O) devices. Figure 3 illustrates how these I/O devices are utilized in the CTU system.

One of the goals in designing the CTU was to reduce the size, required power, and weight of the recorder by at least 50%. The microprocessor would not only control the device but would provide diagnostic aid to the field service personnel responsible for proper system operation.

Several functions have been implemented to date, all requiring some interface with the operator through a terminal (a TI Silent 700 is being used at field sites). With this terminal, data can be read back from tapes for spot checking, and software routines can be read into the random access memory (RAM) and executed to perform analysis or other functions.

A memory diagnostic is included in the programmable read-only memory (PROM) software for checking RAM. A checksum routine monitors the PROM's continuously when the unit is operational and flags those with errors.

Fig. 1 The cartridge tape unit and maintenance terminal.

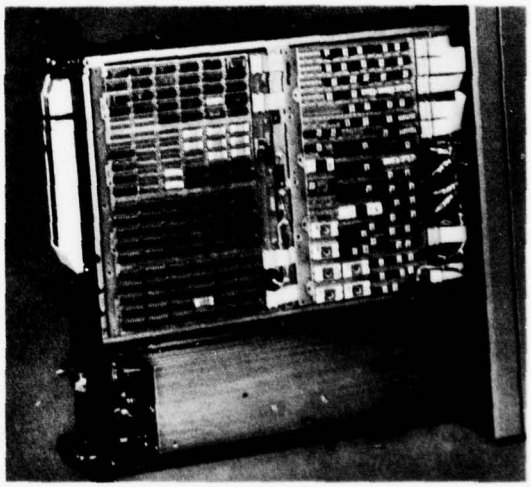

Fig. 2 Internal view of cartridge tape unit.

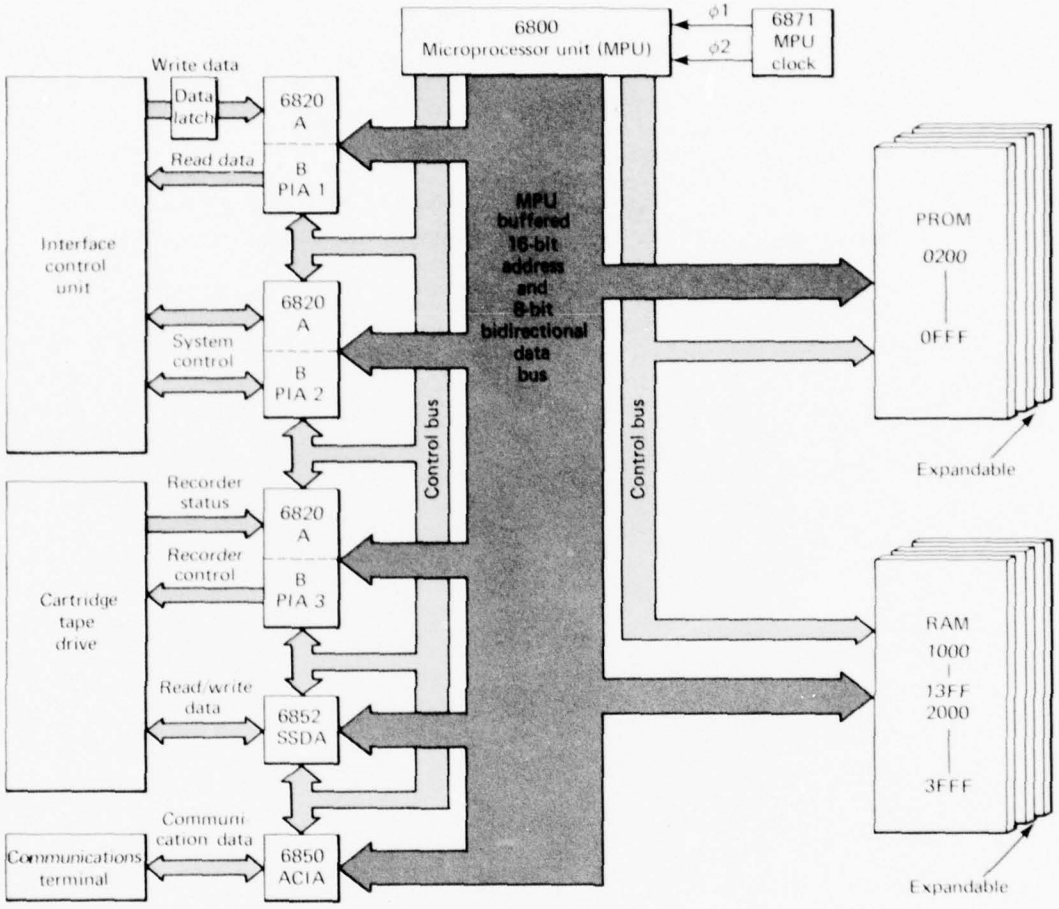

Fig. 3 Diagram of CTU system.

Where the CTU has not replaced the nine-track units, it can be used to check their operation. Tapes from the nine-track unit can be copied on cartridge tape with a simple cable hookup and then dumped to the terminal. The reverse can also be done if a nine-track unit is required for analysis on a large system such as the IBM 360.

The DC&R system was designed to be a turnkey system. As such, during operation, minimal interface with personnel is desirable. Insertion of a new tape when indicated and replacement of the old cartridge if power is interrupted are the only requirements.

The software controls collection of data from the interface control unit while previously collected data are being written. If a power interruption occurs, the cartridge is replaced and the software restores the unit to its state before interruption. This is done by means of a battery back-up RAM that allows pointers to the tape and program states to be saved when a power outage occurs.

Note that the software used in the CTU was tailored to structured programming techniques. Basically, this means that the flow is top-down and that the code is divided into modules by function. Each of these modules has minimal entry and exit points, and all are linked through a change of a "state" variable. The state variable always contains the address of the currently executing module and is one of the pointers saved, should power interruption occur, to enable restoration of the system.

Modular, or structured, programming allows new functions to be added by defining a link to a new state. Should a function be changed, there is minimal impact on the remainder of the software.

Perhaps the most important asset of a microprocessor-based system is the flexibility that can be realized. New functions can be added, often without wiring or other hardware changes, by changing a PROM. Changes can be made and verified in the office and implemented in the field with ease. The diagnostic capabilities that can be implemented are virtually without limit through the use of cartridge tapes for software storage and a terminal for operator interface.

ACKNOWLEDGMENT

The software was developed with the aid of a M6800 cross-assembler program written by A. W. Currano.

Authors: *S. B. Springer and E. L. True*

Support: *NAVELEXSYSCOM, PME-117*

ENERGY RESEARCH AND DEVELOPMENT

INTRODUCTION

Energy management is a key technical area in much of APL's work. Since its inception, APL has been a leader in high-speed combustion research and its application to advanced ramjet and rocket propulsion systems. The development of more efficient subsonic and supersonic combustion ramjets is providing the basis for increased range and performance of future missiles. One recent accomplishment, reported in the Naval Systems Support section of this volume, is the successful design and test of an efficient low-volume ramjet combustor that can extend the range of the Advanced Surface-to-Air Ramjet (ASAR) within the constraints of current shipboard launching and handling systems. The dramatic increase in performance capability provided by another APL propulsion development, the integral rocket-ramjet, is also presented in that section of this volume.

The Chemical Propulsion Information Agency operated by APL supports the national rocket propulsion supplier and user communities by providing definitive component and system information, standardized methodology for measuring and presenting rocket design and performance data, and guidance in areas of continuing R&D needs.

In the civil area, APL combustion technology is applicable to more efficient utilization of increasingly scarce and expensive fossil fuels. A spin-off of APL combustion expertise is the Fire Research Program discussed in the Environmental Programs section.

Energy management is also essential to the APL satellite and space vehicle programs. APL pioneered the development and application of long-life solar cell power systems for satellites. In support of this requirement, research in photovoltaic materials and processes is conducted. This work may provide a basis for lower cost solar photovoltaic systems for civil energy generation. Some recent results on thin-film silicon solar cells are reported herein. Another satellite requirement, momentum storage for spacecraft attitude control, led to the development of highly efficient flywheels. APL's proprietary flywheel designs are applicable to efficient energy conversion and storage for both automotive and stationary civil applications.

As early as 1973, APL had analyzed energy technologies and concluded that utilization of low-grade heat will provide increasingly important alternatives to scarce fossil fuels. These include solar thermal, geothermal, and waste heat sources. Accordingly, programs were initiated in-house in the areas of ocean thermal energy (OTEC, solar energy stored in the tropical oceans), geothermal applications, and annual storage systems that save summer heat for winter use. While some of the efforts are in too early a stage for detailed reporting, they have been endorsed by ERDA and will receive increasing future sponsor support. A common requirement of these applications is more efficient heat exchange at small temperature differences. Engineering design data for heat exchange at small temperature differences were hitherto unreliable or nonexistent. The OTEC heat transfer experiments provide for the first time a firm basis for the design of economical evaporators and condensers for large OTEC plants. Development of mathematical models for heat exchangers provides an analytical basis for more efficient design.

THIN-FILM SILICON SOLAR CELLS

Experimental solar cells were fabricated from vacuum-deposited polycrystalline silicon films using conventional integrated-circuit processing techniques. Solar cell efficiencies of approximately 2% (AM2) were obtained from small devices with no attempt made to optimize the electrode configuration and without an antireflection coating. Suggested ways to improve processing and structure could lead to the development of low-cost, large-area, photovoltaic devices suitable for the terrestrial conversion of solar energy.

BACKGROUND

The requirement for efficient solar cells that could be manufactured in large quantities and at low cost has compelled researchers to consider forms of semiconductors other than single crystals. The possibility of using vacuum-deposited polycrystalline silicon on foreign substrates was examined. Vacuum deposition is a well-known and accepted method for producing large-area layers of metals, dielectrics, and some semiconductors such as selenium and cadmium sulfide. Previous difficulties in the vacuum deposition of semiconducting grade silicon (and germanium) have led researchers to avoid these materials for practical applications.

Original studies had been done by APL on: (a) vacuum deposition and secondary ion mass spectrometry (SIMS) analysis leading to very pure silicon films (Ref. 1), (b) the crystallization kinetics of amorphous silicon films (Ref. 2), (c) the formation of p–n junctions and devices on fused silica substrates by standard diffusion techniques (Ref. 3), and (d) the formation of diodes with some photovoltaic response in thin samples that were deposited in amorphous form on sapphire and subsequently crystallized (Ref. 4).

DISCUSSION

In the present work, silicon was deposited on substrates maintained between 800 and 1000°C. For the most part, the substrates were sapphire in order to avoid complications of mismatched expansion coefficients and impurities introduced from the substrates. Special glass substrates were also used with results equivalent to those obtained with sapphire. The resulting films are polycrystalline with various grain sizes, depending on the substrate temperature. Films up to 33 μm were deposited. Planar p–n junction diodes were formed in the samples by a conventional integrated-circuit double-diffusion process. These diodes were evaluated as potential low-cost solar cells.

FILM PREPARATION. Silicon films were vacuum deposited from a molybdenum-lined, water-cooled, nickel crucible that was heated by means of an electron gun. The precautions necessary for maintaining sample purity have been described elsewhere (Ref. 3).

The deposition parameters are given in Table 1. The predeposition pressures were approximately 5×10^{-9} Torr.

TABLE 1
DEPOSITION AND FILM PARAMETERS

Parameter	Si 130	Si 147	Si 149	Si 155
Pressure (Torr)	1.3×10^{-6}	2×10^{-7}	7×10^{-7}	5×10^{-7}
Substrate temperature (°C)	500	650	800	980
Thickness (μm)	13.8	5.0	8.5	33.0
Deposit rate (nm/min)	490	14	23.6	91.7
Grain diameter (μm)	0.17	1.64	2.06	4.94

The films were examined by scanning electron microscopy immediately after deposition and at various stages in the subsequent processing. There appeared to be little observable change in surface grain appearance that could be attributed to processing. Grain diameters increased with an increase in substrate temperature (Table 1).

FUNCTION OF p–n JUNCTION. Doubly-diffused p–n junction diodes were formed in polycrystalline films by a 15-step, three-level, photolithographic, double-diffusion process. The procedures are based on industrial practice for single-crystal processing and were developed from previous experience with extremely thin, small-grained films on fused silica substrates (Ref. 1). Single-crystal wafers were processed along with the polycrystalline samples. All samples were processed identically to permit comparisons of film specimens.

SIMS ANALYSIS OF DIFFUSIONS. The SIMS analysis of silicon thin films included determining the impurity content and dopant profiles. Typical SIMS profiles are shown in Fig. 1 for Si 147B and Si 149B and their corresponding single-crystal monitor. Profiles such as these have demonstrated that doping levels in films may be controlled in the same manner as in single crystals. The p–n junction is located at the intersection of the phosphorus and boron profile.

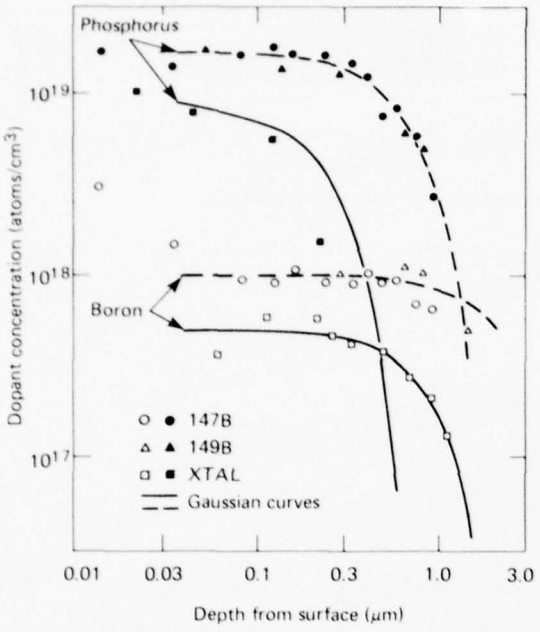

Fig. 1 SIMS dopant concentration profiles for polycrystalline films (Si 147B and Si 149B) and a single-crystal monitor. Curves represent a Gaussian fit.

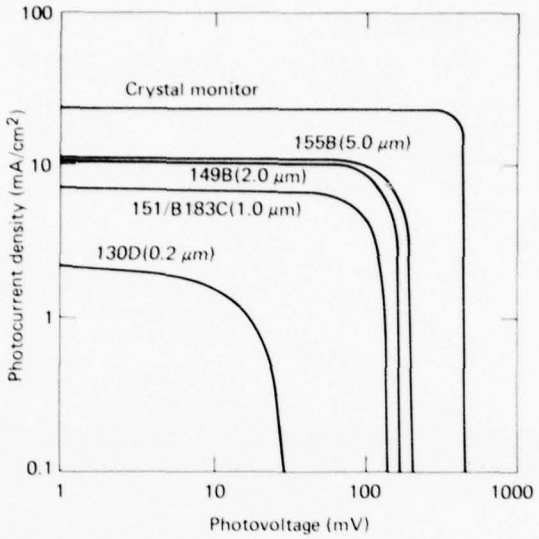

Fig. 2 Illustrated I–V characteristics for polycrystalline films with various grain diameters and a crystal monitor.

In the films, the junction was about 1.2 μm deep. In the single crystal, the junction was 0.48 μm deep. The difference is due to the different diffusion constants of the single crystal and the polycrystalline sample.

PHOTOVOLTAIC RESPONSE. Photovoltaic response *I–V* curves were obtained by illuminating the sample with a radiation flux similar to that received at ground level in the United States. As can be seen in Fig. 2, the photovoltaic response increases with an increase in grain size. Note that the curve labeled 151/B183C in Fig. 2 was obtained from a sample containing a predeposited boron layer and thus the junction was formed by bilateral diffusion. Table 2 gives the photovoltaic response parameters for the samples listed in Table 1. Here, V_{oc} is the open-circuit voltage, J_{sc} the short-circuit current density, ff the fill factor, and η the efficiency of converting the simulated solar radiation to electrical power. This efficiency does not take into account antireflection coatings or special geometries that are commonly used in solar cells. The fill factor, defined as $J_{max}V_{max}/J_{sc}V_{oc}$, is a measure of the sharpness of the bend in the curves shown in Fig. 2. The last row in Table 2 gives the response of the single crystal monitor that was processed with film sample 155B. As expected, the single crystal monitor performs better than its film companion. However, part of this difference is due to the difference in junction depths illustrated in Fig. 1.

TABLE 2
PHOTOVOLTAIC RESPONSE PARAMETERS

Sample	Radiation (mW/cm²)	V_{oc} (V)	J_{sc} (mA/cm²)	ff	η (%)
130D	68	0.029	2.1	0.29	0.03
147B	80	0.18	5.0	0.39	0.44
149B	80	0.19	11.0	0.49	1.3
155B	75	0.22	11.0	0.60	1.9
155 crystal	75	0.41	38.0	0.56	11.6

CONCLUSIONS

It has been demonstrated that high-purity, thick films with large ratios of grain size to thickness can be deposited. Photovoltaic p–n junctions can be formed in the samples by both unilateral and bilateral double diffusions. The devices show promising efficiency (1 to 2%) as solar cells, and optimization of the geometry and deposition conditions is expected to increase the efficiency considerably.

REFERENCES

1. C. Feldman and F. G. Satkiewicz, "Mass Spectra Analyses of Impurities and Ion Clusters in Amorphous and Crystalline Silicon Films," *J. Electrochem. Soc.*, **120**, 1973, p. 111.
2. N. A. Blum and C. Feldman, "The Crystallization of Amorphous Silicon Films," *J. Non-Crystalline Solids*, **11**, 1972, p. 242; N. A. Blum and C. Feldman, "The Crystallization of Amorphous Germanium Films," *J. Non-Crystalline Solids*, **22**, 1976, p. 29.
3. C. Feldman and R. Plachy, "Vacuum Deposited Silicon Devices on Fused Silica Substrates," *J. Electrochem. Soc.*, **121**, 1974, p. 685.
4. C. Feldman, F. G. Satkiewicz, and H. K. Charles, Jr., "Evaluation of Vacuum Deposited Silicon Films and Junctions for Solar Cell Applications," *Proceedings of the National Workshop on Low Cost Polycrystalline Silicon Solar Cells* (sponsored by ERDA), Dallas, TX, 18–19 May 1976, p. 267.

Authors: *C. Feldman, H. K. Charles, Jr., F. G. Satkiewicz, and N. A. Blum*

Support: *Indirectly Funded IR&D*

FULLY DEVELOPED CONVECTIVE THERMAL FIELDS

Finned heating ducts have been examined numerically using a finite-difference program. A surprising result is that not all fins improve convective heat transfer, contrary to the general impression.

BACKGROUND

Energy considerations dictate that heating ducts should be designed to extract maximum heat from a fluid flowing down the duct. Longitudinal fins had been shown empirically to increase average heat transfer (Ref. 1). Indeed, the impression one obtains from the literature is that all fins improve heat transfer; such appears not to be the case. We have developed a finite-difference program that examines any long, straight duct of general arbitrary cross section. The results indicate which fins do and do not improve heat transfer.

DISCUSSION

Fully developed laminar flow in the ducts (parallel to the walls) and fully developed thermal fields for uniform heat loss per unit length of duct are described mathematically by coupled linear partial differential equations similar to those in two-dimensional viscous flow problems (Ref. 2). Applying our modeling experience to the thermal problems, we computed steady velocity fields and temperature fields via a direct finite-difference program for arbitrary ducts (Ref. 3).

The velocity equation for steady parallel flow (Fig. 1) reduces to

$$\nabla^2 u^* = \left(\frac{\partial^2}{\partial X^2} + \frac{\partial^2}{\partial Y^2}\right) u^* = -1 , \qquad (1)$$

with the nonslip viscous boundary condition that the velocity is zero on the surface of the duct, or $u^*|_W = 0$, where W (wall) denotes the plane curve $W(x,y) = 0$, the edge of the cross section of the straight duct. The velocity $U = \mu^{-1} b^2 \, dp/dz$ has been used to normalize velocity, u: $u^* = u/U$. Here, as in Fig. 1, b is the half-height of the duct, μ the fluid viscosity, dp/dz the constant pressure gradient in the axial (z) direction, and $\mathbf{X} = \boldsymbol{x}/b$.

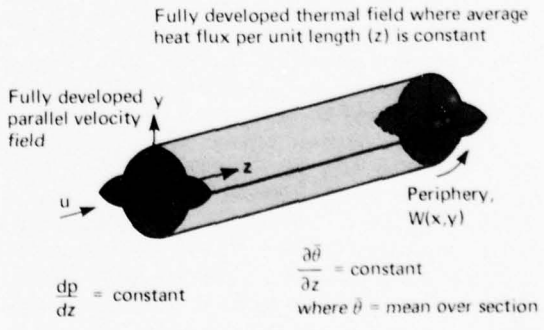

Fig. 1 Defining the duct problem for viscous incompressible fluids of constant physical properties, μ and α.

Neglecting axial heat conduction and frictional heating, the corresponding equation for the convective thermal field reduces to

$$\nabla^2 \theta^* = u^* . \qquad (2)$$

The temperature, θ, is normalized by $\theta^* = (\theta - \bar{\theta}_w)/(Ub^2\alpha^{-1}\ \partial\bar{\theta}/\partial z)$, where α is the thermal diffusivity of the fluid, and $\partial\bar{\theta}/\partial z$ is the average temperature gradient in the axial direction. One can describe a variety of temperature boundary conditions on the curve $W(x,y) = 0$ that reflect various physical situations related to heat conduction in the wall material. One of the most popular for theoretical modeling has been $\theta^*|_W = 0$ (condition a), as if the duct were lined with metal of such high heat conductivity that any peripheral temperature differences would be smoothed out immediately. We have also considered $\theta^*|_W = f(x,y) \neq 0$ (condition b) to cover other situations where temperature distributions are part of the problem.

Equations 1 and 2 are solved by a finite-difference approximation (Ref. 3). Briefly, a square grid is superimposed on the region. The usual five-point difference approximation to ∇^2 is applied to each internal mesh point not adjacent to the boundary. Near a curved boundary, a Shortley-Weller approximation (Ref. 4) is applied, and boundary mesh values are imposed. The resulting linear system of equations is solved directly using a capacitance matrix approach (Ref. 5).

The absolute accuracy of the method has been tested against a variety of duct sections for which the exact analytic solutions are known. The agreement was excellent as is shown in Table 1 where the numerical values of u^* and θ^* are compared with the exact analytic solutions. The agreement is to three or more significant figures for u^* (Ref. 6) and θ^* (Ref. 3) everywhere within the field. The examples included round and elliptical sections, indicating that the curved boundary approximation is valid. The method is competitive with finite-element and over-determined collocation methods for obtaining convective field solutions numerically.

TABLE 1

COMPARISON OF NUMERICAL AND ANALYTICAL TEMPERATURE SOLUTIONS—CENTERPLANE PROFILES (θ_c^* IS CENTRAL VALUE)

(a) Square ($a/b = 1$)†

	Absolute, θ^*		Relative, θ^*/θ_c^*	
$Y(X)$	Numerical	Analytical	Numerical	Analytical
0	−0.064990	−0.064998	1.0	1.0
0.25	−0.060413	−0.060418	0.9296	0.9296
0.5	−0.047010	−0.047011	0.7233	0.7233
0.75	−0.025976	−0.025972	0.3997	0.3996
1.0	0	0	0	0

(b) Ellipse of fineness ratio 2 ($a/b = 2$)‡
($\theta_c^* = -0.12303$, num; $\theta_c^* = -0.12293$ anal)

Y	Numerical	Analytical	X	Numerical	Analytical
0	1.0	1.0	0	1.0	1.0
0.25	0.9235	0.9235	0.5	0.9049	0.9048
0.5	0.7054	0.7055	1.0	0.6459	0.6460
0.75	0.3789	0.3790	1.5	0.3013	0.3008
1.0	0	0	2.0	0	0

† $b = 1/32$ ‡ $b = 1/16$ } finite-difference mesh size

When the temperature boundary condition a is applied to Eq. 2, the resulting thermal field tends to resemble the velocity field (Fig. 2). There are differences, since isovels and isotherms coincide exactly only when the duct is circular. In the case considered here, the peak velocity occurs at two symmetrical off-center points (x-mark); the temperature extremum is is still at the center. The surface heat conductivity (dimensional) is directly proportional to the normal temperature gradient, $\partial\theta^*/\partial N$, along $W(x,y)$. It is very close to being proportional to the velocity shear, $\partial u^*/\partial N$, along the surface. The extrema are located at the tips of the fins.

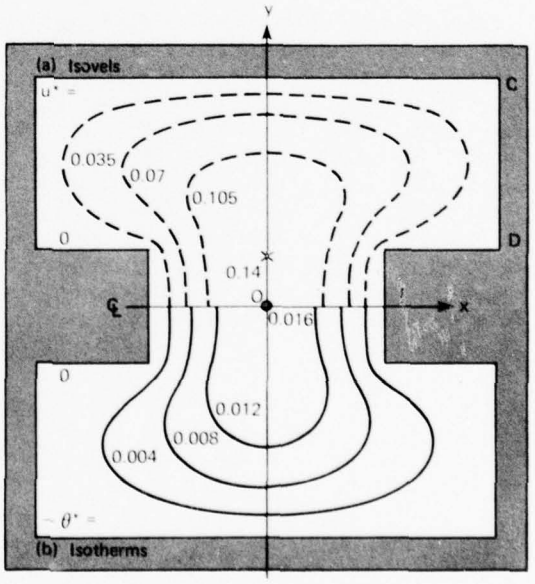

Fig. 2 Velocity and temperature contours in a finned square duct. Isovels (dashed curves; cross is at peak velocity) are in the upper half and isotherms (solid curves) in the lower half of the duct.

We have considered four different fin geometries (Fig. 3). The letter denotes the width of the fin (W is wide and M, medium) and the number is the

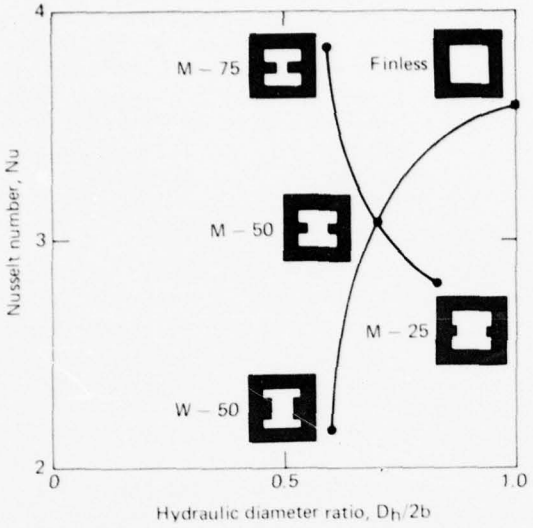

Fig. 3 Nusselt number as a function of $D_h/2b$ for finned square ducts.

percentage length of the fin. The Nusselt number (Nu) is the usual way of comparing the average heat transfer of different ducts. It is a normalized overall heat conductance based on the hydraulic diameter, D_h, for noncircular ducts. For the finned square ducts, the hydraulic diameter is always less than the actual height. (The two agree for the finless square duct.) Figure 3, a plot of Nusselt number versus hydraulic diameter ratio, $D_h/2b$, shows that only one of the four finned configurations has a greater average heat conductivity than the finless square duct. Short fat fins definitely degrade heat transfer, but long thin fins improve it.

The effect of boundary condition b does not appear very much in the literature. Yet we have found that it makes a considerable difference in surface conductivity and overall heat transfer, even for the finless convex ducts where exact analytic solutions have always been possible (Ref. 3). No longer do isovels and isotherms resemble each other. The peak surface conductivity shifts from the tips of the fins and/or midsides of finless configurations, and the bulk temperature (a mixed-mean average of $u^*\theta^*$, essentially) can even go to zero (theoretically). However, the bulk temperature occurs in the denominator of the Nusselt number and infinite values cannot occur physically. Still, the numerical modeling indicates that significant changes will occur with nonuniform peripheral temperatures or corresponding concentration distributions (Ref. 7).

REFERENCES

1. A. E. Bergles, "Survey and Evaluation of Techniques to Augment Convective Heat and Mass Transfer," *Progress in Heat and Mass Transfer*, 1, Pergamon Press, Elmsford, NY, 1969, pp. 331–411.
2. L. W. Ehrlich, "Solving the Biharmonic Equation as Coupled Finite-Difference Equations," *SIAM J. Numer. Anal.*, **8**, No. 2, 1971.
3. V. O'Brien, *Developed Convective Thermal Fields in Noncircular Ducts*, APL/JHU TG 1303, September 1976.
4. G. H. Shortley and R. Weller, "The Numerical Solution of Laplace's Equation," *J. Appl. Phys.*, **9**, 1938, pp. 334–348.
5. B. L. Buzbee, F. W. Dorr, J. A. George, and G. H. Bolub, "The Direct Solution of the Discrete Poisson Equation on Irregular Regions," *SIAM J. Numer. Anal.*, **8**, No. 4, 1971, pp. 722–736.
6. V. O'Brien, "Steady and Unsteady Flow in Noncircular Straight Ducts," *ASME J. Appl. Mech.*, **44E**, No. 1, 1977, pp. 1–6 (with Appendix by L. W. Ehrlich).
7. V. O'Brien, "Convective Field Theory to Predict Dialysis Oxygenator Efficiency," *Proceedings of 29th Annual Conference on Engineering in Medicine and Biology*, November 1976.

Authors: *V. O'Brien and L. W. Ehrlich*

Support: *NAVSEASYSCOM*

INTERNAL HEAT TRANSFER EXPERIMENTS FOR OTEC EVAPORATOR TUBES

In the APL Ocean Thermal Energy Conversion (OTEC) plant-ship concept, large-diameter (3 to 4 in.) aluminum tubes with ammonia flowing inside are being proposed for use as a low-cost multipass evaporator. Experiments measuring the internal two-phase heat transfer coefficients of ammonia flowing inside a 3-in.-diameter, 20-ft-long aluminum tube have been conducted at the APL Propulsion Research Laboratory. Prior to these tests, no data were available for large-diameter tubes at the heat fluxes that will occur during OTEC operations (1000 to 3000 Btu/h-ft²). The results provide a basis for predicting the internal heat trans-

fer characteristics needed for the design of an evaporator core unit to be tested in the next phase of the development program.

BACKGROUND

In an OTEC plant, warm surface seawater will be used in evaporators to vaporize ammonia. The ammonia will drive a power turbine and then will be condensed by heat exchange with cold seawater drawn from a depth of 2500 ft. The electric power will be used on board to produce ammonia, aluminum, or other energy-intensive products.

The plants will succeed commercially only if the overall system cost is low. A promising low-cost heat exchanger concept (Ref. 1) has arrays of large-diameter (3 to 4 in.) multipass aluminum tubes for both the evaporator and the condenser, with ammonia as the working fluid inside the tubes. Seawater is pumped to head ponds above the tube banks and flows vertically downward by gravity. The use of a large diameter tube results in a configuration that allows sufficient space in the vertical planes between the rows of tubes to permit the use of a low-cost system of water-jet cleaning heads to remove the biofouling from the outside of the tubes. The large diameter also reduces the number of joints required, thus reducing fabrication costs (Ref. 1).

The internal heat transfer experiments described herein were needed to validate correlations that have been employed in system studies—correlations that were obtained by others from experiments on smaller diameter tubes and at relatively high heat fluxes. Full details of the APL experiments are given in Ref. 2.

DISCUSSION

Figure 1 is a simplified schematic of an internal flow test loop simulating a single evaporator pass. Ammonia is transferred from a storage tank to fill the ammonia sump to an automatically controlled head. This precludes cavitation in the ammonia pump and provides a constant mass flow to the circuit. The quality of the ammonia (mass percent vapor) entering the test section is altered by varying the heat input from a horizontal, digitized steam-jacketed preheater.

The test section is wrapped with electric heating tape to provide a uniform external heat flux to the outside wall. The ammonia flows from the test section into a demister that returns the liquid to the sump. To avoid the need for a large condenser in the loop, the vapor is discarded via a pressure regulator into the facility water-cooling system and escapes from a spray basin by gradual evaporation. Liquid ammonia

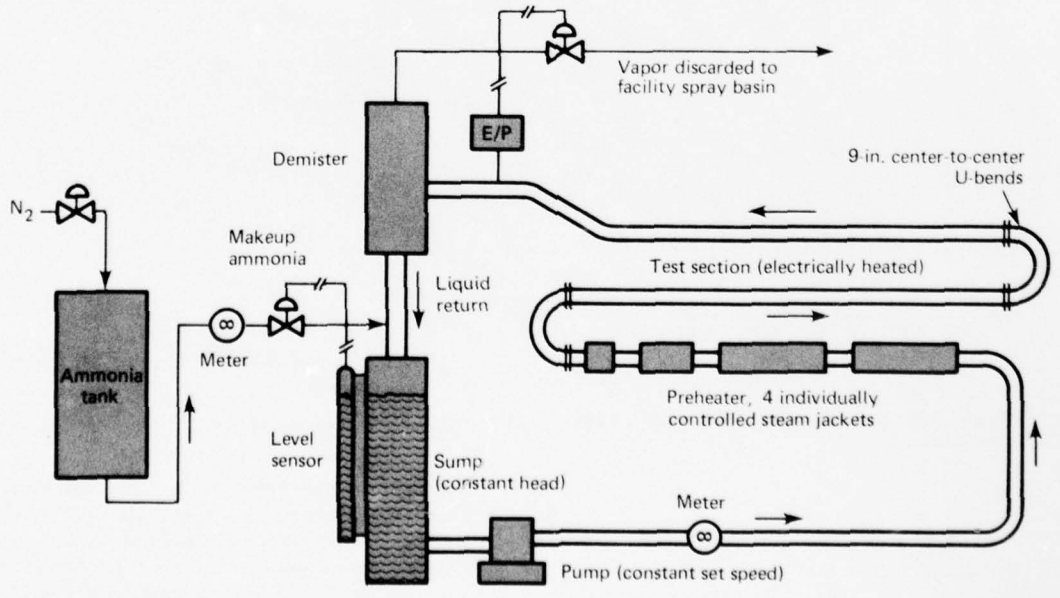

Fig. 1 Simplified diagram of an internal flow test loop.

is metered continuously to the sump to make up for the discarded vapor, and the ratio of the makeup flow to the total flow in the loop serves as the measure of quality. The test section is a tube of 6061–T aluminum alloy, 3.02 in. OD and 20 ft long, with a 0.131–in. wall thickness. Thermocouples and pressure transducers measure bulk ammonia temperatures and pressures at the inlet and the outlet. The wall temperatures of the aluminum tube are measured by thermocouples and thermopiles at four stations along the tube length.

Data were obtained at 29 test conditions for ammonia mass flow rates ranging from 1.0 to 2.8 lb/s, heat flux values from 1100 to 2300 Btu/h-ft², tube inclination angles from 0.26° downward to 2.0° upward, and mass qualities up to 20%. Run 6, which had the most complete instrumentation, covered 16 test conditions at a 2° upward tilt.

Results from the all-liquid-inlet tests of run 6 are compared with the Dittus-Boelter correlation in Fig. 2. Although heat balances indicated that very small amounts of boiling did occur in these all-liquid-inlet tests (qualities of 0.02 to 0.8% for the various points), agreement with the correlation is good.

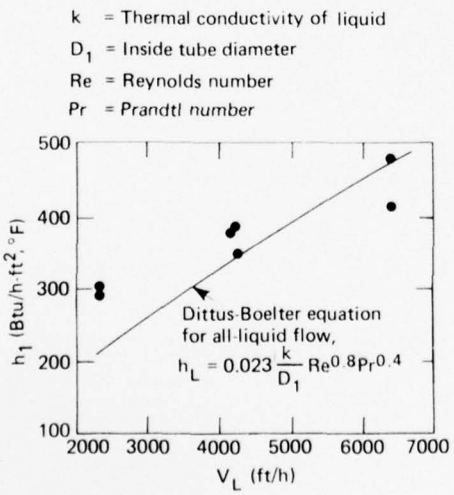

Fig. 2 Comparison of all-liquid-inlet tests and Dittus-Boelter correlation.

In Fig. 3, the overall averages of the two-phase-flow heat transfer coefficients from run 6 are compared with the following Chaddock-Brunemann correlation for two values of the boiling number chosen to bracket most of the data:

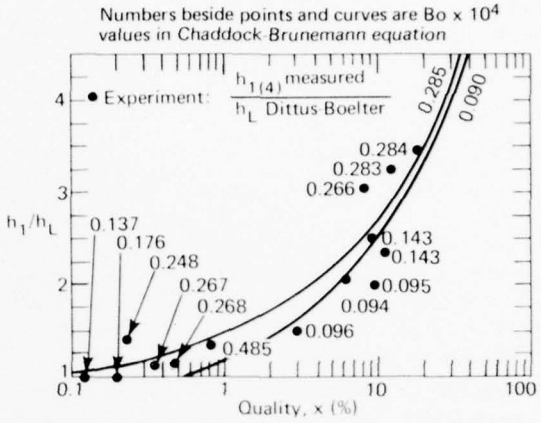

Fig. 3 Comparison of measured heat transfer coefficients and Chaddock-Brunemann correlation.

$$h_1 = 1.91\ h_L\ (Bo \times 10^4 + 1.5\ X_{tt}^{-2/3})^{0.6} \quad (1)$$

where

h_1 is the two-phase heat transfer coefficient,

h_L is computed by the Dittus-Boelter correlation (Fig. 2),

Bo is the boiling number (heat flux divided by weight flow rate multipled by latent heat), and

X_{tt} is the Martinelli parameter.

The Martinelli parameter is defined by

$$\frac{1}{X_{tt}} = \left(\frac{x}{1-x}\right)^{0.9}\left(\frac{\rho_f}{\rho_g}\right)^{0.5}\left(\frac{\mu_g}{\mu_f}\right)^{0.1} = 7.148\left(\frac{x}{1-x}\right)^{0.9} \quad (2)$$

where

x is the mass quality,

ρ_f and ρ_g are densities of liquid and gas, respectively, and

μ_f and μ_g are viscosities of liquid and gas, respectively.

The experimental points are in good agrement with these correlation curves. Therefore, it is concluded that the Dittus-Boelter and Chaddock-Brunemann correlations can be used in further analyses and design work for predicting heat transfer coefficients of ammonia flowing inside tubes of diameters up to 3 in.

REFERENCES

1. G. L. Dugger, H. L. Olsen, P. P. Pandolfini, and W. H. Avery, *Experiments on and Design of Low-Cost Aluminum Heat Exchangers for OTEC Plant Ships*, APL/JHU AEO-77-073, March 1977; also presented at the Fourth Ocean Thermal Energy Conference, 1977, New Orleans, LA, 22–24 March 1977, sponsored by the Solar Energy Division of ERDA.
2. H. L. Olsen, P. P. Pandolfini, and J. L. Rice, *Internal Heat Transfer Experiments in a Simulated OTEC Evaporator Tube*, APL/JHU AEO-76-066, November 1976.

Authors: *P. P. Pandolfini and J. L. Keirsey*

Support: *U.S. Energy Research and Development Administration, Division of Solar Energy*

COMPOSITE FLYWHEEL DEVELOPMENT

The feasibility of two Superflywheel configurations conceived at APL has been confirmed through spin tests. The flywheels are especially suitable for a wide variety of applications involving both stationary and mobile equipment. One configuration is capable of storing a great deal of energy per unit cost in typical stationary applications where weight and volume are not critical. The other configuration apparently has the ultimate capability of storing more energy per unit weight than any other known type of flywheel.

BACKGROUND

APL has been engaged continuously since 1968 in improving modern flywheel performance through the use of a wide range of new "super" materials such as fiberglass, boron, Kevlar (trade name of DuPont de Nemours Co., Wilmington, Delaware), and steel wire.

The new materials, having a strength-to-weight ratio many times that of bulk steel, theoretically are capable of being made into Superflywheels that can outperform steel flywheels. However, for optimal results these typically filamentary materials must be used in pure tension. APL has experimented with Superflywheel configurations with this objective in mind. In March 1976, the National Science Foundation awarded a grant of $189,000 for evaluation of two of the more promising concepts.

DISCUSSION

The Superflywheel configuration being evaluated for very-low-cost stationary systems is the pseudo-isotropic disk illustrated in Fig. 1 and described in detail in Ref. 1. Although the performance of this configuration is relatively poor in terms of weight,

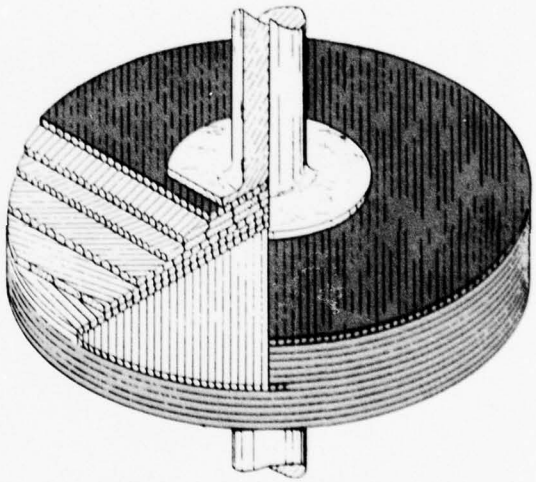

Fig. 1 The APL pseudo-isotropic rotor concept.

it is modest in terms of volume and excellent in terms of cost. The configuration consists of adjacent layers of unidirectional filamentary composite materials oriented in a prescribed manner so that the resulting disk structure can sustain equal loads in all directions—hence the term pseudo-isotropic. This type of flywheel has the demonstrated capability of storing 30 W-h per dollar when made of fiberglass/epoxy, and 40 W-h per dollar when made of ordinary plywood. The principal problem has been to find a method of attaching the hub to the rotor without impairing rotor performance. The most satisfactory is the rubber-bonded hub illustrated in Fig. 2.

For the high-performance Superflywheel, APL has proposed a bare filament rotor (Fig. 3). In theory,

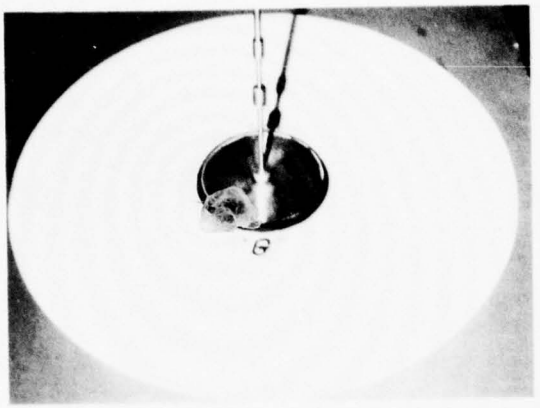

Fig. 2 Pseudo-isotropic disk with Lord-bonded flexible hub attached.

Fig. 3 Balancing the wound rotor.

this configuration offers the highest possible energy-to-weight ratio of any known flywheel, since as much as 95% of its total weight is comprised of high strength-to-weight materials utilized in pure tension. Typical composite flywheels are comprised of 30 to 50% resin, which contributes little to strength but adds proportionately to weight, thus reducing the energy storage capability by a corresponding amount.

A major problem in both programs has been the development of a suitable rotor suspension system that would permit repeated excursions through a wide range of rotational speeds encompassing the various critical speeds of the rotor system. A soft, resilient rotor suspension system with a conventional elastomer shock and vibration isolation unit (Fig. 3) has given consistently satisfactory results.

The bare filament rotor has demonstrated the principal program objective of storing more than 30 W-h/lb. Further tests are expected to yield a definition of the usable energy density level of this configuration in terms of the usable strength of the material. This value for a bare filament Superflywheel made of Kevlar is about 80 W-h/lb, compared to 3 to 14 W-h/lb for a steel flywheel.

REFERENCE

1. G. L. Dugger et al., *Heat Engine/Mechanical Energy Storage Hybrid Propulsion Systems for Vehicles—Final Report*, APL/JHU CP 011, March 1972.

Author: *D. W. Rabenhorst*

Support: *NSF Grant AER–75–20607*

APPLICATION OF ENERGY CONSERVATION IN BUILDING 8

In the fall of 1975, APL completed and occupied a new office facility (Building 8) comprising 83 000 gross square feet. This four-story building (Fig. 1) does not contain a conventional heating system of any type. It uses no fossil fuel, no solar heat, and has an electrical resistance heating system only for backup use in case of failure of the system described below.

BACKGROUND

During a building planning session in the spring of 1974, the architect, his mechanical consultant, and the author were discussing APL's desire to use double-glazed windows and superior insulation in the planned

Fig. 1 Building 8.

Building 8 to help conserve energy. The mechanical consultant indicated that if this approach were used, there might be enough surplus heat from lights and people during the building's occupied period to make up for heat losses during the night when the lights are out and when heating and cooling systems are inoperative. Because of the energy crisis, all APL heating and cooling systems were already being shut down during nights and weekends. Further discussions led to an agreement to explore the possibility of eliminating a conventional heating plant. A heat-balance analysis indicated that the concept was valid even in the coldest weather. The system that was subsequently designed and installed has been operating continuously ever since, with excellent results.

DISCUSSION

During the building's occupied cycle, the heat output from the fluorescent lighting (approximately 3 W/ft^2) was more than enough to heat the building. Instead of additional cold air being introduced when a building overheats as is done with conventional systems (usually called a free cooling or economizer cycle), fresh air is held to the minimum ventilation requirements, and the conventional air-conditioning system is operated to keep the building from overheating. The condenser water from the refrigeration machines is circulated through underground storage tanks (approximately 25 000 gallons capacity) until its temperature reaches 95°F. If the building continues to overheat, the system enters the conventional economizer cycle mode and more fresh air is introduced for cooling. At the end of the work day, all systems are turned off and the building temperature drops during the night.

Early the next morning, exactly when depending on how cold it has been, the system comes back on with the ventilation off until the people arrive. In this mode, called the warm-up cycle, the refrigeration is in reverse operation and is chilling the water in the storage tanks. The heat removed from the tank water is added to heat generated by the compressor and leaves the condenser in the form of 105°F water that is circulated through oversized heating coils in the air duct system. The heat lost during the night therefore is replaced by that saved during the previous day. Later, when the building begins to overheat, the heat storage cycle comes on and the sequence is repeated.

The system works. The cost of Building 8 was virtually unchanged by the installation of this system since the additional cost of the energy system was offset by the omission of boilers, a chimney, and fuel tanks. During the reporting period, electrical energy consumption per unit area in Building 8 was approximately 45% lower than in the rest of the APL buildings. This saving is in addition to the complete elimination of fossil fuel for heating.

A bonus to energy savings was realized when unanticipated computers were installed after the building was completed. The heat from the computer air-conditioning condenser water is also stored in the tanks. This extra heat shortens the time that the heat storage cycle must be run and thus saves electrical transfer energy. When the computers are run at night and the storage tanks are heated to 95°F, the heating system is cycled to keep the building from cooling as much as it otherwise would, thus shortening the morning warm-up cycle. The oversized water-to-air heating coils make it possible to use the computer heat output. If another system were to be built in the future, the coils would be made even larger in order to further shorten the time it takes to warm the building in the morning, thus saving additional electrical transfer energy.

The arrangement of the automatic valves, dampers, and piping in Building 8 that circulate the water and air in different modes for the six cycles is considered to be too complex to be maintained by average commercial office building operating engineers without special training. The reason for this is that the reverse-cycle winter feature, together with the normal summer mode of operation, results in an extremely complex system of piping and automatic control mechanisms. There is a warm-up cycle, a heat-recovery cycle, an economizer cycle with refrigeration off, an economizer cycle with refrigeration on, a minimum-ventilation summer cooling cycle, and an add-on night cycle for saving surplus computer heat. However, this difficulty can probably be overcome in future applications through engineering simplifications and the increased use of automation.

Author: *A. C. Stucki*

Support: *The Johns Hopkins University*

COMPUTER TECHNOLOGY APPLICATIONS

INTRODUCTION

The use of computers at APL began in 1948 with the acquisition of a Reeves Instrument Company REAC (Reeves Electronic Analog Computer). Subsequently, APL pioneered in the application of analog computers for both simulation of guided missile systems and as components in missile guidance and fire control subsytems.

In 1956, APL entered the field of digital computing with the acquisition of an IBM 650 computer. The need for a general-purpose digital computation center was soon recognized, and by 1957 a UNIVAC 1103A digital computer was acquired. This computer was sequentially replaced by the more powerful IBM 7090, the IBM 7094, and the IBM 360/91. Recently an IBM 370/158 has been added to work in concert with the 360/91. The main memory for this combination currently totals 7 million bytes and is supplemented by auxiliary on-line storage of 8.2 billion bytes.

The large general-purpose computer has been the only type of computer that can handle a load encompassing a wide variety of tasks of an unpredictable nature, especially tasks requiring large amounts of memory, but there is an increasing demand for small "minicomputers" to meet long-term specialized needs, in which portability, a guaranteed time response, simplicity of management, or the ability to embed in other equipment is paramount.

In the 1970's, a further trend developed as a result of the cost and size breakthrough of microcomputers. The radical price-to-performance reductions achieved by the microcomputers, along with substantial reductions of the same nature for certain types of peripheral devices, has demonstrated that a mix of maxi-, mini-, and microcomputers is the most cost-effective way to provide support to the Laboratory. Any type of computational problem can now be matched to the computer more efficiently than in the past when only large control computers were available. Articles in this section describe two such new facilities.

Despite the rapid development of powerful digital computers, analog computers have continued as essential support tools. Their value has been greatly enhanced by integration with digital computers, thus providing "hybrid" computing systems. A key advantage of hybrid systems is the capability to simulate accurately, and relatively inexpensively, very large physical systems composed of both discrete and continuous processes. As a result, APL now operates two hybrid computer laboratories, and stand-alone analog computers have been essentially replaced.

A great advantage that analog computers have had over digital computers is the easy paralleling of the analog components and their much greater speeds. The possibility now of fully integrating linear circuits with digital, and paralleling digital with digital and digital with linear, opens the door to computer systems much more powerful in computation speed compared to the present capabilities of digital and hybrid. These systems may be easily and inexpensively configured in such a wide variety of forms that, not only will the differentiation among various forms of digital computers blur, but the differentiation among analog, hybrid, and digital will essentially disappear.

The papers in this section are a limited selection of computer-related accomplishments. Several other projects, however, require mention: the use of a microcomputer to collect and format data and automate the associated tape recorder for virtually unattended shipboard operation; a microcomputer space probe experiment checkout unit; a microcomputer-based satellite under an altimeter data analyzer and telemetry command system; a modularized general-purpose microcomputer system to standarize a wide variety of instrumentation for field use; a microcomputer as an on-line diagnostic tool for a navigation system; a data conversion microcomputer for a scientific surveillance aircraft; and a group of 12 microcomputers controlled by a microcomputer to provide a realistic hardware configuration for the SATRAC data collection system.

A SOFTWARE DEVELOPMENT AND R&D FACILITY FOR MINI- AND MICROCOMPUTERS

A Computer-Aided Programming (CAP) facility has been developed at APL to aid the development of software for a variety of mini- and microcomputers and to construct or evaluate advanced software development tools. The facility supports these functions in three different modes of operation. Hosted tools reside at the facility, remote tools may be accessed via the facility, and mini- and microcomputers with self-hosted tools may use the components of the facility as their own sophisticated set of peripherals.

Advanced tools have been developed to access remote time-sharing hosts, to provide graphic representations, to assist in editing textual data, and to provide a common application-oriented software debugging capability for different computers. Users access the facility through work stations comprising high-speed graphics terminals, hard-copy devices, and dual-drive floppy disk systems. The facility aids in traditional software development and in the research and development of new tools.

BACKGROUND

The proliferation of mini- and microcomputers at APL has aroused interest in having a common facility to support the development of software for many types of computers. In addition, APL is assisting DoD in the construction and evaluation of new software development tools. The CAP facility at APL (Refs. 1 and 2) provides a flexible means to support the development of many target mini- and microcomputers and to construct and evaluate advanced software development tools.

DISCUSSION

An essential part of the concept is the provision for access to support items that are not physically located at the CAP facility. Figure 1 is an overview of the facility. The support items (called tools) are depicted as either hosted in the facility, self-hosted on the target computer, or hosted in a different facility. The result is that the facility acts as a common interface for the user. He sees a multitude of possible ways to accomplish his development. In some cases, the facility acts as the peripherals that may not exist on his own computer. In other cases, he can reduce the load on his own computer or reduce the cost of using a sophisticated large-batch or time-sharing system. He accesses the common interface through a work station that contains a high-speed graphics terminal, an associated hard-copy device, and a dual-drive floppy disk system. Thus, he can record a terminal work session and also has a very convenient portable medium for data storage. He can therefore view the facility as a means of having one common way of developing software for several computers, with immediately available local support.

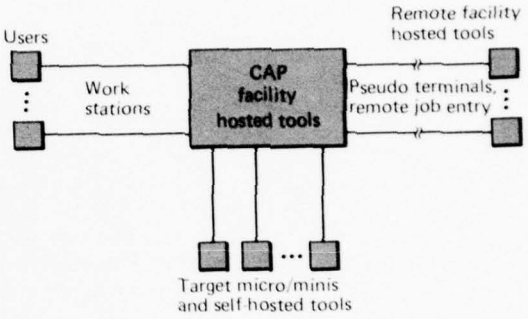

Fig. 1 Overview of the CAP facility.

The support of software development encompasses the more-or-less traditional areas of computer programming but may in some cases be accomplished in a nontraditional manner. The facility provides for multiuser editing and storage of program sources, listings, and object code (as is inherent in most multiuser operating systems). This capability is currently being used to replace tedious, time-consuming keypunch and card-to-tape functions that are inherent in many minimally configured target computers.

Software has been developed in the CAP facility to exchange data sets between the various military computers at APL. Since many military computers have a minimum of peripheral devices, software development may be enhanced by granting the users the more extensive resources of the facility, such as disk storage, magnetic-tape and line printer devices, cross-assemblers, and cross-compilers.

To aid in editing and storing text (e.g., source code), an IBM Selectric magnetic card typewriter is linked to the facility. Software developed at the CAP facility can transfer data sets between the magnetic cards and any peripheral at the facility, thus providing all the power of sophisticated editors and high-speed graphics terminals.

The capability to assemble or compile the target computer's source code is provided by any of the three hosting mechanisms (Fig. 1). When the assembler or compiler operates only in a self-hosted configuration, the CAP facility acts as the peripherals. In many applications, this approach is less costly and less time-consuming than purchasing the necessary peripherals. When a cross-assembler or cross-compiler already exists at another facility, the CAP facility can act as a submittal station (remote facility hosting). If preferred, the cross-assembler or cross-compiler can be installed or developed in the CAP facility. Cross-assemblers have been implemented this way for the Intel 8080 and the Motorola 6800 microprocessors.

Frequently the need arises to develop an advanced tool, or an advanced tool must be evaluated. These nontraditional tools must be distinguished from the traditional tools mentioned previously.

A graphics editor that can be used easily by scientists, engineers, and secretaries allows text editing in context. Instead of constructing commands that search for an existing character string and change it to a new string, the user points with a crosshair cursor and types the correction. This can be done while the complete text is displayed on the face of a CRT, as shown in Fig. 2.

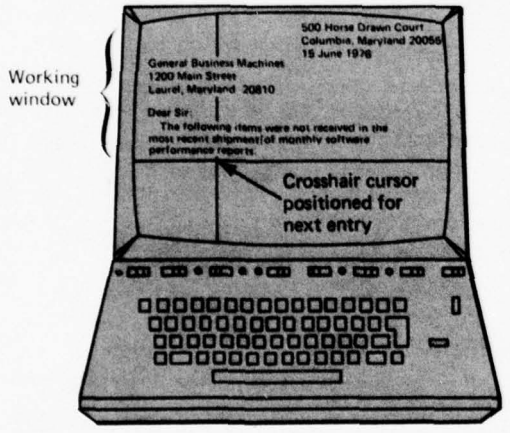

Fig. 2 Graphics editing on CRT.

Another graphics package allows pictorial representations to be created at a CRT and maintained in the facility. Again, crosshairs are used to locate specific positions, and special control commands are used for the generation of a wide variety of graphic constructs, such as rectangles and circles, at any particular location on the CRT. The graphic constructs can be annotated with independently positioned textual descriptions to complete the presentation.

To assist in the evaluation of existing tools, a software communications package has been developed that allows the CAP facility to act as a terminal to remote computer time-sharing systems, including the APL central computer facility. This software tool has considerable potential as it not only allows users to access software tools on remote computers but also provides access to all the peripherals at the CAP facility.

APL acts to some degree as an evaluation center for new software development tools on remote computers. The communications package has interacted with many different computers including those on the DARPA network. It allows the user to transmit files from any CAP peripheral to a remote computer as far away as Hawaii or England as if he were typing the information in manually, but of course at a much higher transmission rate.

A technique also in the area of advanced tools allows one debugging aid to support different types of target computers in their application environments. The standard tool for the CAP facility computers was modified to perform such functions as inspecting and changing the core memory, setting break points, and executing single instructions in a target computer (e.g., NOVA 1200) via a communications interface. Thus, the tool itself runs on the CAP facility and communicates with a small interface program in the target computer.

The CAP facility (Fig. 3) consists of two minicomputer-based systems: the Basic Support System and the Research and Development System. The Basic Support System is used to execute the tools previously described, whereas the Research and Development System is used to develop new tools that enhance the capabilities of the Basic Support System. Thus, existing tools can be run on the Basic Support System while complex advanced peripherals and tools are being installed, on a noninterfering basis, on the Research and Development System. This approach has been found to be necessary since, during development, many of the advanced tools require operation in a priority state that would otherwise interfere with the support function.

The principal components of the Basic Support System are a Digital Equipment Corporation (DEC) PDP-11/45 minicomputer with 80 000 16-bit words of core memory, a 44-million 16-bit word removable disk drive, and a broad range of peripheral devices including a high-speed line printer, seven- and nine-track magnetic tape drives, card and paper-tape readers, and four work stations.

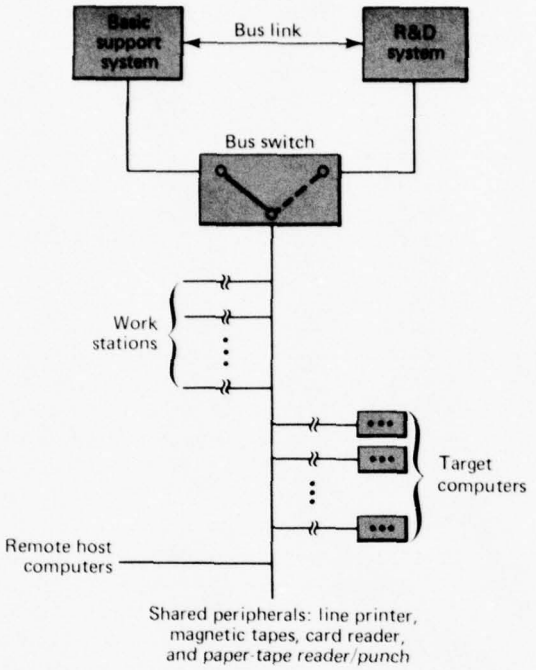

Fig. 3 Configuration of CAP facility.

A work station consists of a Tektronix 4014 Graphic Display Terminal, generally operational at 9600 bits per second, a hard-copy device that makes facsimile copies of the Tektronix screen, and a dual-drive floppy disk system. The use of floppy disks instead of more typical on-line disks is important because the user retains (as with cards) physical control of his source data. In addition, synchronous and asynchronous interfaces and modems are available for dial-up access to the facility.

The Research and Development System consists of a DEC PDP–11/40 minicomputer with 64 000 16–bit words of core memory and two 1.25–million 16–bit-word removable disk drives. The system is connected to the Basic Support System through a DEC Unibus link. This linkage and a Unibus link-handler software package allow the Research and Development System to access the Basic Support System and its peripherals, thus creating a shared peripheral environment. A bus switch provides convenient backup switching of Basic Support System peripherals to the Research and Development System in the event of a problem with the latter.

A multiprogramming real-time operating system (RSX–11D) executes asynchronously on both the Basic Support System and the Research and Development System. Both operating systems contain such capabilities as reentrant system programs and libraries and line-printer spooling, which help create a multiuser environment. A bus link handler, developed at the CAP facility, has been implemented on both systems so that they can access the shared peripherals (Ref. 3). The software executes as a normal input/output handler under the operating systems. Not only are all peripherals available to both systems, but a new tool is easily transferred to the Basic Support System by simply rebuilding it to the core resident system routines.

A CAP facility librarian plays an active and integral role by providing software development assistance to users of the facility and by ensuring its proper operation. Typical librarian functions include orienting new users to the facility, assisting in initiation of actual software development, and helping to maintain hardware, software, and documentation.

Some additional software components not developed at the facility include a sophisticated Tektronix graphics package, a FORTRAN preprocessor that allows programs to be written using structured programming constructs, and an RJE 2780 emulator package that provides access to the IBM 360/91 batch-processing system. Extensive word processing software is also available. A powerful editor, TECO, was adapted from the PDP–10 computer, and RUNOFF is a program to facilitate the preparation of typed or printed manuscripts such as memos and manuals.

An LSI–11 microprocessor is in use at the CAP facility. Experiments are being performed to evaluate the possibility of off-loading some of the larger or more time-consuming tasks, such as graphics translation and remote host communication, onto the LSI–11. This microprocessor is also treated as a target computer for the purpose of software development.

REFERENCES

1. W. J. Sederowitz, *The Computer-Aided Programming Facility*, APH/JHU FS–76–126, June 1976.
2. T. P. Sleight and W. J. Sederowitz, "A Software Development and R&D Facility for Mini- and Microcomputers," *Thirteenth IEEE Computer Society International Conference*, Fall 1976, pp. 290–294.
3. C. S. Potter, "A Method for Implementation of Transparent Sharing of Peripherals by Two Processors," *IEEE Symposium on Trends and Applications, 1976: Micro and Mini Systems*, pp. 43–45.

Author: *W. J. Sederowitz*

Support: *NAVSEASYSCOM*

IN-HOUSE FACILITIES IN SUPPORT OF MICROPROCESSOR-BASED SYSTEM DEVELOPMENT

Many hardware designers have been reluctant to use microprocessors in their systems because of the high cost of the hardware and software required for efficient system development. As a result, a program was undertaken by APL's F. T. McClure Computing Center to provide in-house facilities that enable designers to develop microprocessor-based systems effectively without a large initial expenditure. They also have complete freedom to choose the most suitable microprocessor for each application.

BACKGROUND

Major changes have taken place in hardware system design due to the advent of microprocessors. Figure 1 shows the principal stages of development of a microprocessor-based system. In the partitioning phase, the designer makes tradeoffs to determine which functions will be performed in hardware and which in software. The hardware and software designs then proceed in parallel. At some point, the hardware and software subsystems must be integrated into a working unit.

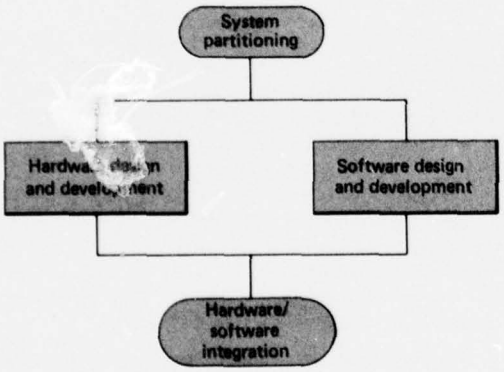

Fig. 1 Major phases of microprocessor-based system development. Note that the software development should not depend on the hardware being operational.

As a result of these changes, the design, development, and testing of microprocessor-based systems require tools different from those traditionally used to develop hardwired systems. In particular, efficient software development requires the use of assemblers to translate programs into machine language, simulators to help uncover logical errors and to expedite software development before the hardware is operating, and an efficient means of loading programs into microprocessor memory and of programming programmable read-only memories (PROM's).

To get such design aids, the designer typically had to purchase a so-called "development system" from the microprocessor manufacturers. In addition to their high initial cost, most development systems have the disadvantage that they can be used only with the microprocessors of a limited number of manufacturers. Furthermore, the requirement that the equipment be in close proximity to the system under development limits the use of a development system to one user at a time. These problems often made it difficult to justify the purchase of a development system. As a result, many designers were reluctant to use microprocessors in their systems or resorted to time-consuming and error-prone hand coding and debugging techniques.

DISCUSSION

The present effort was undertaken to provide the APL staff with the tools necessary to develop software efficiently for all of the more common microprocessors. Figure 2 is an overview of the microprocessor development facilities implemented at the Computing Center.

CROSS-ASSEMBLER PACKAGE. One of the first and most important tools required for efficient software development is an assembler. It is a computer program that translates software for a particular processor from a form that is easier for people to write and to understand (assembly language) to the form that the processor can execute (machine language). A microprocessor "cross-assembler" is an assembler that is run on a larger computer system, such as a minicomputer or a large time-sharing system, rather than on the microprocessor itself.

The first component of our in-house development facilities is a cross-assembler package that runs under the APLSV timesharing system of the Computing Center. The package consists of a set of cross-assemblers for a number of popular microprocessors, as shown in Table 1. The assemblers have a common

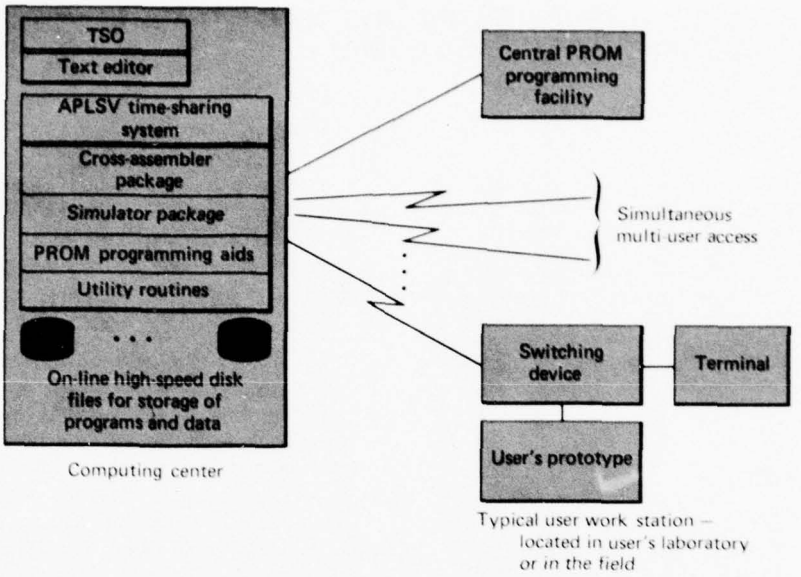

Fig. 2. Overview of in-house microprocessor development facilities of the F. T. McClure Computing Center.

framework, with a few processor-specific tables and subroutines to tailor the basic assembler to each of the supported microprocessors. With this approach, we can add an assembler for a new microprocessor in a very short time, generally less than one man-week. Therefore, we do not restrict designers in their choice of microprocessors. Also, the uniform assembler syntax and commands mean a shortened learning time associated with different microprocessors.

TABLE I
MICROPROCESSORS CURRENTLY SUPPORTED BY THE APL CROSS-ASSEMBLER PACKAGE

Microprocessor	Manufacturers
6800	Motorola, AMI
8080	Intel, Texas Instruments
6502	MOS Technology
9900 (16 bit)	Texas Instruments
F8	Fairchild, Mostek
IM6100	Intersil
PACE (16 bit)	National Semiconductor

The interactive nature of the APLSV system enables the user to get his results almost immediately at the terminal without the turnaround time normally associated with large "batch" computer systems. A file system on high-speed disk storage allows permanent storage of source (assembly language) and object (machine language) programs. Virtually unlimited space is available for program storage. A powerful editor facilitates the creation and editing of source programs.

Simulator Package. The second major part of the facility is a simulator package that currently includes support for the two most popular microprocessors, the 8080 and the 6800. Processor operation is simulated at the instruction cycle level. External input/output devices can be simulated to any desired degree of detail using the powerful APL (*A Programming Language*) language. The simulators allow designers to develop, test, and check programs before the hardware is operating. Accurate program timings are generated to aid the designer in making the necessary hardware/software tradeoffs early.

The simulators are a valuable aid for understanding the internal operation of a microprocessor. The state of all registers and condition flags can be traced dynamically as the simulation proceeds. This can be especially helpful to engineers who are unfamiliar with software concepts. The simulators can also be used as a software "breadboarding" facility. Instruction sequences and subroutines can be tested very quickly and easily before they are integrated into the final software subsystem. Checking out software algorithms is simple and straightforward using the extensive trace and breakpoint facilities.

COMMUNICATION WITH THE CENTRAL FACILITIES. A microprocessor program must eventually reside in the microprocessor memory before it can be tested in the actual system environment. During early development and checkout, programs are often loaded into random access read-write memory (RAM) for testing. Data are usually entered manually with a keypad or front panel, which is very tedious and time-consuming, or via paper tape, which is cumbersome at best. When a system is somewhat stable, the programs are normally stored in PROM by means of a device called a PROM programmer. Again, data are usually entered by a means of a keypad or a paper-tape reader.

To simplify the transfer of programs to RAM or to a PROM programmer, a simple communicating line switching technique was devised. Program loading and PROM programming are performed directly from the time-sharing system. Thus, the designer can compose and assemble his programs with the cross-assembler package and then immediately load the microprocessor RAM or program a PROM by merely entering the appropriate commands at his terminal and flipping a switch. The only hardware requirements are a simple switchbox and a standard RS–232 serial interface in the microprocessor system or PROM programmer. A software loader/monitor for the microprocessor can be written easily or can be obtained in ROM from most microprocessor manufacturers. The Computing Center supplies the necessary software in the central time-sharing system.

This technique has been used successfully with microcomputer kits, several types of PROM programmers, vendor development systems, and various user prototypes. The initial cost is quite small, and no maintenance is required since the switchbox is passive. The technique can be used in the laboratory with hardwired communication lines or in the field with an acoustic coupler or modem to connect to the central system over a telephone line. Those who are not using the cross-assemblers may still use this technique to store and retrieve programs and data in central disk files. This can eliminate the need to purchase slow or expensive peripherals such as paper-tape units and floppy disk systems for program storage.

USER CONSULTATION. One of the most important aspects of the in-house facilities is the availability of individual consultation at no cost. A user can be taken, step by step, all the way through the development process. We encourage designers to request support for new microprocessors when the need arises or to suggest improvements in the existing facilities. Close interaction with a user leads to quick resolution of problems that do arise. Thus, he can quickly learn to use the in-house facilities most effectively for his particular application and environment.

Author: *A. W. Currano*

Support: *NAVSEASYSCOM*

A GRAPHICAL INTERACTIVE COMPUTER ROOM PLANNER

The Computer Layout Installation Planner (CLIP) is an interactive graphics program for arranging a computer machine room (Fig. 1). Written in PL/I language for the Tektronix 4015 Storage Tube Graphics Terminal, it allows up to 99 component units to be maneuvered into position by typing in commands and indicating positions with a crosshair cursor. Each unit has a label, a cable port opening marker, and a symbol to indicate its front side. The final layout is plotted on a CalComp 925/1036 30–in.-wide plotter, using preruled grid paper (one square per floor tile) to serve as a placement chart for the installers.

BACKGROUND

A typical commercial computer consists of many components linked together by a network of cables. The exact placement of each component is determined by many constraints, some of the more obvious being maximum cable lengths, operator traffic clearance, access space for maintenance, wall clearance, doorway entrance space, and areas for future expansion. Power and air-conditioning requirements are

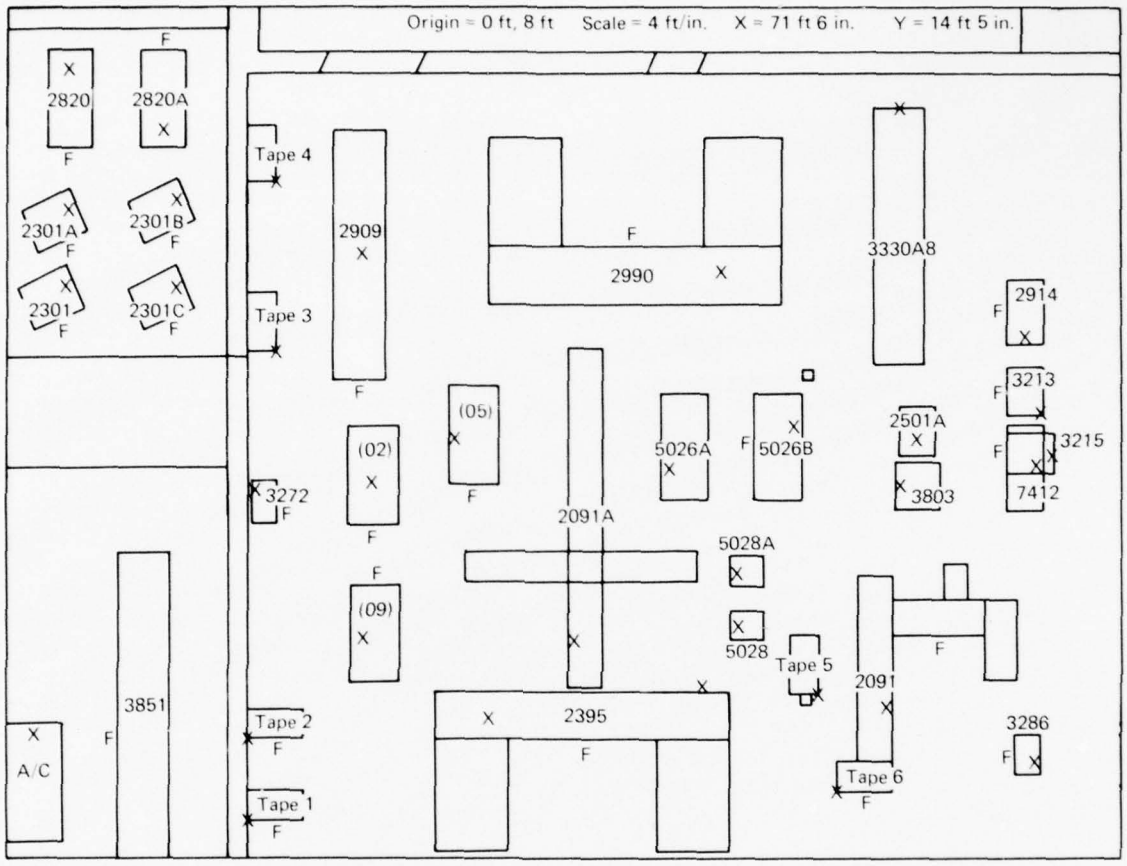

Fig. 1 The APL F. T. McClure Computing Center machine room.

easily calculated once for a proposed configuration, but the placement of the computer components is iterative in nature. Many plans are usually considered before an acceptable one is agreed upon. A mistake in planning the computer layout can prove very costly to correct after the installation has been completed.

The planning process is usually approached by placing plastic templates of the machine units upon a piece of grid paper. This technique leaves much to be desired: the templates can be inadvertently moved out of place, the diagonal distances between units must be measured with a ruler, and the onerous task of recording the final placement on paper must be done manually. (Any changes made after this step are a nuisance at best.) Dissatisfaction with the old method provided the motivation for writing the CLIP program. Since the planning process is essentially two-dimensional and requires a good deal of list-keeping, it was an obvious candidate for implementation on an interactive computer graphics terminal.

DISCUSSION

DATA MANAGEMENT COMMANDS. An on-line data set is used to store a particular layout. It can be modified by means of the Time Sharing Option (TSO) Editor if further processing is required.

"FETCH" fetches a layout stored on a disk. "STORE" stores the current layout on a disk.

LAYOUT MANIPULATIVE COMMANDS. The function used most often is the command to shift a unit from one position to another. The target location is indicated by moving crosshair cursors on a cathode ray tube (CRT) display. An alternative technique would be to type in the exact coordinates, if known, but this would deny the freedom of a purely graphical operation. The other obvious maneuvering function is that of rotating a unit. The angle of rotation is arbitrarily fixed at +90°, since most machine rooms have a rectangular aspect and all units are parallel to the walls.

"UNIT" allows a current unit to be selected. "MOVE" repositions the current unit. "ROTATE" pivots the current unit by 90°. "END" halts the program and returns control to TSO.

UNIT INFORMATION COMMANDS. Each unit is represented as a rectangle or a cluster of rectangles identified by a manufacturer's number. Other markings include an X to indicate the cable port at the bottom of the unit (needed for cable distance calculations), and an F to indicate the front side of the unit. The X,Y coordinates of a unit are displayed in feet and inches from the origin.

Most units have hinged doors or extending panels called gates for service access. This clearance area can be displayed optionally to indicate obstructions. To avoid excessive display demands, the spaces are shown as rectangles instead of curved arcs because of the number of line segments involved. It has been proven adequate to simply indicate which sides of the units have doors and where the maximum point of swing falls. (*Fig. 2*).

A major concern for computer installers is the length of cable runs between units. The maximum wiring distance is often determined by the electrical characteristics of the signals on the lines. The longer the lines, the greater the risk of transmission error. The cables are precut into standard lengths and priced accordingly, so it is most economical to use short cables. The CLIP program will find the point-to-point distances between cable ports of two or more units.

"DOORS" indicates the door clearance around each unit. "CABLES" gives the cable length between two or more units.

GRAPHICAL INTERACTION COMMANDS. One of the primary benefits of interactive computer graphics is

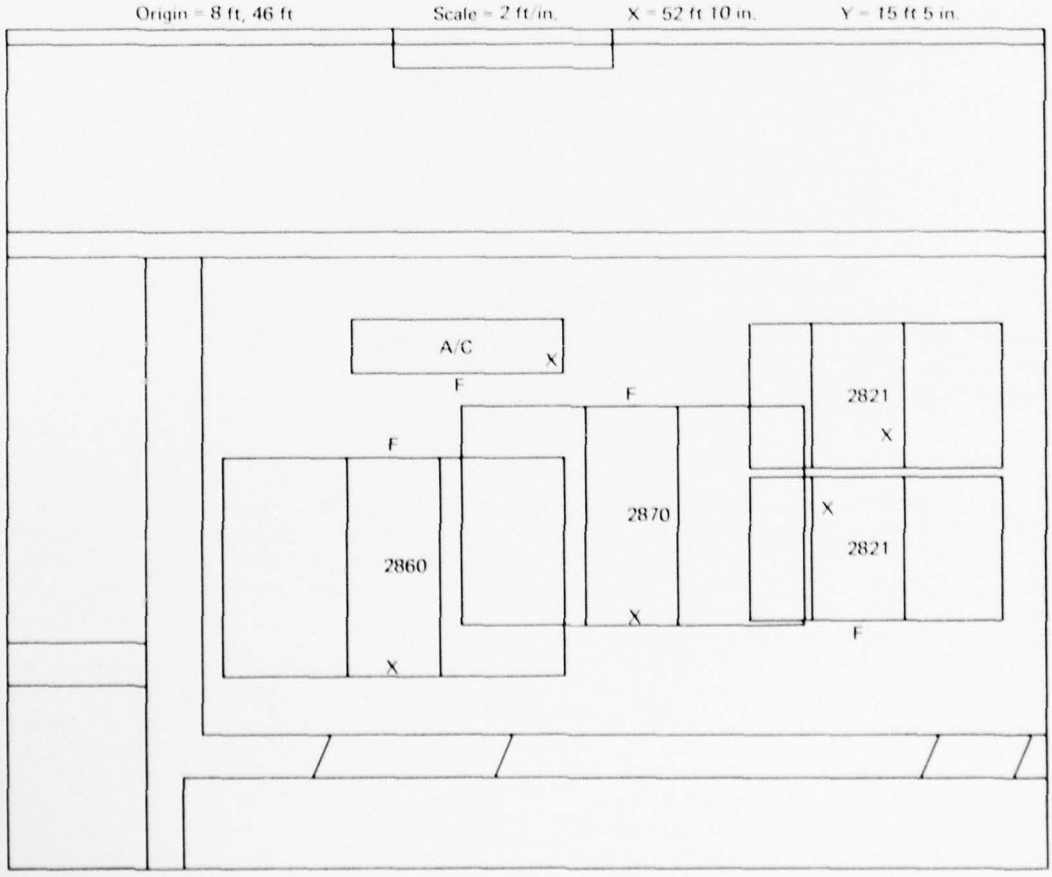

Fig. 2 Viewport showing door clearances.

the ability to change quickly the scale or area of the data being displayed. This gives complete freedom in choosing a viewing port.

A choice of 10 different scales is available for the 1-in. grid pattern on the CRT. The current scale is displayed in feet per inch. At 2 ft/in., each grid line represents one square tile of raised flooring. This is the same size used to generate the preruled plot paper that serves as a guide for the installers.

"SCALE" selects the current scale. "GRID" turns the 1-in. grid on or off. "BIG" resets the scale to 10, the viewpoint origin to 0,0. "WALLS" causes the wall outline to appear or disappear. "ORIGIN" shifts the viewpoint origin.

DATA STORAGE. The data base for the computer units is a 99 by 22 array of 16-bit words. The wall outline is stored in a separate array at the time of compilation, since these data rarely need to be changed. If a new room is being considered, the program is recompiled with a new set of coordinates. The storage requirements are 20 000 bytes of core memory and approximately 1100 words of disk space.

CONCLUSION

The CLIP program has proven to be extremely useful, not only for designing an original layout but also for modifying an existing layout. It was run for almost two years at APL on an IBM 1130/2250 Model IV computer and has subsequently been rewritten for the Tektronix 4015. In that time, the configuration of the main computer (an IBM 360/91) has been steadily upgraded. On several occasions when new equipment was to be installed in phases, a series of plots was generated to indicate the situation clearly and precisely at each stage. The installation proceeded smoothly, and no errors were encountered.

Author: *S. E. Anderson*

Support: *NAVSEASYSCOM*

REPLACEMENT PROGRAM STORAGE ASSEMBLY FOR THE AN/AYN–1 AIRBORNE NAVIGATION COMPUTER

APL has successfully completed the design and development of a new program storage assembly for the AN/AYN–1 airborne navigation computer. One hundred and ten of the assemblies are being fabricated for the U.S. Coast Guard with the expectation that their introduction into the AYN–1 computer systems will substantially reduce maintenance costs.

BACKGROUND

During the past decade, the Coast Guard has equipped many of its helicopters and fixed-wing aircraft with the AYN-1 airborne navigation computer. This computer operates under the control of a program comprising 143 360 bits of information formatted as an array of 4096 35-bit words. In the original version of the computer, the program is stored in a core-rope, read-only memory (ROM) assembly enclosed in a metallic housing (Fig. 1). The housing, about 5 in. square and 6 in. high, plugs into a base plate for connection to other parts of the computer.

The circuitry of the core-rope memory is mounted on seven printed circuit boards. While it has many flat-pack integrated circuits and discrete components, its distinguishing features are 280 toroidal memory cores distributed over five of the printed circuit boards. All seven boards are linked by a continuous "rope" consisting of 521 fine copper wires selectively routed through the memory cores. The resulting assembly can perform its electrical function adequately but is mechanically delicate. This delicacy has been

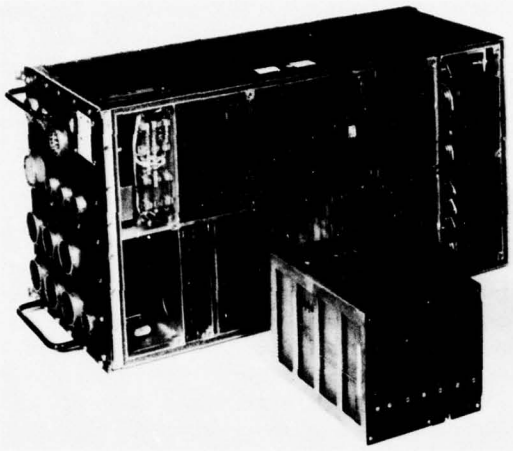

Fig. 1 AYN–1 computer with read-only memory assembly removed.

a contributing factor to an undesirably high failure rate of the assemblies. Moreover, it has precluded their being serviced at avionics depots. The resultant requirement for factory maintenance has proven to be an excessive logistic and financial burden to the Coast Guard.

The attempt to find relief from that burden led to a search for a substitute for the core-rope memory assembly. Several years ago, the search focused on a new device—a large-scale integrated circuit capable of performing the ROM function. The Coast Guard authorized APL to design, develop, and produce a replacement memory system that would exploit the characteristics of the new device.

DISCUSSION

The MC8316A ROM integrated circuit was chosen as the basis for the design because its 16 384–bit storage capacity was the largest then being commercially manufactured, its single supply voltage and modest power requirement were compatible with the AYN–1 system, and its manufacturer was prepared to screen and process the device in accordance with pertinent military specifications.

The specification of the data patterns to be embodied in these devices was delayed because of the initial lack of a machine-readable version of the AYN–1 program. Such a program was ultimately obtained by means of a specially designed and assembled program extractor. The program extractor generated a perforated paper tape representation of the program on the basis of its ability to interrogate electrically one of the existing core-rope storage assemblies. The tape was then used as the input for a general-purpose computer that had been configured to prepare ten punched card decks specifying the data patterns (in a format designated by the manufacturer of the ROM integrated circuits) for the ten MC8316A devices required in a complete memory system (Ref. 1).

SYSTEM DESIGN. The redesign concept entailed replacement of all memory cores and associated sense amplifiers on each of the five central boards of the storage assembly with a pair of ROM integrated circuits. All other small-scale integrated circuits included on the boards for the formation of output registers and gating networks were retained intact in the new design, thus assuring electrical compatibility between the output signals produced by the new storage assembly and other elements of the AYN–1 computer. The collateral aspect of the compatibility problem (establishing compatibility between the new storage assembly and the input signals provided to it by other functional elements of the computer) was resolved by redesigning the program counter. This counter, which is embodied in the circuitry on two printed circuit cards external to the storage assembly, provides the address-defining signals that are applied to the storage assembly. The new program counter (Fig. 2) retains the circuitry in the original version that is actually associated with the counting function, but the elaborate array of associated discrete component current drivers that provided a suitable address interface to the 521–wire rope were replaced with a few integrated circuit buffers.

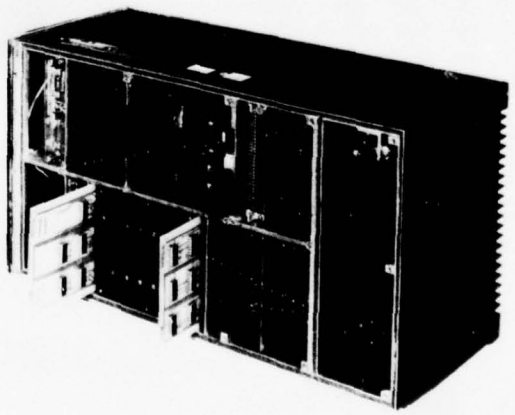

Fig. 2 AYN–1 computer with read-only memory installed between partially removed program counter boards.

The electrical design of the assembly proceeded smoothly, but two significant problems arose in the mechanical design. The address-defining signal ensemble had to be communicated to the five central boards in the assembly. (In the core-rope system, this role was filled by the rope that linked all seven boards, both physically and electrically.) The housing cover plate was modified to include a flat cable assembly that provided the required interboard connections, so that base-plate rewiring was not needed.

The second mechanical problem became apparent when initial attempts to develop a workable layout for the five central printed circuit boards proved unsuccessful. The difficulty was largely attributable to high component density and the desire to avoid multilayer boards with their higher cost and more complex maintenance procedures. All flat-pack integrated circuits (which had been used exclusively in the core-rope version) were replaced with electrically equivalent devices in dual-in-line packages. This substitution permitted circuit tracks to be routed between the more widely spaced leads of the dual-in-line devices and thereby eliminated the need for many interconnections between board surfaces. A computer-aided layout service provided by a subcontractor completed the solution to the problem.

PROTOTYPE EVALUATION. Two prototype storage assemblies conforming to the new design were fabricated and subjected to extensive functional tests, which were successful. One prototype was then installed in a computer aboard an HH–3F helicopter. During two months of routine flight activities, it exhibited more than 200 hours of fault-free operation. Termination of the flight tests was dictated at that point by reassignment of the helicopter.

Subsequent to the successful prototype demonstration, effort was directed toward the assembly of 110 new memory systems. The first phase of this activity consisted of procurement and inspection of approximately 20 000 components processed in accordance with pertinent military standards (Ref. 2). The second phase, now nearing completion, has involved the negotiation and monitoring of a subcontract calling for the fabrication and assembly of the 990 printed circuit boards that will be the constituents of the new systems. The third and final stage of this effort will be the electrical testing of these boards.

In preparation for the third-phase test program, two special-purpose test units have been designed and assembled. The memory/register test unit automatically exercises and evaluates the performance of the boards that occupy the five central positions in the new program storage assemblies. A program counter test unit performs an analogous role for the two program counter boards that complete the new systems. A noteworthy feature of this unit is its use of an eight-bit microprocessor that operates under the control of a 470-byte stored program.

After completion of the test activities and delivery of the new memory systems to the Coast Guard, it is anticipated that the program will be concluded with several instructional sessions for Coast Guard maintenance personnel and the preparation of formal documentation.

REFERENCES

1. R. T. Stellabuto and B. J. Condon, *AN/AYN–1 Computer Memory Conversion Software Support*, APL/JHU SSE–75–246, 11 December 1975.
2. R. W. Cole and H. E. Reichenberg, *SOR QA Program on Electronic Piece Parts and Assemblies for the AN/AYN–1 Computer Conversion*, APH/JHU SOR–77011, 22 February 1977.

Author: *C. A. Blackburn*

Support: *U.S. Coast Guard*

BIOMEDICAL ENGINEERING

INTRODUCTION

The Johns Hopkins University School of Medicine, the School of Hygiene and Public Health, and APL have collaborated in a program of biomedical research and development since 1965. An important objective of the program is to apply the "know how" of engineering and physical sciences, acquired in defense and space research and development by APL, to solve problems in medical research and health care delivery. This program has grown to include collaboration with nearly all of the clinical departments and with many of the basic science departments of the medical divisions. More recently, a collaborative program has been established with the Johns Hopkins Hospital. There are active programs in Nuclear Medicine, Ophthalmology, Neurosensory Instrumentation, Radiography, Cardiovascular Systems, Prosthetic Systems, Biomedical Engineering, and Clinical Engineering.

This application of state-of-the-art technology has contributed to many areas of basic medical research and to clinical diagnosis and therapy through improvement of instrumentation, techniques, and knowledge. The application of systems engineering techniques has contributed to solutions for problems of the health care delivery system. These activities have a focus in the Department of Biomedical Engineering at the Johns Hopkins Medical Institutions. In addition, a new educational program developed in collaboration with members of the Department of Biomedical Engineering leading to the Master's Degree in Clinical Engineering was established in September 1973 at the Medical School.

The results of the research and development in this program are reported in the open literature, principally in biomedical, biological, and medical journals. During the program's relatively short life, more than 150 papers have been published along with a few book chapters, more than 65 instruments for research and clinical application have been developed, and a number of APL staff members have assumed line responsibility for the JHMI in areas where technology can make specific contributions to patient care and the health care delivery system. Examples of the latter are in radiation physics, in information processing, and in defining technical requirements

for the maintenance of the highly technological medical equipment used in patient care.

At any given time, there are 40 to 60 active projects within the collaborative biomedical program. They have ranged all the way from the development of a rechargeable heart pacemaker to eliminate the repeated implant surgery usually required—to the discovery of a method for observing the blood flow in usually inaccessible regions of the human eye—to the specification of monitoring equipment and communication systems for better patient care.

The projects reported herein are heavily research oriented. Two deal with the analysis of data taken from dynamic measurements of blood flow using radioactively tagged molecules of blood. These studies have defined parameters that quantitate the efficacy of heart function and allow assessment of cerebral blood flow in humans. Another deals with sophisticated techniques of measurement of light scattering from the tissue of the cornea of the eye and its correlation with analytic models of both normal and swollen corneas. The fourth describes a novel membrane transport cell that enables the simultaneous measurement of hydraulic conductivity, reflection coefficient, and effective permeability of a membrane. Results for sucrose transport across a Cuprophan–150 PM membrane are described.

Other activities of importance within the current biomedical program are the application of a two-dimensional scanned echocardiographic system to the measurement of left ventricular wall motion. Along with the development of sophisticated data processing methods, this will enable quantitation of infarct size and progress in heart attack victims and may be extended to the early detection of preinfarct ischemia. The clinical evaluation of two instruments developed under this program is currently under way—a novel three-dimensional radiographic device and a sensor for detecting abnormal intracranial pressure. Finally, the application of the techniques of holography to measure and study the healing of cornea wounds is progressing well. Any of these may well be the subject of future accomplishments.

tains a high-speed graphics terminal, an associated

graphics terminal

EVALUATION OF CARDIAC FUNCTION USING MEDICAL RADIONUCLIDES

The poor resolution of previous radionuclide tracer images of the heart has been a major limiting constraint to the quality of the diagnostic information. A new imaging technique "freezes" the motion of the heart during each of 16 time divisions within the cardiac cycle. The data frames may then be displayed to the physician in a repeating motion-picture format.

BACKGROUND

Noninvasive measurements of global and regional cardiac function by means of radioactive tracers are being used increasingly in the diagnosis and monitoring of patients with heart disease. These procedures supplement and often replace more expensive and technically complicated invasive techniques such as cardiac catheterization (Ref. 1). Nuclear medicine techniques, on the other hand, cannot provide the exquisite resolution of conventional roentgenology.

In radionuclide imaging of the heart, organ motion has been a significant problem. The ventricles of the heart demonstrate major volume changes with attendant translation of the cardiac walls. In addition, torsional movement is an important component of overall motion. In most systems, the image data are collected with an "open-shutter" gamma camera. Obviously, any organ movement tends to blur the image, and the blurring is most severe near the apex of the heart where many infarctions and aneurysms occur.

DISCUSSION

The principal recent advances (Ref. 2) have been in the application of new programs for use with a computerized scintillation camera system. It has the following distinctive characteristics:

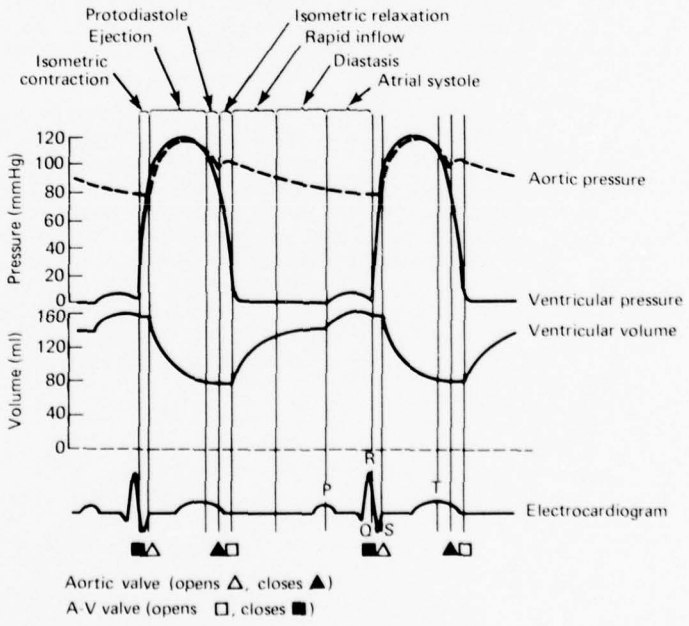

Fig. 1 Various physiological events that occur during the cardiac cycle. The shape of the left ventricular volume curve can be determined noninvasively using radio-tracer techniques.

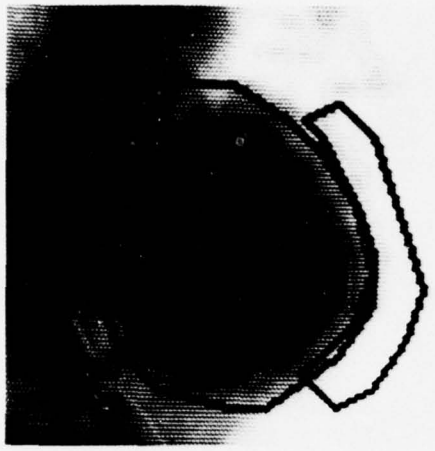

Fig. 2 Regions of interest superimposed on a radionuclide image of the heart at end diastole. The larger *region encircles the left ventricle; the smaller region* defines a background area in this left anterior oblique view. These regions are used in the computer program to generate time/activity curves of the activity within the left ventricle.

1. The system has an EKG-synchronized data-acquisition capability that uses a buffer memory to separate the gamma camera data into as many as 64 individual data matrices. Each data field (image) contains only the events recorded during a discrete predetermined portion of the cardiac R–R interval. However, the data accumulated in each of the time slots are integrated over 1000 heartbeats.
2. The resultant data matrices can be displayed as images of the beating heart and recycled repeatedly as an "endless tape" motion picture.

For most patients, a conventional nuclear angiocardiogram is recorded in one-second frames for 30 seconds after the intravenous injection of ^{99m}Tc-albumin. The data provide a visual evaluation of the "first-pass" characteristics as the bolus enters the right side of the heart, exits to the lungs, returns to the left side, and exits again to the rest of the body. Overall sluggish circulation, left-to-right and right-to-left interchamber shunts, and lung transit times may be noted. An EKG-synchronized study of the cardiac blood pool is then acquired, with the cardiac cycle divided into 16 time segments. The events of the cardiac cycle are illustrated in Fig. 1.

Following the acquisition phase, the data are corrected for inherent spatial nonuniformities in sensitivity in the camera's detection system. In addition,

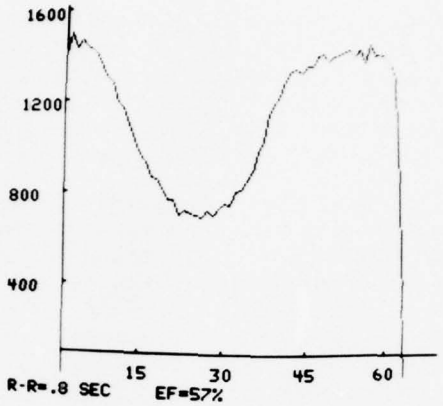

(a) Normal ejection fraction 57%

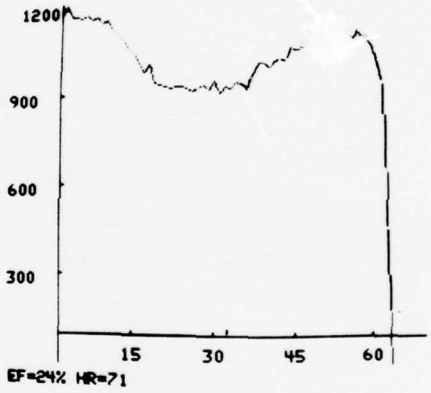

(b) Patient with marked decrease in cardiac function ejection fraction 24%

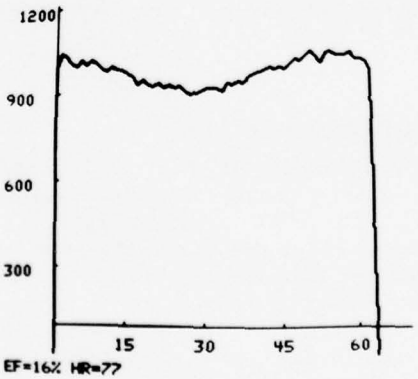

(c) Patient in congestive heart failure ejection fraction 16%

Fig. 3 Several clinical examples of left ventricular volume curves determined by EKG-synchronized scintigraphy.

a data-bounding process is applied so that any element that differs by more than two standard deviations (2σ) from its immediate neighbors is set to the 2σ value. The left ventrical is outlined as the cardiac region of interest, and a periventricular area is defined as a background region of interest (Fig. 2).

The activity within these regions of interest is plotted as a function of time within the R–R interval. The background curve is subtracted from the ventricular curve to yield the corrected blood pool data. These data are then analyzed further to yield the ejection fraction of the left ventricle, the pre-ejection period (a measure of the time from the R-wave to the beginning of ventricular contraction), the emptying and filling times of the left ventricle as a fraction of the R–R interval, and the ejection fraction divided by the emptying time (Fig. 3).

In addition to the quantitative data, the matrices are displayed in a "cine" format. The images are in essence a scintigraphic movie of the beating heart. A visual evaluation of wall motion of both ventricles may be made by the physician. Areas of diskinesia and/or akinetic portions of the heart wall are easily identifiable.

REFERENCES

1. H. N. Wagner, Jr., "The Heart and Circulation," *Nuclear Medicine*, HP Publishing Co., New York, 1975.
2. M. G. Lotter, K. H. Douglass, L. G. Knowles, E. L. Nickoloff, and H. N. Wagner, Jr., "A Technique for the Evaluation of Global and Regional Ventricular Function," *Proceedings of the Symposium on Computer Assisted Data Processing in Nuclear Medicine*, 16–17 January 1977, Atlanta, GA (to be published).

Authors: *L. G. Knowles (APL) and H. N. Wagner, Jr. (JHMI)*

Support: *U.S. Public Health Service Grant GM–10548*

DEPTH-DEPENDENT CORNEAL LIGHT SCATTERING

The use of light-scattering measurements to probe structural features within the stromal region of the eye's cornea assumes that the primary scatterer is the stroma and not the epithelial and endothelial cell layers. Our studies show that the stroma contributes more than 60% of the total corneal scattering at angles greater than 20° and about 80% at backward angles.

BACKGROUND

Light scattering in the normal cornea is small and is determined in part by the spatial arrangement of collagen fibrils within the stromal region. The relationship between corneal light scattering and structure was the basis for our earlier study (Refs. 1 and 2), which showed that the variations of corneal light-scattering intensity with light wavelength evidence a short-ranged ordering of fibrils in rabbit corneas of normal thickness and the presence of regions void of fibrils in cold swollen rabbit corneas. The use of light-scattering measurements to probe stromal ultrastructure assumes that most of the scattering occurs from within the stroma and not from the limiting cellular layers. We cited preliminary experiments in Ref. 1 that supported this assumption. However, in a subsequent study (Ref. 3), other investigators attempted to measure the distribution of scattered light as a function of depth into the cornea and concluded, "the main contribution to the integrated scattered intensity from the cornea comes from regions close to the limiting layers, i.e., the epithelium and endothelium." Recently we have demonstrated that these investigators did not measure directly the actual light-scattering profile and that a proper interpretation of their data *actually* shows that most of the scattering is from within the stroma (Ref. 4). Additionally, our own measurements show that the stroma is the primary scatterer within the cornea over a wide range of scattering angles from forward to backward directions (Ref. 5).

DISCUSSION

When a normal cornea is examined under a slit lamp in lateral directions, the notable features are (a) the nonscattering epithelium bounded by two narrow bright bands, (b) the stroma in which the scatter-

software development requires the use of assemblers to translate programs into machine language, simula-

blers for a number of popular microprocessors, as shown in Table 1. The assemblers have a common

ing is relatively less intense than in the two bright bands, and (c) a bright band at the endothelium. The scattering geometry used in the experiments of Ref. 4 is illustrated in the top line of Fig. 1a, where the shading suggests the distribution of scattering intensity in the cornea. If this distribution were viewed at an angle, as illustrated, the viewer would see a distorted picture of the actual distribution shown by the geometric projection on the second line of Fig. 1b.

This distortion of the true distribution is caused by the finite width of the incident beam and is related to the beam width, the viewing angle, the stromal thickness, and the epithelial thickness. An ideal detector would reproduce this projection exactly; however, the actual detector had a spatial response function that could be approximated by the isosceles triangle shown in Fig. 1c. The finite width of the detector response function causes further distortion of the ideal geometric projection.

The curve labeled "calculated" in Fig. 1d is the result of scanning the distribution of Fig. 1b with this triangular response function, where 72% of the scat-

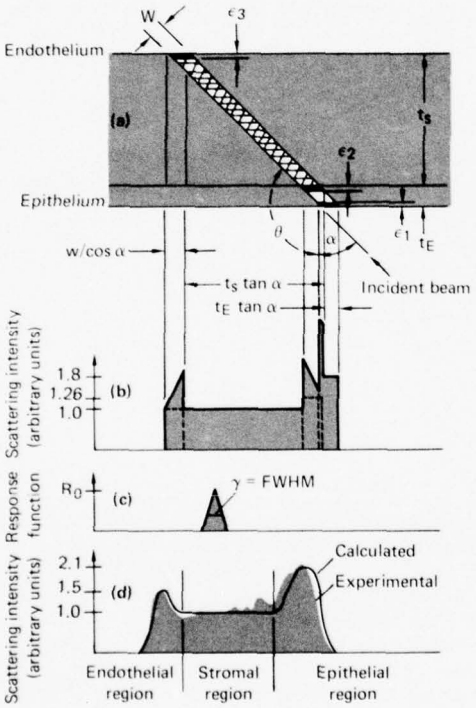

Fig. 1 The finite width, w, of the incident beam causes the intensity distribution to be distorted when the sample is viewed at an angle, θ. The true intensity is represented at the top of the figure, and the distortion introduced by the width of the beam is represented by the projection in the center of the figure. The amplitudes of the various regions are also adjusted by appropriate trigonometric factors to account for the projection. The final result, obtained by scanning this distribution with the slit response function of the detector, is shown at the bottom of the figure. The line labeled "calculated" is the distribution predicted from the above model using the parameters of Ref. 4, and the line outlining the tinted area is the measured trace. The breakdown into epithelial, stromal, and endothelial regions is that of Ref. 4.

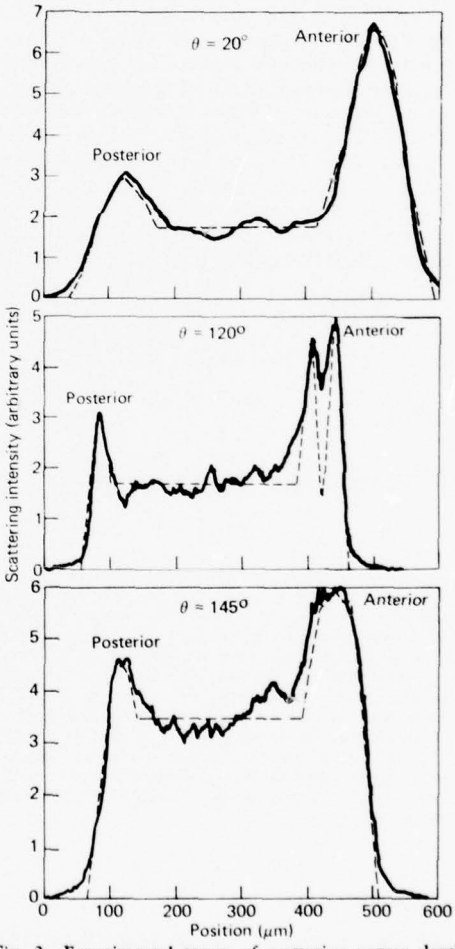

Fig. 2 Experimental traces of scattering versus depth into the cornea (solid curves) and calculation for the model discussed in text (dashed curves). The results show that most of the scattering occurs within the stroma at all the angles studied and, for backscattering configurations, the stroma is responsible for approximately 80% of the scattering.

system on high-speed disk storage allows permanent storage of source (assembly language) and object

rithms is simple and straightforward using the extensive trace and breakpoint facilities.

tering intensity is assumed to originate from within the stromal region. For comparison, the curve outlining the tinted region in Fig. 1d is the experimental trace of Ref. 4. This agreement between theory and experiment suggests that most of the scattering occurs within the stroma, at least at the scattering angles used in these experiments.

In Ref. 5, we presented our traces of light scattering versus depth into the cornea at a series of scattering angles between 20 and 145° using green light. Typical experimental results are given by the solid curves of Fig. 2. The trace at a scattering angle of 120° shows two distinct peaks in the anterior corneal region. The total spatial response function of the apparatus was measured at each of the scattering angles and was used to interpret the experiments. The dashed traces in Fig. 2 are calculated based on the measured response function and the model of the depth dependence of corneal scattering illustrated in Fig. 1a (however, in our experiments the light was incident normal to the corneal surface). The calculated curves compare favorably with the measured signal. Our analyses of such traces show that the stroma contributes more than 60% of the scattering at all angles and approximately 80% at backscattering angles.

REFERENCES

1. R. A. Farrell, R. L. McCally, and P. E. R. Tatham, "Wavelength Dependencies of Light Scattering in Normal and Cold Swollen Rabbit Corneas and Their Structural Implications," *J. Physiol.*, 233, 1973, pp. 589–612.
2. R. A. Farrell and R. L. McCally, "On Corneal Transparency and Its Loss with Swelling," *J. Opt. Soc. Am.*, 66, No. 4, 1976, pp. 342–345.
3. J. Lindstrom, T. Feuk, and B. Tengroth, "The Distribution of Light Scattered from the Rabbit's Cornea," *Acta Ophthalmol.*, 51, 1973, pp. 656–669.
4. R. A. Farrell and R. L. McCally, "On the Interpretation of Depth Dependent Light Scattering Measurements in Normal Corneas," *Acta Ophthalmol.*, 54, 1976, pp. 261–270.
5. R. L. McCally and R. A. Farrell, "The Depth Dependence of Light Scattering from the Normal Rabbit Cornea," *Exp. Eye Res.*, 23, 1976, pp. 64–81.

Authors: *R. L. McCally and R. A. Farrell*

Support: *U.S. Public Health Service Grant EY01019*

MEMBRANE TRANSPORT CELL

A novel membrane transport cell that uses laser interferometry to measure solute flux has been developed. With this apparatus, all of the transport properties describing solute and volume flow across artificial or biological membranes can be obtained from a single experiment and processed to provide new information regarding the organization of transport pathways across the preparation. The cell has been used to measure the hydraulic conductivity (solvent flow under a hydrostatic or osmotic pressure head), reflection coefficient (related to the sieving properties of the membrane), and sucrose permeability of Cuprophan dialysis membrane.

BACKGROUND

The passive transport properties of membranes typically are measured in separate experiments and then combined to predict membrane performance under boundary conditions that, in general, differ from those under which the transport properties were measured. We have shown (Ref. 1) that if membrane structure is ignored in both property measurement and performance prediction, the predicted solute flux across parallel pathway membranes will generally be in error. The error depends on the distribution of the reflection coefficients (heteroreflectivity) of the parallel paths. For the simplest case of a heteroporous membrane bounded by nonelectrolyte solutions whose concentrations are close enough to permit linearization of the governing flux equations, the solute flux is given by

$$J_s = J_v\,(1-\sigma)\bar{C} + [\omega + gL_p\sigma(1-\sigma)\bar{C}]RT\Delta C\ , \quad (1)$$

where J_v is volume flux across the membrane, σ is the conventionally determined reflection coefficient, $\bar{C}$ is a mean concentration, ω is the tracer permeability, L_p is the conventionally determined hydraulic conductivity, R is the gas constant, T is absolute temperature, ΔC is the concentration difference across the membrane, and g $(0 \leq g \leq 1)$ measures the influence of parallel path structure on solute flux. We term the bracketed coefficient in Eq. 1 the effective permeability, ω_{eff}. Independent measurements of ω_{eff} and ω can provide g

when L_p and σ are known. These measurements give insight into the transport structure of the membrane.

The simultaneous measurement of all transport properties in a single experiment can conserve time and material and improve the consistency of the data, particularly for biological membranes. Laser interferometry provides a noninvasive means to monitor transmembrane solute flux and to obtain useful transport properties not previously measured by conventional techniques.

DISCUSSION

The membrane transport cell shown in Fig. 1 was developed to permit the simultaneous measurement of σ, L_p, and ω_{eff}. The membrane with an effective transport area, A, separates two fluid chambers; C_i, P_i, and V_i are the concentration, pressure, and volume of the ith chamber. A large reservoir at a fixed height, h, maintains a constant pressure head across the membrane. A calibrated capillary tube is used to measure changes in V_2.

The laser interferometric technique is used to measure the concentration difference across the membrane, $\Delta C = C_1 - C_2$, in a stirred cell. A helium-neon laser illuminates the optical mask whose four apertures permit light to pass through the membrane cell. Glass spacers cause the relative phase of two of the rays passing through the cell to change by an amount that depends on the difference between the refractive indices, and thus the concentrations, of the solutions in each chamber. A cylindrical lens causes these rays to form an interference pattern. The additional two rays that do not pass through the spacers are also brought together by the lens to provide a reference pattern independent of ΔC.

A typical pair of diffraction patterns is shown in Fig. 1. As the concentration difference across the membrane changes with time in an unsteady experiment, the distance between the nulls of the two patterns changes correspondingly.

The time courses of both volume flow (measured using capillary tubes) and solute flow are measured simultaneously. The experimental protocol employs a

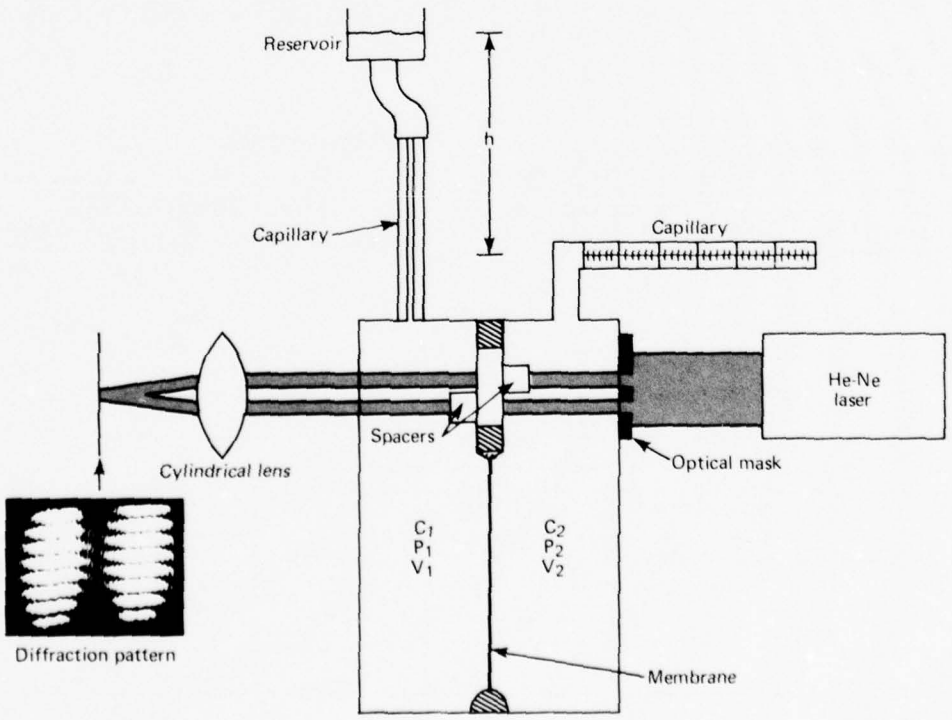

Fig. 1 Schematic diagram of experimental system.

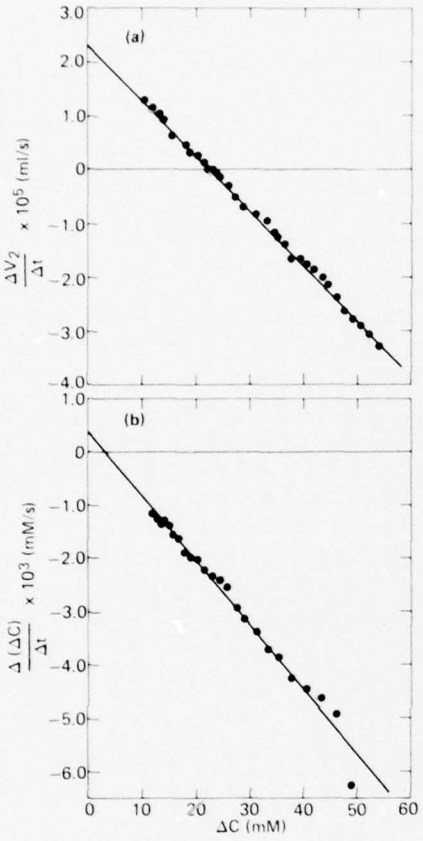

Fig. 2 Plots of experimental data for Cuprophan at 37°C with a stirring rate of 75 rpm. (a) Volume flow rate into chamber 2 versus concentration difference across membrane. (b) Rate of change of concentration difference across membrane averaged over ±20 minutes versus concentration difference across membrane.

constant pressure head and an initial concentration difference across the membrane; the driving forces are such that volume flow and solute flow are linearly dependent on the concentration difference across the membrane. The phenomenological transport coefficients are determined from the slopes and intercepts of these linear relationships.

Our initial experiments used Cuprophan 150 PM membrane, a constant pressure head consisting of 140 cm of 170 mM sucrose solution, and an initial concentration difference of 60 mM sucrose with an average concentration, $\overline{C}$, of 140 mM. A typical plot of the data measured over a six-hour period is shown in Fig. 2. The straight lines are linear least-square fits to the data. The ΔC intercept and slope of the plot of $\Delta V_2/\Delta t$ versus ΔC provide the values of the reflection coefficient, σ, and the hydraulic conductivity, L_p. The slope of the plot of $\Delta(\Delta C)/\Delta t$ versus ΔC provides the effective membrane permeability, ω_{eff}.

Transport coefficients obtained at three different stirring speeds are compared with published data in Table 1. The phenomenological coefficients are not clearly dependent on stirring speed, suggesting that unstirred layers were of negligible importance. Our values of L_p and ω_{eff} are well within the range of published values. Membrane heteroreflectivity contributes to the effective permeability by no more than 15%.

REFERENCES

1. M. H. Friedman, "The Effect of Membrane Structure on the Predictability of Fluxes, with Application to the Cornea," *J. Theor. Biol.*, 61, No. 2, 1976, pp. 307–328.
2. E. Klein, J. K. Smith, and F. F. Holland, *Membrane and Materials Evaluation; Cuprophan 150-PM Artificial Kidney Reference*

TABLE 1

PHENOMENOLOGICAL COEFFICIENTS FOR CUPROPHAN AT 37° C WITH SUCROSE AS THE SOLUTE

$L_p \times 10^{11}$ $\left(\frac{\text{ml}}{\text{dyne-s}}\right)$	σ	$\omega \times 10^{15}$ (moles/dyne-s)			Source
		ω_{eff}	ω_{min}†	ω	
3.82 ± 0.01	0.233 ± 0.001	6.03 ± 0.12	5.07 ± 0.12	—	This study (75 rpm)
3.89 ± 0.03	0.231 ± 0.001	6.01 ± 0.10	5.04 ± 0.10	—	This study (150 rpm)
3.84 ± 0.02	0.250 ± 0.001	5.96 ± 0.14	4.95 ± 0.14	—	This study (300 rpm)
3.06	—	—	—	6.67	Ref. 2
4.78	0.17‡	—	—	5.67	Ref. 3
—	—	—	—	6.55	Ref. 4
—	—	—	—	8.74	Ref. 5
4.90	—	—	—	—	Ref. 6

† $\omega_{min} = \omega_{eff} - L_p\sigma(1-\sigma)\overline{C}$

‡ Reflection coefficient was obtained using the following formula: $\sigma = 1 - 2T_R/(1 + T_R^*)$, where T_R and T_R^* are defined in Ref. 3.

Material—Evaluation and Experimental Procedures, NIH Department of Health, Education, and Welfare Report AK-2-72-2221-A, 1974.

3. D. M. Grecc, G. D. Antwiler, J. W. Moncrief, J. F. Decherd, and R. P. Popovich, "Measurement of the Transmittance Coefficient Spectrum of Cuprophan and RP69 Membranes: Applications to Middle Molecule Removal via Ultrafiltration," *Trans. Am. Soc. Artif. Internal Organs*, 22, 1976, pp. 627–636.
4. C. K. Colton, K. A. Smith, E. W. Merrill, and P. C. Farrell, "Permeability Studies with Cellulosic Membranes," *J. Biomed. Mater. Res.*, 5, 1971, pp. 459–487.
5. P. C. Farrell and A. L. Babb, "Estimate of the Permeability of Cellulosic Membranes from Solute Dimensions and Diffusivities," *J. Biomed. Mater. Res.*, 7, 1973, pp. 275–300.
6. Y. Nose, G. L. Mrava, D. C. Weber, T. Kon, S. Nakamoto, K. L. Popowniak, and K. C. Juruvila, "Clinical and Engineering Evaluation of Disposable Envelope Inserts for the Kiil Dialyzer," *Trans. Am. Soc. Artif. Internal Organs*, 15, 1969, pp. 118–126.

Authors: *M. H. Friedman and R. A. Meyer*

Support: *IR&D*

PHYSIOLOGICAL INTERPRETATION OF TIME/ACTIVITY CURVES FROM CEREBRAL FLOW STUDIES

Regional cerebral perfusion may be evaluated by imaging the first circulation of a relatively nondiffusible radiotracer labeled with technetium-99m following an intravenous injection. The data can be quantitatively interpreted by generating time/activity curves from selected regions of interest in the brain. Certain patterns within these activity curves can be assigned to proven disease states.

BACKGROUND

Noninvasive radiotracer methods for the evaluation of regional cerebral perfusion in patients with ischemic strokes have been shown by others (Ref. 1) to have a sensitivity of approximately 50% with visual interpretation alone and up to 74% when the data are also quantified. The improvement in sensitivity with quantitative interpretation is attributable to the ability to generate time/activity curves, measure parameters associated with these curves with good reproducibility, and establish normal ranges for these parameters. Previous methods of interpreting the time/activity curves have suffered from the use of nonphysiological parameters or the use of only one physiological parameter that evaluates blood flow incompletely.

DISCUSSION

A well known medical axiom states that there is more similarity in function between paired organs (e.g., left and right lung fields) within a particular person than there is between the same type of organ in two different people (e.g., the left kidneys of any two randomly chosen persons). This basic principle has been applied to this study to evaluate regional abnormalities in the brain. Paired and symmetrical "regions of interest" (Fig. 1) in the brain can be expected to exhibit essentially identical blood flow patterns when subjected to the same bolus of radioactive tracers, so that regions in the left side of the brain can reasonably be compared to similar areas in the right side.

The time/activity curve generated by detecting the passage of the radionuclide through the region of

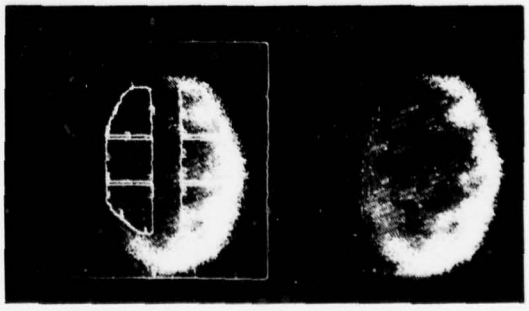

Fig. 1 Six regions of interest defining areas in a vertex radionuclide image of the brain. The abnormal distribution is due to metastatic lesions caused by a primary cancerous prostate gland.

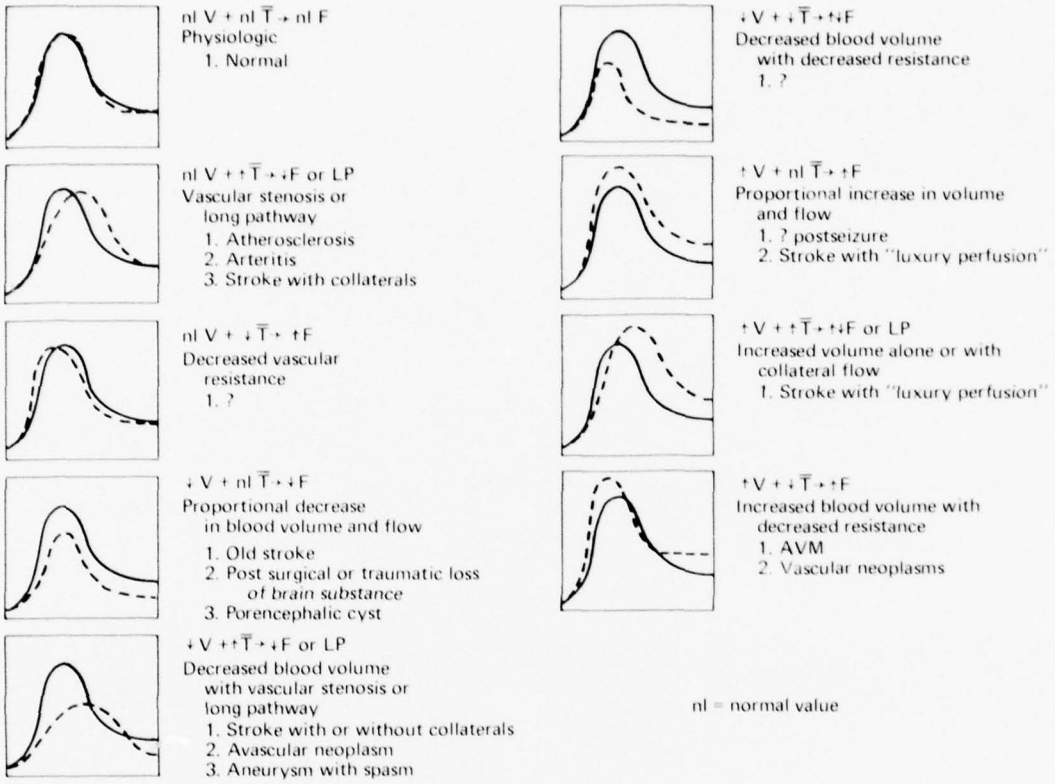

Fig. 2 Interpretation of time/activity curves from paired regions of interest.

TABLE 1
NORMAL ABSOLUTE VALUES FOR TIME PARAMETERS (MEAN ±1 STD DEV)

Time (s)	Hemisphere		Anterior	Middle	Posterior
T_1: Injection-to-first-arrival time	Right	11.3 ± 2.5	11.4 ± 2.5	11.2 ± 2.5	11.3 ± 2.6
	Left	11.3 ± 2.5	11.4 ± 2.5	11.2 ± 2.5	11.3 ± 2.6
T_2: Injection-to-peak-activity time	Right	18.0 ± 3.5	18.3 ± 3.9	17.6 ± 3.3	17.8 ± 3.7
	Left	18.0 ± 3.5	18.3 ± 3.9	17.6 ± 3.3	17.8 ± 3.7
T_3: Mean transit time	Right	22.3 ± 3.8	22.4 ± 4.3	21.8 ± 3.8	22.8 ± 3.7
	Left	22.3 ± 3.8	22.4 ± 4.3	22.0 ± 4.1	22.7 ± 3.8

interest is related to the injected dose and cardiac output by the Stewart-Hamilton equation

$$Q = F_{co} \int_0^\infty C(t)dt.$$

It states that if a given amount of tracer, Q, is injected into the proximal circulation and undergoes uniform mixing in a central chamber, the measurement of the concentration of the tracer, $C(t)$, at some distal point during the first calculation will permit calculation of the cardiac output, F_{co}. When this equation is modified for the evaluation of relative regional cerebral perfusion to symmetrical paired regions of interest within the brain, the equation reduces to the simple relationship: relative flow equals relative volume divided by the relative mean transit time of the tracer through the region of interest (Ref. 2).

A group of 50 patients who did not have organic brain disease at the time of discharge (or follow-up)

was studied by this method. An automated data acquisition and processing system was used to determine the time course of the radioactive bolus through six regions of interest within the brain. Computer programs have been developed to calculate objectively a number of physiological parameters. The values of the injection-to-first-arrival times, injection-to-peak-activity times, and mean transit times for these normal patients, are given in Table 1.

There are nine possible combinations of normal, increased, or decreased relative regional blood volume and normal, increased, or decreased relative mean transit time of the bolus through the region of interest. When the two physiological parameters are compared, a pathophysiological interpretation relating to regional blood flow can be constructed (Fig. 2).

REFERENCES

1. W. H. Oldendorf and M. Kitano, "Radioisotope Measurement of Brain Blood Turnover Time as a Clinical Index of Brain Circulation," *J. Nucl. Med.*, **8**, 1967, pp. 570–587.
2. W. C. Klingensmith, III, M. G. Lotter, L. G. Knowles, A. Motazedi, and H. N. Wagner, Jr., "Modification of the Stewart-Hamilton Principle for Clinical Evaluation of Regional Cerebral Circulation" (Submitted for publication in *J. Nucl. Med.*).

Authors: *L. G. Knowles (APL) and H. N. Wagner, Jr. (JHMI)*

Support: *U.S. Public Health Service Grant GM–10548*

ENVIRONMENTAL PROGRAMS

INTRODUCTION

Environmental concerns have emerged as a major area affecting public policy, especially in regard to minimizing potentially adverse effects of new technologies. In keeping with its mission of using its technical expertise in service to the nation, APL has maintained a diverse program in several environmentally related areas, notably power plant siting, fire-related problems, and water purification.

The Detailed Site Evaluation Program is a joint program of APL and the Chesapeake Bay Institute (CBI). The program was initiated in 1972 in response to legislation requiring that all proposed power plant sites in Maryland be subjected to an environmental impact study and that environmental acceptability be assured as a part of the approval process. APL provides program management and conducts impact assessment in all areas other than marine biology and hydrography. These two study areas are covered by CBI. The remaining areas, consisting in part of air pollution, meteorology, plant design, geology, radiation releases, noise, transmission line effects, groundwater problems, and chemistry, provide APL with the opportunity of a highly interdisciplinary study area. Since 1972, detailed site evaluations have been completed on a number of sites encompassing both fossil and nuclear generation, and ranging from 50 to 2000 MWe in size.

In 1976, a one-year study was initiated under sponsorship of the Electric Power Research Institute (EPRI) to develop a computerized method for locating major energy facilities. The method is being developed for a five-state mid-Atlantic region but is intended for eventual nationwide use. A linear programming model is the basis for the method, which determines probable locations for sets of future energy facilities such as power plants and oil refineries. The results will be suitable for use in predicting the cumulative regional environmental impact of sets of proposed energy facilities. Information on state siting objectives and constraints will be provided by representatives from the five states within the region.

Other topical studies related to energy facilities and the Maryland coastal environment have included a study report, "Environmental and Socio-

economic Analysis for Proposed Petroleum Related Coastal Facilities in Maryland," and a wetlands study through the Chesapeake Research Consortium. A current project in collaboration with local governments studies the feasibility of developing methane from solid waste disposal areas.

A second area, broadly included under the environmental heading, is the APL Fire Program. It deals with four major areas related to fire including combustion research, fire casualties analysis, fire operations assessment, and technical information transfer, both within the fire community and between the fire community and the public. The effort is interdisciplinary in scope and includes collaboration with the School of Hygiene and Public Health of The Johns Hopkins University and with fire and health agencies of the State of Maryland. The program objectives address four questions: (1) What are the physical causes and medical consequences of fires that lead to fatalities or injuries? (2) What useful devices or practices can be designed for the fire service or the population at large? (3) What are the information needs of the fire field, and how can they be strengthened? (4) What chemical factors determine the ignition and extinction of flames?

The specific articles included in this section deal with the information transfer and combustion aspects of the fire program. However, the general areas of fire tactics and casualty assessments are continuing parts of the program as well.

The final topic included in this section concerns an experimentally based research effort directed at bacteria suppression in public water supplies by photo-generated singlet oxygen. The investigation showed that coliform levels present in untreated Potomac River water are substantially reduced by exposure to singlet oxygen generated by laser absorption at 1.064 μm. The results show a dependence on dissolved oxygen concentration, laser intensity, and irradiation time. In contrast with ultraviolet sterilization, this process does not produce photochemical changes in substances present in water. Moreover, it avoids problems associated with disinfection using chlorine, a subject of recent environmental concern in light of the possible hazards of chlorinated hydrocarbons in the biosphere.

ENVIRONMENTAL EFFECTS OF PROPOSED DOUGLAS POINT NUCLEAR POWER PLANT

An evaluation of the environmental effects of the proposed nuclear power plant at Douglas Point on the Potomac River 30 miles south of Washington, D.C. has been performed by APL, the Chesapeake Bay Institute, and the Department of Geography and Environmental Engineering of The Johns Hopkins University. A site evaluation report was published, public testimony was given before the U.S. Nuclear Regulatory Commission and the Maryland Public Service Commission, and the proposed findings of fact were prepared.

BACKGROUND

The siting of a power plant is affected by many competing considerations. The plant must be near a body of water in order for its condensers to be cooled economically, and the water preferably should be fresh to reduce corrosion problems. Nuclear plants must be situated away from populous areas because of safety regulations designed to protect the public in the event of a serious accident. New fossil fuel plants usually must be sited away from cities because of the problems associated with air emissions and fuel handling. Approaches to airfields must be avoided. Barge or rail facilities should be nearby to facilitate construction and transportation of fuel. Long distances between the plant and its service area are undesirable because of the cost of transmission lines.

The result of these relatively inflexible constraints is that several major power plants in Maryland have been proposed for estuarine areas at the interface of fresh water and salt water at places such as Douglas Point on the Potomac River, at the mouth of the Susquehanna River, and on the Chesapeake and Delaware Canal. These areas are quite productive biologically and serve as spawning grounds for many species of fish, the most prominent being the striped bass, or rockfish. Aquatic organisms can be damaged by being drawn into the cooling water system (entrainment), impinged on the intake screens, or affected by the discharge of chemicals or heat. To reduce these effects in biologically important areas, plants must use cooling towers that dissipate most of the heat by evaporation. They thus require only approximately 2% of the water that is required in "once-through" cooling systems with conductive heat transfer. But cooling towers create fog and deposit salt from their plumes, and their height (up to 150 m) makes them highly visible, especially in a rural setting.

There are many other environmental effects of power plants, including dredging and dredge spoil disposal, noise during construction and operation, electric fields from transmission lines, and diversion of groundwater. In addition, there are social impacts and site-specific safety factors to be considered.

The State of Maryland initiated in 1972 a Power Plant Siting Program to promote the orderly development of power plants and to protect the State's environment and natural resources. One component of that program, the evaluation of proposed new plant sites, has been carried out under subcontract by a Johns Hopkins University team presently comprising APL and the Chesapeake Bay Institute and coordinated by APL. Activities include collecting field data, performing analyses, constructing models, and predicting the environmental impacts for specific power plant sites. Alternative designs in problem areas sometimes are proposed and evaluated. The end product is a site evaluation report that describes the site and the predicted effects of the proposed plant.

Approval for construction of a power plant requires that permits be issued by a number of state and federal regulatory bodies. Public hearings are usually held on issues such as environmental impact, the need for power, and health and safety considerations. Permit decisions are based on the public record submitted by the utility, governmental bodies, and other interested groups.

The site evaluation reports prepared by APL draw no conclusions about the suitability of a site but do provide technical information from which the state can make policy decisions. The reports are submitted to hearing boards as part of the evidentiary record, and the authors are subject to cross-examination on the validity of their work.

DISCUSSION

The proposed Douglas Point site is a 1386-acre tract located on the Potomac River 30 miles south of Washington, D.C. (Fig. 1). Major features of the proposed design include a lagoon for docking and the withdrawal of cooling water, two 400-ft cooling towers, and a dredge spoil disposal basin (Fig. 2).

The environmental evaluation included extensive field programs in hydrology, aquatic biology, and

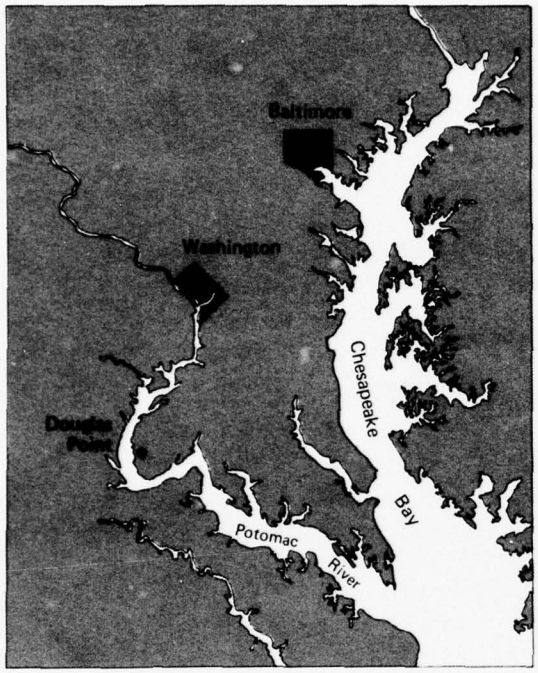

Fig. 1 The proposed Douglas Point site.

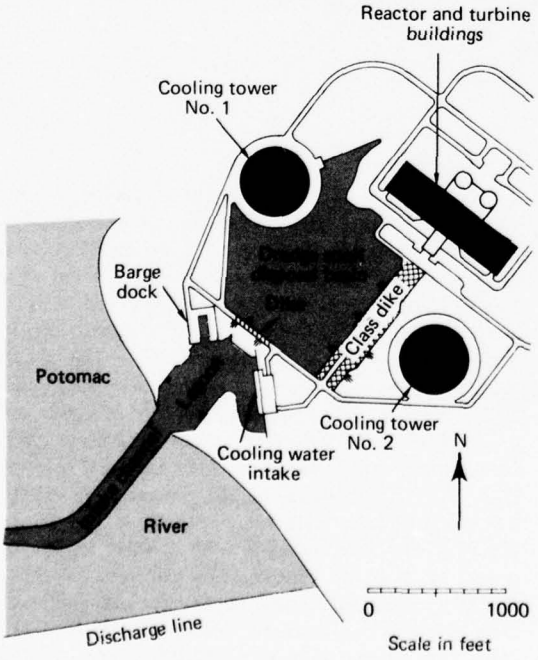

Fig. 2 Details of proposed design.

meteorology and the development of analysis and models in many technical disciplines. Environmental effects were predicted and alternatives in plant design to mitigate certain environmental impacts were proposed and evaluated. A final site evaluation report has been published (Ref. 1) in addition to supporting technical documents, testimony, and draft proposed findings of fact for regulatory hearings. Interaction with the staff of the utility during the course of the study resulted in a number of cost-effective design modifications to reduce environmental effects.

A principal concern about the proposed Douglas Point site was that it is located in the center of a major striped bass spawning ground; a large fraction of the entire East Coast striped bass population originates in the Potomac and several Chesapeake Bay spawning areas. Numerous potential impacts were examined in the site evaluation report, but only the striped bass issue will be discussed here as an illustration of the type of analysis performed.

An extensive biological field program was conducted by The John Hopkins University in 1974 to determine the distribution of striped bass eggs and larvae along the axes of the river in the vicinity of Douglas Point and to ascertain if the organisms exhibited a preference for the shore, the bottom, the channel, or other special locations. In a related effort in 1974 through 1976, another element of the Power Plant Siting Program surveyed egg and larvae distributions over a broader expanse of the river and sampled the adult spawning stock with gill nets and sonar. The Chesapeake Bay Institute conducted a hydrographic program to determine the river's water circulation patterns and dilution capabilities.

A hydrological-biological computer model was developed of the spawning process, the water circulation, the behavior of the larvae, and the operation of the plant. Inputs were based on the field program data and on an extensive review of the literature on striped bass spawning. The model predicted the percent of eggs and larvae that would be entrained and destroyed by the plant cooling system. A sensitivity analysis was conducted by determining the effect of uncertainties in the data and the assumptions. A change in the cooling system was suggested to the utility that would reduce water usage and thus entrainment during the spawning period by 70%. The final prediction was that plant operation would reduce the number of eggs and larvae by a yearly average of 0.6%.

The question of what effect such a reduction in eggs and larvae has on the subsequent adult population hinges on the manner in which compensation or

density-dependent factors regulate the population. Data on spawning, eggs, juvenile fish, and commercial catch in several estuarine systems were reviewed; analysis suggests that the adult population originating in the Potomac River will be reduced at most by the same 0.6%.

Information on commercial and recreational fishing and tagging studies of fish migration and mortality was analyzed to determine the actual size of the adult population and the contribution of the Potomac River to the total stock of fish. The result was a prediction that the probable average yearly loss to the East Coast fishery would be less than 29 000 lb of striped bass. For comparison, the average annual catch of striped bass in Maryland is 9 000 000 lb.

Other damage to the striped bass could result from chlorine discharges used to prevent biofouling of the condensers, from corroded metals in the cooling system, from the discharge of heated water, and from the impingement of adult fish on the screens at the cooling water intake. Each of these effects was examined. It is not always possible to be quantitative about possible effects but some bounds were determined and mitigating alternatives and their costs were discussed.

REFERENCES

1. *Power Plant Site Evaluation Final Report, Douglas Point Site,* JHU PPSE 4–2, 1, February 1976, 2, January 1976, prepared by APL and the Chesapeake Bay Institute for the Maryland Power Plant Siting Program.
2. K. L. Warsh, *Hydrological-Biological Models of the Impact of Entrainment of Spawn of the Striped Bass (Morone Saxatilis) in Proposed Power Plants at Two Areas in Upper Chesapeake Bay,* JHU PPSE–T–1, June 1975.

Author: *E. M. Portner*

Support: *State of Maryland Power Plant Siting Program*

REDUCTION OF TOTAL COLIFORM COUNTS OF NATURAL WATER SAMPLES BY MEANS OF LASER RADIATION

Experimental investigation of the combined effects of laser radiation at 1.0642 μm and oxygen pressurization on coliform levels in Potomac River water samples has yielded the following results. A substantial reduction in coliform levels may be induced, the magnitude of which exhibits a fundamental dependence on the concentration of dissolved oxygen, laser intensity, and irradiation time. A reduction of coliform levels by oxygen pressure alone is observed but, on the average, the effect is small compared to that observed when the sample is irradiated simultaneously. Thermal effects accompanying irradiation are negligible. The inactivation rate is inhibited for oxygen pressures in excess of 10 atm.

A consideration of the first three results in conjunction with the established experimental fact that bacteria are unaffected by radiation alone for wavelengths that are large compared to 260 nm (where nucleic acids absorb strongly and genetic damage occurs) implies that laser-excited singlet molecular oxygen, $O_2(^1\Delta_g)$, is the single cause of bacterial destruction, the role of the laser being solely to produce selective excitation of oxygen from the ground electronic state.

DISCUSSION

Investigations described in this article were conducted with the cooperation of the Washington Suburban Sanitary Commission, Patuxent Filtration Plant. All water samples processed and analyzed were obtained from the Potomac River. Since raw samples were required, they were unfiltered, the first step in water treatment being chlorination. Thus, the optical quality of the water samples was usually poor, with high turbidity and significant amounts of algae and other unidentified filterable matter. Therefore, it is felt that the results presented here represent a lower limit to the effectiveness of the process. The experimental procedure involved sterilizing a cell in an autoclave and then filling it with a water sample by means of a sterile pipette. The coliform count of the water was determined separately and compared with that obtained from the processed sample. In all cases, two plate counts were made to give an indication of the statistical spread of the resulting data.

Figure 1 is an overall view of the experimental arrangement. A GTE Sylvania Model 606 cw Nd:YAG laser is used as the irradiation source. Details of the construction and operation of the high-pressure cell are presented in Fig. 2. The cell was machined from stainless steel and is designed to withstand gas pressures in excess of 1000 psig. It consists of two vertically connected compartments. In the one for oxygenation, a maximum surface area of the sample is exposed. Irradiation occurs in the other cylindrical compartment, which has windows sealing both ends. The cross-sectional area of the irradiation chamber is 0.77 cm^2 and the length is 4 cm, providing a capacity of 3.1 cm^3.

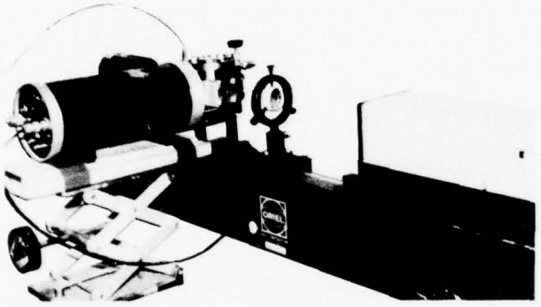

Fig. 1 Laser used to kill bacteria in water is in the oblong housing at right. The water sample is in the small bolted block at left.

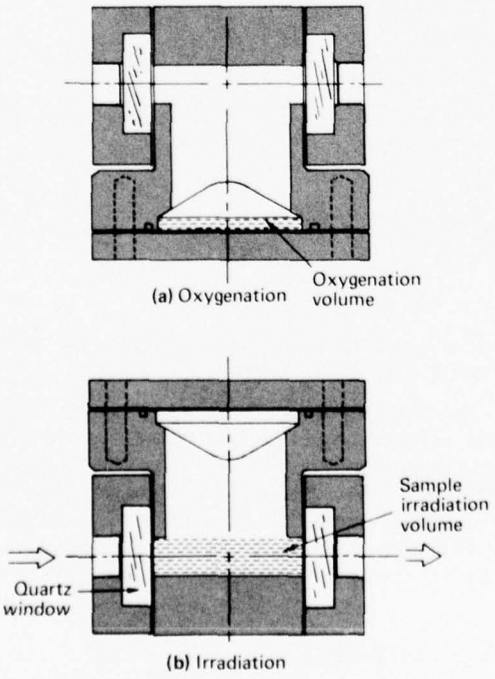

Fig. 2 Schematic diagram of high-pressure cell.

Operation of the cell involves filling the irradiation chamber with the water sample, placing the top in position, tightening the retaining bolts, applying the desired oxygen pressure, and closing the gas supply valve. The cell is then inverted, causing the sample to fill the conically shaped oxygenation compartment to a depth of 0.27 cm with an exposed area of 11.4 cm^2. To ensure that the dissolved oxygen is in equilibrium, the cell, still inverted, is shaken vigorously. The cell is still connected to the oxygen supply by a length of stainless steel hypodermic needle tubing of small diameter. Finally, the cell is rotated to its original position and set in place for irradiation.

The results obtained are summarized in Fig. 3. The kill rate constant, k, is plotted against oxygen pressure, p_O. Thus, if the initial coliform count is M_0 (determined from the control sample), the number remaining after time, t, is

$$M = M_0 e^{-kt}.$$

The fact that k decreases at high levels of dissolved oxygen is probably due to quenching of the laser-excited oxygen by unexcited oxygen molecules.

The single most important result emerging from this investigation is that bacteria in an aqueous envi-

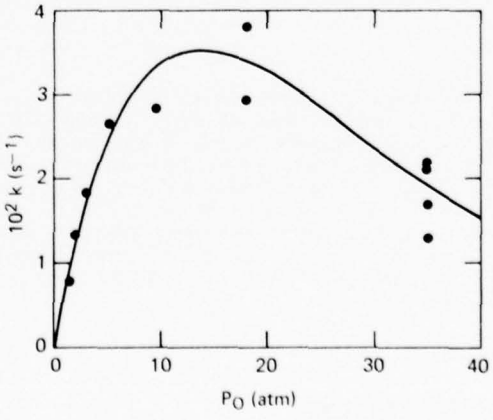

Fig. 3 Plot of effective kill rate constant, k, versus oxygen pressure.

ronment may be inactivated by interaction with dissolved oxygen excited to the $^1\Delta_g$ electronic state by means of laser radiation at 1.0642 μm. It is clear that this is not a thermal effect since in all experiments the rise in water temperature was less than 1°C. Furthermore, it is deduced that the rate of energy transfer from excited oxygen molecules averaged over the surface of a typical bacterium is negligibly small; thus damage to the organism must be highly localized, i.e., confined to the point of energy release.

Theoretical interpretation of the experimental data indicates that 10^5 collisions of $O_2(^1\Delta_g)$ molecules with a single microorganism are required for inactivation. It is to be emphasized that these experiments were performed with raw, unfiltered water samples, representative of realistic conditions. The presence of various organic and inorganic chemical substances could only shorten the collisional deactivation time, and the presence of particulate matter increases the overall optical transmission loss. Of great importance in any future research is the development of a means to measure the collisional deactivation time of $O_2(^1\Delta_g)$ in solution to permit correlation of this quantity with coliform deactivation rates for a wide variety of water samples.

The determination of the collisional deactivation time is important for another reason. It is an empirical fact that chemical substances that can quench $O_2(^1\Delta_g)$ efficiently are often high in carcinogenicity. An example of this is evidenced by experimental studies of quenching by aromatic hydrocarbons. Therefore, samples exhibiting high deactivation rates should be subjected to a thorough chemical analysis to determine whether or not potentially harmful substances are present.

In contrast to direct sterilization with radiation (as with ultraviolet at 260 nm), the process investigated here has the decided advantage that the exciting radiation is infrared and thus is unable to produce photochemical changes in substances present in the water. Also, since no chemicals are added, problems associated with disinfection using chlorine are avoided.

ACKNOWLEDGMENT

The author would like to express his gratitude to the individuals who cooperated in with work. In particular, credit is due to Mr. R. von Briesen of APL, who carried out the experimental tests, and to Mrs. B. Tonguette of the WSSC Patuxent Filtration Plant, who analyzed the water samples.

Author: J. G. Parker

Support: NAVSEASYSCOM

STEADY-STATE POLYMER COMBUSTION

The combustion of two common polymers, PVC and Teflon, was studied quantitatively. A new experimental technique was required to resolve the instantaneous stages of combustion and fix them in steady state, and a theory has been developed to interpret some of the observations. It was found that the ignition of a polymer is characterized by a critical surface temperature defined to within 1%. We also determined for PVC the chemical sequence of events taking place at ignition.

BACKGROUND

Fires commonly involve polymeric materials, solids of high molecular weights whose molecules are made up of repeating units. Some examples are fabrics, plastics, rugs, foam cushions, and wood.

Improvements in fire engineering require a scientific understanding of polymer combustion; therefore, we studied the combustion of two common polymers, PVC and Teflon. Previously, the time-dependent nature of the combustion of solids made quantitative studies difficult. Our first task was to develop a new technique to avoid this difficulty.

DISCUSSION

The method we developed, called the moving wire technique (Refs. 1 through 4), resolves the instan-

taneous stages of polymer combustion and holds them fixed in steady state (Ref. 5). In addition, it defines the ignition and extinction transitions with a precision typically better than 1%.

The polymer is coated on a supporting metal wire or glass fiber and is pulled by a variable speed motor through a stationary flame (Fig. 1). The speed is controlled to within 0.1% and is monitored. Polymer burning is then fixed with respect to a laboratory observer. The observation time is limited primarily by the supply of material, and precise measurements can be made. Samples of the solid phase (Refs. 2 and 3) may be obtained for any stage of combustion by cooling the wire rapidly as it emerges from the flame by means of a cross flow of cold helium gas. The chemical composition of gases emitted from the polymer is observed by microprobe sampling with mass spectral analysis (Ref. 3).

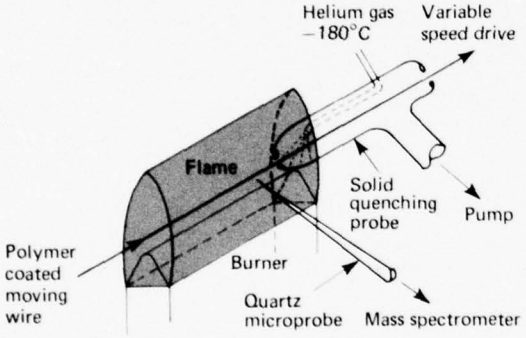

Fig. 1 The moving wire apparatus with an O_2-rich flame, showing a mass spectral sampling probe and the cold helium heat extractor.

The surface temperature of the moving wire is measured by any of three methods (Ref. 4). In the first, a thermocouple is in rubbing contact with the wire; the thermocouple is surrounded by a small oven whose temperature is adjusted to a null point. The second method makes use of thermal paints (in the nonburning regimes only). In the third, the polymer is coated directly on a thermocouple.

The application of these techniques to the combustion of Teflon (Ref. 4) reveals the behavior shown in Fig. 2. Teflon burns when its surface temperature exceeds 500°C. If the wire speed is initially too fast for the Teflon to burn but is gradually decreased, no chemical changes are observed until the surface temperature reaches 500°C. Then burning is suddenly established, the transition being reproducible to 1%. The transition temperature is independent of the heat source flame and the wire diameter.

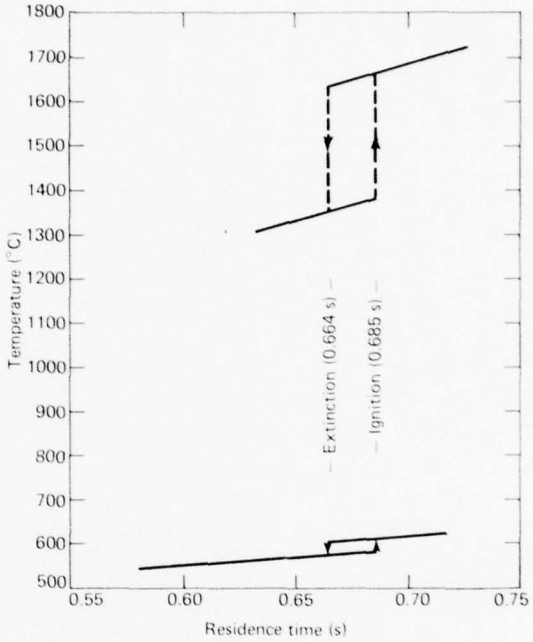

Fig. 2 Temperature hysteresis at ignition and extinction of #30 Teflon wire. Arrows on the graphs indicate irreversible transitions. The gas phase temperature (upper graph) was measured without radiation corrections by a 3-mil Pt versus Pt+10% Rh thermocouple positioned where the polymer flame front occurred. The surface temperature was measured by a null point technique.

When the technique is applied to PVC (Ref. 3), the results (Fig. 3) suggest the following behavior. As the surface temperature increases, HCl is evolved first. This gas is not flammable. Evolution of gaseous benzene begins at 295 ± 5°C. When O_2 is present in the heat source flame, the benzene is oxidized with a liberation of heat, some of which feeds back to the surface. The feedback apparently exceeds surface losses if, and only if, the O_2 level exceeds 24 ± 2%, since only then does burning occur. The concentration of benzene at ignition is less than 10^{-4} mole fraction (100 ppm).

We are currently working toward a more detailed understanding of ignition, including extensions of the theory and an improved experimental resolution of the chemical and thermal sequences of events.

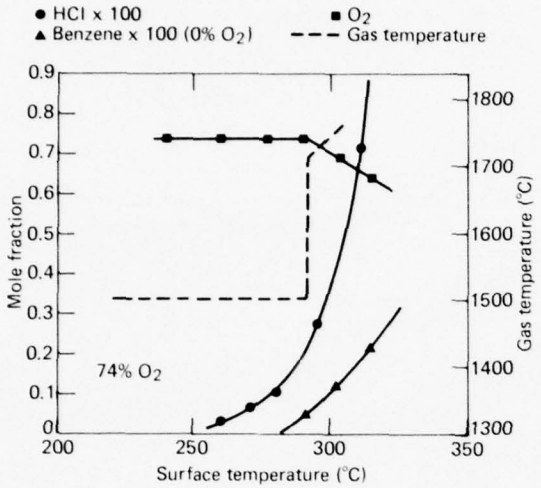

Fig. 3 Chemical and thermal sequence of events for pure PVC. The gases were sampled at the right edge of the source. The surface temperature was controlled by the speed of the wire. Flames of O and 74% O_2 are compared.

REFERENCES

1. R. M. Fristrom and C. Grunfelder, "Moving Wire Technique Studies of Ablation, Ignition and Extinction," *Fire Mater.*, 1, 1976, p. 48.
2. R. M. Fristrom, C. Grunfelder, and L. W. Hunter, "Exploratory Studies in Polymer Ablation, Ignition and Extinction by the Moving Wire Technique," *Combust. Flame*, **27**, 1976, p. 33.
3. H. Schacke, L .W. Hunter, R. M. Fristrom, and C. Grunfelder, "Combustion of PVC Studied by the Moving Wire Technique," presented at the Sixteenth Symposium (International) on Combustion, The Combustion Institute, 1976.
4. L. W. Hunter, H. Schacke, C. Grunfelder, and R. M. Fristrom, "Surface Temperature Measurements in the Moving Wire Technique," *Combust. Sci. Technol.*, **15**, 1976, p. 41.
5. L. W. Hunter, *Theory of the Moving Wire Technique for Studying Polymer Flammability. I. The Temperature in the Wire Under Forced Convection*, APL/JHU TR25, February 1976.

Authors: *L. W. Hunter, R. M. Fristrom, and C. Grunfelder*

Support: *U.S. Department of Commerce, National Fire Prevention and Control Administration*

FIRE INFORMATION

Unwanted fire is a complex problem whose solution calls for expertise in many disciplines. To promote understanding and information transfer between the various professionals engaged in fire problems and thus enhance the probability of successful solutions, a Fire Sciences Dictionary was compiled and the publication of a bimonthly Fire Technology Abstracts journal was undertaken.

BACKGROUND

In this age of change and technological innovation, there is an increasing interdependence between workers in specialized fields and a commensurate need for freer-flowing channels of communication. As each specialty grows, so does its particular vocabulary. Language intelligible to one group is likely to be gibberish to everyone else.

The difficulty with the technical literature is that specialists tend to publish their papers in journals devoted to their particular specialty and, largely because of time constraints, to follow regularly only a restricted set of journals. Thus, useful papers can be missed because they are published in unfamiliar journals. Moreover, patents, reports, and unpublished or irregular types of literature are not announced conveniently and thus are not seen by those who could benefit most from them.

The language and literature problems are so prevalent that a well-known authority in management science, Kenneth Boulding, was provoked to lament: "Physicists only talk to physicists, economists to economists, . . . [so that] one wonders sometimes if science will not grind to a stop in an assemblage of walled-in hermits, each mumbling to himself words in a private language that only he can understand."

DISCUSSION

The decision to compile a dictionary was predicated on the broad technical background held by members of the Fire Problems Program group in the research, technical, and practical aspects of the fire problem. However, background alone is insufficient to produce a useful dictionary. The intended compiler must first learn the art of lexicography. Procedures must be worked out to find appropriate terms, define them, and arrange them in order, with cross-references. To perform this task, the APL computer and the INFO–360 package of programs proved to be a boon. Use of the computer to maintain the dictionary file eliminated an enormous load of housekeeping, file cards, alphabetizing, and other manual chores. Clean drafts could be produced at regular intervals, and reciprocity loops could be checked automatically.

In 1973, a preliminary version of the dictionary contained about 5000 terms drawn from 75 fields of science, technology, and practice, ranging from anatomy to transportation. It was printed as an APL report and circulated to approximately 250 fire specialists for comment. Responses were uniformly encouraging, and the decision was made to seek a commercial publisher.

Wiley Interscience offered a contract, and work commenced on enlarging and refining the manuscript. More than 4000 terms and definitions were added. Since each term was tagged with the discipline from which it was drawn, it was a simple matter to print selected lists of terms on the computer. A panel of reviewers was organized to ensure accuracy. Medical terminology was submitted to a medical doctor, forestry terminology to a forestry specialist, fire service terminology to a fire chief, and so on. When the review was completed, the file was updated and a fair copy was delivered to the publisher for reproduction.

There is little doubt that this book will be a useful reference tool, not only for scientists and practitioners in the fire community but also for students who in ever-increasing numbers are taking courses in the fire sciences.

Efforts to organize fire literature and to make it more easily accessible to the fire community ran parallel to preparation of the dictionary. The only prior fire information reference source in English, aside from *Fire Research Abstracts and Reviews* (*FRAR*), which is devoted largely to basic research, was the monthly *Library Accession Lists* of the British Building Research Establishment's Fire Research Station and its semiannual cumulations, *References to Scientific Literature on Fire*. Unfortunately, the *Lists* have only titles and bibliographic data and lack indexes until the cumulations are published. Moreover, the subject scope is biased toward the needs of the Building Research staff.

In 1972, the Soviet *Abstracts Journal* (*Referativny Zhurnal*) began publication of a monthly reference journal, *Fire Protection* (*Pozharnaya Okhrana*), as No. 68 in its series devoted to specific information areas. Although well conceived and executed, this journal is useless unless one reads Russian.

In 1974, the documentation section (Fachdokumentation) of the Fire Protection Engineering Center at Karlsruhe University in the Federal Republic of Germany began issuing, on a small scale, a monthly set of some 100 abstracts of the world's fire literature in the form of 4– by 6–in. cards designed to become a file index. But here again language is a difficulty.

In view of the lack of an adequate fire-technology reference source in English, the staff of the Fire Problems Program of APL proposed, in 1973, a modest project of translating the Soviet *Abstracts Journal* into English. They illustrated the feasibility of this endeavor by preparing a trial issue, which was published in *FRAR* in early 1974.

Simultaneously and subsequently, other expedients were tried to help bridge the fire-literature information gap. A trial issue of *Fire Information Summaries* with journal tables of contents and meeting announcements was published in the fall of 1973. Toward the end of 1974, *Fireliter*, a fire literature review, was patterned essentially after the preceding effort but with the addition of a subject index prepared from individual words and word strings in the article titles. "Fireliter 1974" and "Fireliter 1975" were published in *FRAR*.

In the spring of 1975, APL submitted a proposal to the National Fire Prevention and Control Administration for the preparation of *Fire Technology Abstracts*, an announcement journal devoted exclusively to literature on fire technology. This proposal led to an agreement that APL would compile the journal and the Government Printing Office would publish it bimonthly.

A topical arrangement of 13 categories and a suitable number of subcategories was devised. Journal formatting was to be accomplished by means of the APL INFO–360 package of computerized text-writing programs, which allows for the generation of indexes of author, subject, source, and report number. Quality control of the journal was assured by the enlistment of prominent members of the international fire community as Editorial Advisory Board. The first issue of

Fire Technology Abstracts, Vol. 1, No. 1, was delivered in the middle of August 1976. Sample copies distributed nationally and internationally have been received with considerable favor. Publication of the first six issues by GPO is assured.

ACKNOWLEDGMENT

APL staff members who contributed to this project include W. G. Berl, R. M. Fristrom, B. E. Hess, J. B. Jernigan, and G. T. Trotter.

Authors: *B. W. Kuvshinoff and L. J. Holtschlag*

Support: *National Fire Prevention and Control Administration*

TRANSPORTATION PROGRAMS

INTRODUCTION

Efficient transportation of people and commodities has a high economic and environmental value to our society. This is illustrated by the fact that the transportation sector of the economy consumes approximately 25% of the U.S. energy budget. APL has conducted major programs to improve transportation in our urban centers since 1969. It also conducts other programs in other transportation areas including transport of bulk commodities on our inland seas and waterways.

Public transportation in the U.S. has suffered a severe decline in recent decades as a result of the dispersed travel patterns characteristic of our urban areas, the inability of public transportation to compete with the automobile in convenience and travel time, and the sharply rising labor costs of the last decade. However, because of the need to provide an alternative to the automobile, interest has increased in the development of fully automated transit systems that eventually may be able to provide a high level of service to an entire metropolitan region. Current interest in these systems has focused on their ability to provide circulation within high-activity areas, such as central business districts, large shopping and commercial areas, universities, and airports. These high-activity areas are characterized by a high level of street congestion and by trips beyond convenient walking distance but too short to be accommodated by the automobile when parking and unparking considerations are taken into account. The interest in these systems is reflected in the Federal Government's Downtown People Mover Program, which will install these automated systems in several downtown locations.

APL has been involved in two aspects of the development of a research and development effort directed at establishing the requirements and constraints of the automated control system, at investigating various approaches to solving the control problem, and at a technical support effort that provides technical assistance to public agencies in the conduct of their automated transit system programs. The following articles describe specific aspects of this work performed during the past year.

The Laboratory has been investigating for a number of years the requirements imposed upon the automated control system as the headway (i.e., the

spacing between vehicles) is reduced. This work showed that the requirements imposed by passenger comfort conflicted with the requirements imposed by safety during transitions by a vehicle from long to short headways (less than three seconds between vehicles) in such a manner as to create instabilities in the operation of a vehicle. The work by Pue describes an approach that includes these requirements in the control law and thus results in improved performance throughout the range of operating headways. This work is continuing in an effort to define the hardware requirements for the control system.

The technical support effort has assisted public agencies in planning their programs, in monitoring and reviewing system suppliers, designs, and studies, and in conducting test programs and analyzing test results on specific systems. This work has been primarily funded by the Federal Urban Mass Transportation Administration (UMTA) but also includes safety studies on automated transit for the Province of Ontario and involvement in the Baltimore City Downtown People Mover Program. An example of this work is provided by Kershner in the description of a computer model for assessing the performance of Automated Guideway Transit Systems. This model is to be used in assessing the impact of various operational policies on system performance and for examining the tradeoffs among various design parameters such as vehicle size, fleet size, operating costs, passenger service quality, and system dependability. This work is continuing as part of the UMTA Advanced Group Rapid Transit Program to provide information on the requirements imposed upon these systems by potential applications.

Reliable, uninterrupted flow of commodities is essential to the economic health of our nation. Our inland waterways have long provided a secure, low-cost means for transportation of materials and bulk. APL has participated in a continuing effort to maintain this system at the level of the currently available technology by a program, under Coast Guard sponsorship, directed at improving navigational aids on inland waterways. The specific problem addressed is that of adapting a loran-C navigational system to guiding ore carriers on the confined waters of the Great Lakes.

A STATE-CONSTRAINED APPROACH TO VEHICLE-FOLLOWER CONTROL FOR SHORT-HEADWAY AUTOMATED TRANSIT SYSTEMS

The longitudinal control of automated transit vehicles at very short headways (0.5 to 3.0 s) presents several control problems that preclude the use of a linear time-invariant feedback design. Thus, a control that is a nonlinear function of states was developed and is shown to resolve the difficulties encountered at these short headways.

BACKGROUND

Vehicle following in an automated transit system is a longitudinal control scheme wherein the state (i.e., velocity and position) of a given vehicle is determined by the behavior of the preceding vehicle. Several investigators (Refs. 1 and 2) have studied the feasibility of this approach when a linear constant-gain regulator is used to control perturbations from a nominal operating condition. Recently, Stupp et al. (Ref. 3) have shown that at time headways (i.e., the time between successive vehicles passing a fixed point on the guideway) of less than 3 s, a fundamental kinematic constraint creates bounds on vehicle motion. This constraint dictates a minimum allowable spacing between vehicles that is a function of trailing vehicle state, preceding vehicle state, and the future maneuver capability of each vehicle.

For a situation where a trailing vehicle is overtaking a slower moving preceding vehicle, it is shown (Ref. 3) that the kinematic constraint determines the point at which the trailing vehicle must switch to a closed-loop regulation mode of operation. As a result, the bandwidth requirement for the closed-loop regulator at short headways is inconsistent with the large initial values of vehicle motion; i.e., the system response to these initial conditions typically leads to violations of comfort criteria and the kinematically required spacing.

The nonlinear controller discussed below explicitly includes the kinematic constraint in the control law and consequently provides near-optimal performance while satisfying safety requirements under all operating conditions. The importance of this approach is that, for the first time, the state constraints inherent in a vehicle-following strategy are expressed as part of the control scheme. Thus, it affords a general formulation and systematic method that designers may adapt for future work.

DISCUSSION

The kinematic constraint is a result of a fundamental characteristic of vehicle following; i.e., future maneuvers of a preceding vehicle are not known by a trailing vehicle. During normal operation, safety considerations require that the trailing vehicle controller anticipate a nonemergency minimum time deceleration to minimum line speed by the preceding vehicle at any time. The time and distance required to complete such a maneuver are functions of the velocity limits (V_{min} and V_{max}), service acceleration limit (A_s), service jerk limit (J_s), vehicle velocity (V), and vehicle acceleration (A). The resulting time and distance required of each vehicle for a given set of vehicle states then determine the minimum allowable spacing (Fig. 1). The minimum spacing is given by

$$S_{min} = X_P - X_T = d_r^T - d_r^P - V_{min}(t_r^T - t_r^P) + hV_{min} \quad (1)$$

where X_P and X_T are the trailing and preceding vehicle positions, d_r^T and d_r^P are the distances required for the trailing and preceding vehicles to decelerate to minimum line speed, t_r^T and t_r^P are the times required for the trailing and preceding vehicles to decelerate to minimum line speed, and h is the desired headway.

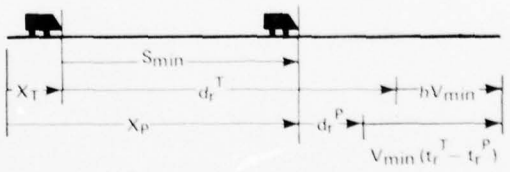

Fig. 1 Minimum spacing required by kinematics.

The term hV_{min} represents the desired spacing when both vehicles are at V_{min} with zero acceleration. Hence, it constitutes a residual term that specifies the desired spacing when the kinematically required spacing is zero. As a result, any suitable factor may be used and not necessarily hV_{min}. In fact, it will be shown that using hV_T (V_T is the trailing vehicle velocity) rather than hV_{min} simplifies the control problem. Moreover, other vehicle-following strategies may be used by including the appropriate term in the constraint function.

The kinematic constraint, $c(\mathbf{x})$, is described in terms of vehicle spacing, S, as follows:

$$c(\mathbf{x}) = S_{min} - S \leq 0 \tag{2}$$

where S_{min} is given by Eq. 1. Note that the presence of this constraint is only significant at short headways because the nominal spacing, hV_T, typically is less than S_{min}. As h becomes larger, the nominal spacing always exceeds the minimum required spacing and the constraint may be ignored.

The vehicle following problem may now be formulated into the optimal regulator with a linear plant and an infinite time integral quadratic performance index. That is, a plant of the form

$$\dot{\mathbf{x}} = A\mathbf{x} + \mathbf{b}u \tag{3}$$

is assumed, where $\mathbf{x}$ is the n-dimensional state vector, u is the scalar control, A is a constant $n \times n$ matrix, and $\mathbf{b}$ is a constant n-dimensional vector. The performance index is of the form

$$I = \int_0^\infty \left[\mathbf{x}^T Q \mathbf{x} + \frac{1}{2} u^2 \right] dt \tag{4}$$

where Q is a constant positive semidefinite $n \times n$ matrix. In addition, a constraint vector is given by

$$\begin{bmatrix} |A| \\ |J| \\ c(\mathbf{x}) \end{bmatrix} \leq \begin{bmatrix} A_s \\ J_s \\ 0 \end{bmatrix} \tag{5}$$

where A is vehicle acceleration and J is vehicle jerk.

The design problem is to minimize Eq. 4 subject to Eqs. 3 and 5 with the aim of producing an instrumentable solution. Saridis (Ref. 4) presents an approximate solution based on observations of the geometric features of the optimal constrained trajectories. A dual-mode controller is proposed such that the system follows the optimal unconstrained trajectories determined by the steady-state Ricatti equation when the presence of the constraint has little effect upon the solution. When the unconstrained solution tends to violate the constraint, a nonlinear mode is introduced to keep the solution on the boundary of the constraint region. The technique may be adapted to the present problem with some modification.

A triple integration plant is assumed, with the state equation given by

$$\dot{\mathbf{x}} = A\mathbf{x} + \mathbf{b}J_T + gJ_P$$

where

$$\mathbf{x} = (S \; V_T \; A_T \; V_P \; A_P)'$$

and A_P, V_P, and J_P are the preceding vehicle's acceleration, velocity, and jerk, respectively. The prime denotes transpose. The control input to the trailing vehicle is a jerk command, J_T. If the initial states are such that $c(\mathbf{x})$ is zero, then a necessary and sufficient condition for $c(\mathbf{x})$ to remain zero is that its time derivative is zero or

$$J_T = -(\nabla c' \mathbf{b})^{-1} \nabla c' (A\mathbf{x} + \mathbf{g}J_P) \; . \tag{6}$$

This constitutes the nonlinear mode of the dual-mode controller proposed by Saridis. Rather than solving for the linear gains in the unconstrained problem, however, an on-limits jerk command is used at a specified distance from the kinematic constraint boundary. The controller structure then takes the form shown in Fig. 2.

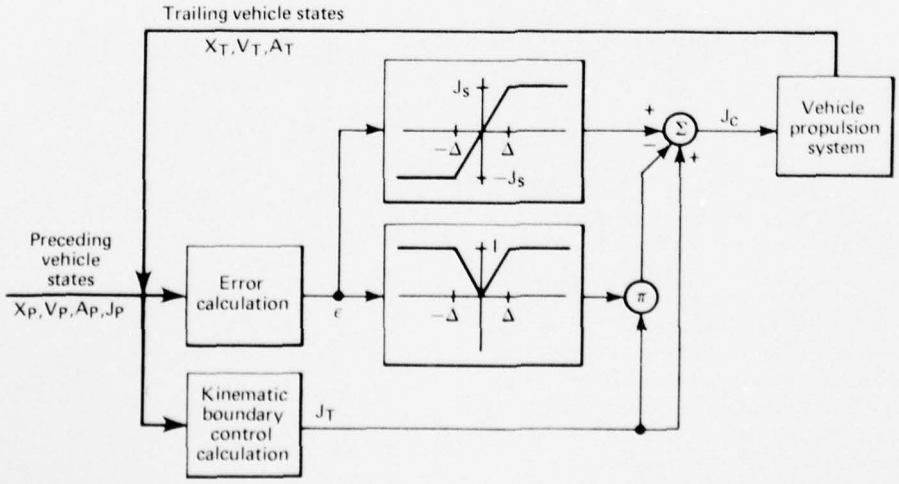

Fig. 2 Controller structure.

The error calculation consists of determining the difference, $\varepsilon = -c(\mathbf{x})$, between the actual vehicle spacing and the kinematically required spacing. When this error is zero, the kinematic boundary control given by Eq. 6 is implemented ($J_c = J_T$). When it is less than zero, the vehicle is violating the constraint (i.e., it is too close). The negative jerk limit is gradually applied until, when the error is $-\Delta$, the on-limit negative jerk command becomes the input to the system ($J_c = -J_s$). Similarly, when the error is greater than zero, the vehicle is safely satisfying the kinematic constraint and a positive jerk may be applied ($J_c = J_s$). The parameter Δ, effectively a gain in the system, is selected through consideration of closed-loop stability using a describing function analysis (Ref. 5).

The kinematic constraint (Eq. 2) may be modified to replace the desired final spacing, hV_{min}, with hV_T. Therefore, the kinematic boundary will coincide with the nominal operating headway and the controller will act to maintain the desired spacing for any value of V_P greater than V_{min}.

The performance of this controller has been evaluated by means of computer simulations for a variety of circumstances (Ref. 5). It reacts properly to any nominal maneuver of a preceding vehicle during both an overtake situation and at the desired headway while precisely maintaining the kinematically required spacing. As seen in Eq. 6, however, the informational requirement consists of the complete state vector, $\mathbf{x}$, and the preceding vehicle jerk, J_p. This requirement may be reduced by simplifying the kinematic constraint so that the resulting control will always keep the vehicle outside the actual kinematic boundary but will require less information. As a result, a variety of suboptimal controls may be generated where each increasingly simplified controller takes progressively longer to complete a maneuver (Ref. 5).

The simplest controller consists of a kinematic boundary control law that is a linear combination of error states (i.e., spacing, relative velocity, relative acceleration) and trailing vehicle states. An example of its implementation in a five-vehicle string is shown in Fig. 3. Initially, the first two vehicles are spaced 100 m apart while the remaining vehicles are spaced 50 m. The lead vehicle is traveling at 15 m/s and the four following vehicles have velocities of 25 m/s. At 20 s, the lead vehicle decelerates on limits to 10 m/s, where the jerk and acceleration limits are set at 2.6 m/s^3 and 2.6 m/s^2, respectively. All trailing vehicles respond appropriately to the maneuver and decelerate to 10 m/s. If each vehicle had not been at the proper spacing as demanded by the kinematic con-

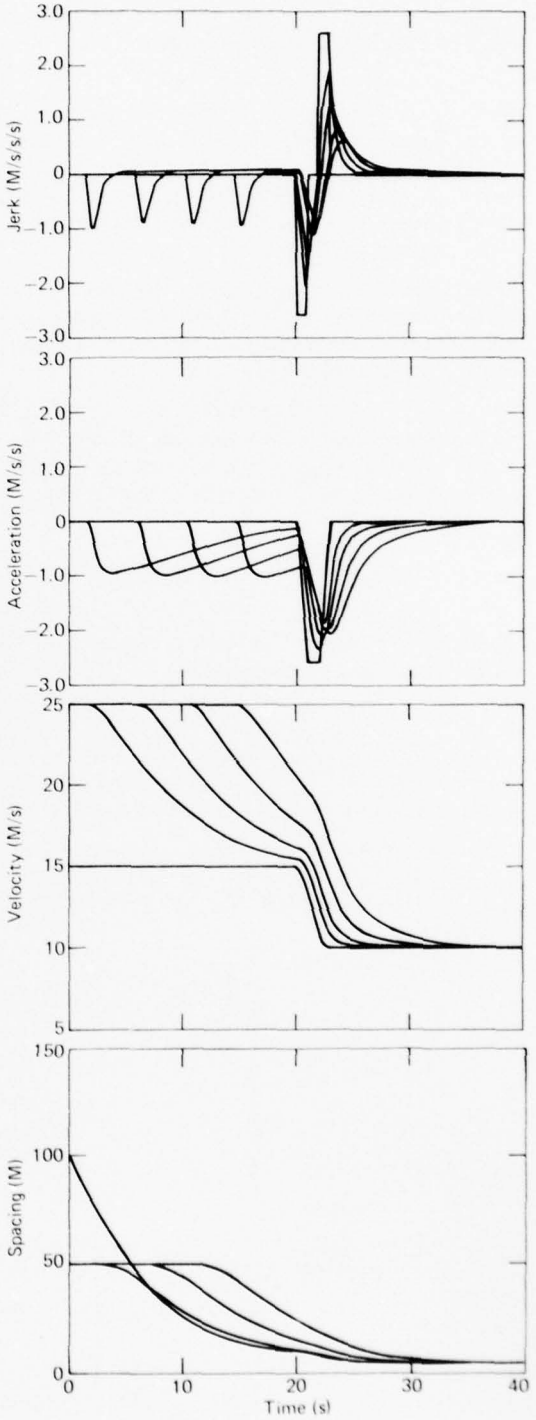

Fig. 3 Response of five-vehicle string with headway of 0.5 s.

straint, collisions would have occurred. Also note that the response exhibits string stability, i.e., disturbances do not propagate with increasing amplitude through the vehicle string.

In conclusion, a vehicle following control law has been designed that explicitly considers the state constraints defining the capabilities of each vehicle as determined by the jerk and acceleration limits imposed to assure passenger safety and comfort. These constraints lead to an approximately optimal nonlinear controller design that may satisfactorily control transient events such as overtaking a slower moving vehicle at short headways.

The major advantage of the state constrained approach would be to provide uniformity in control for a variety of situations such as merging, emergency operation, and overtaking a preceding vehicle. Consequently, it suggests a simplified controller as opposed to a collection of ad hoc procedures to handle these conditions.

REFERENCES

1. S. J. Brown, Jr., "Design of Car-Follower Type Control Systems with Finite Bandwidth Plants," *Proceedings of the Seventh Annual Princeton Conference on Information Sciences and Systems*, March 1973.
2. E. P. Cunningham and E. J. Hinman, "Approach to Velocity/Spacing Regulation and the Merging Problem in Automated Transportation," presented at the Joint Transportation Engineering Conference, Chicago, IL, October 1970.
3. H. Y. Chiu, G. B. Stupp, and S. J. Brown, "Vehicle-Follower Control with Variable-Gains for Short Headway AGT Systems," presented at the Fourth Intersociety Conference on Transportation, Los Angeles, CA, July 1976.
4. G. N. Saridis and Z. V. Rekasius, "Design of Approximately Optimal Feedback Controllers for Systems with Bounded States," *IEEE Trans. Autom. Control*, AC-12, No. 4, August 1967.
5. A. J. Pue, *A State Constrained Approach to Vehicle-Follower Control for Short Headway AGT Systems*, APL/JHU TPR-038, August 1977.

Author: *A. J. Pue*

Support: *Urban Mass Transportation Administration*

A PERFORMANCE ASSESSMENT TOOL FOR AUTOMATED GUIDEWAY TRANSIT SYSTEMS

The planning and preliminary design of Automated Guideway Transit (AGT) for urban applications requires decisions concerning subsystem design approaches and performance specifications. A computer model developed to perform these studies relates system-oriented and passenger-oriented performance measures to system design characteristics and operating policy options.

BACKGROUND

AGT is currently under consideration at both the local and federal levels as a future mode of urban transportation. The systems are characterized by vehicles of small to intermediate capacity (6 to 40 passengers) operating under fully automatic control over a network of dedicated rights-of-way. The development status of AGT systems ranges from conceptual design to fully operational systems in special-purpose applications (e.g., airports, college campuses, and amusement parks). Near-term urban deployment of AGT is anticipated under the Urban Mass Transportation Administration's Downtown People Mover Program. Four cities have been chosen for preliminary design studies of AGT systems used in downtown circulation.

Because AGT is a new and undemonstrated form of urban transit technology, its performance, design, and operating tradeoffs and interactions are not well established. The planning, development, and acquisition of an urban AGT system involves both the system owner/operator and system developers in an iterative design process (Fig. 1). The objective of the process is to decide on a mutually acceptable design configuration, set of performance specifications, system cost, and construction schedule. Many alternative network configurations, system design characteristics, and operating policies must be evaluated. The computer model developed in this study provides a tool for the operator and system developer to use in these evaluations. A more complete description of the model and a demonstration of its application in the evaluation of two types of AGT network configurations are presented in Ref. 1.

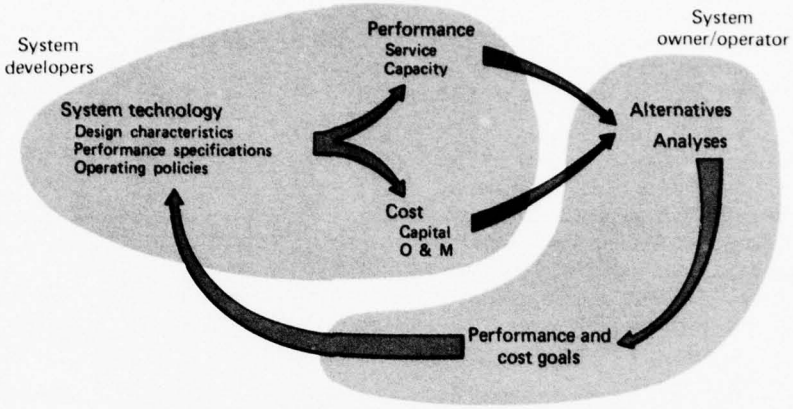

Fig. 1 AGT design process.

DISCUSSION

The AGT performance assessment model is structured to provide an effective, low-cost method for performing design-performance tradeoff studies in the planning and preliminary design stages for an urban AGT system. The model assumes steady-state operating conditions and requires a description of the AGT system at the major subsystem level. This level of analysis is appropriate for preliminary design purposes when many design alternatives and operating policy options are evaluated for a variety of network configurations and demand models.

The assessment model consists of four program modules (Fig. 2). The first module creates data files containing descriptions of the network characteristics, the travel demand data, and the "shortest paths" between all station pairs in the network. The second develops a system of service routes that are consistent with the operating policy parameters input to the module by the user. The third allocates service frequencies (vehicles per hour) to each route by formulating and solving a linear programming problem that minimizes vehicle-miles traveled, subject to constraints on route demand, link capacity, and conservation of flow. The fourth computes the resulting system operating statistics, passenger service measures, and system dependability measures. The dependability measures are computed by incorporating the trip dependability model of Ref. 2 in the program module.

The model has been applied to assess the performance characteristics of AGT systems in a variety of network configurations. The studies demonstrated the sensitivity of system performance to operating policy parameters and to vehicle capacity. The rate at which vehicles can be processed through stations was identified as potentially being the most limiting factor to AGT system capacity. System dependability is a key factor in the success of urban AGT applications. The potential improvement in system dependability resulting from more reliable equipment and from the implementation of techniques to expedite recovery from a system malfunction was investigated.

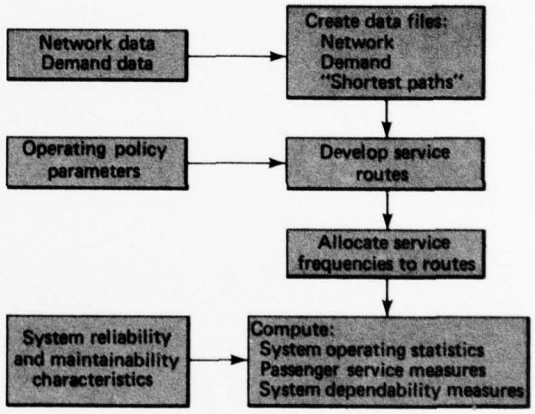

Fig. 2 AGT performance assessment model.

One of the network configurations evaluated is shown schematically in Fig. 3. Consisting of approximately 200 lane-miles of guideway and 58 station locations, it includes a downtown circulation section, multiple line-haul corridors, and several circumferential lines for direct corridor-to-corridor travel. The morning peak travel demand was assumed to be 61 000 passengers per hour.

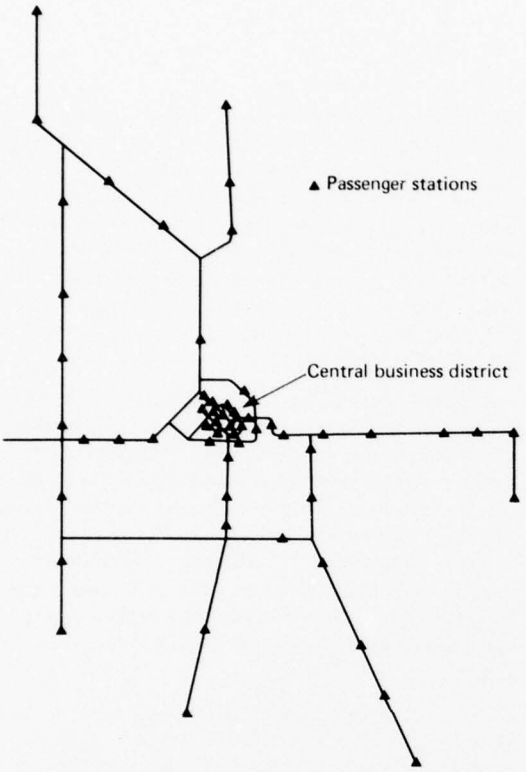

Fig. 3 Configuration of an urban regional AGT network.

This network was studied to compare the performance of 12– and 24–passenger vehicles. More than 300 service routes were generated by the model to satisfy the operating policy constraints that all station-to-station trips have a maximum waiting time of five minutes, a maximum of six stops at intermediate stations, and no vehicle transfers. The results of the comparison are presented in Table 1. Although the levels of service are nearly equivalent for both vehicle sizes, the traffic management problem is substantially reduced with 24–passenger vehicles because of the smaller link and station flows. In addition, the dependability of service, as measured by the probability of a delay-free trip, was significantly greater for the larger vehicles (vehicle failure rates were assumed to be equal for the two sizes).

TABLE 1
COMPARISON OF SYSTEM PERFORMANCE FOR 12– AND 24–PASSENGER VEHICLES

Vehicle Capacity	12–Passenger	24–Passenger
Link flow (vehicles/hour)		
Maximum	1100	700
Average	583	400
Station flow (vehicles/hour)		
Maximum	678	359
Average	385	252
Fleet size (vehicles)	3135	2121
Vehicle-miles/hour	89 130	61 050
System load factor	0.42	0.31
Passenger service		
Average waiting time (minutes)	1.2	1.8
Average trip speed (mph)	27.9	26.7
Average No. of intermediate stops	1.8	1.7
Average excess trip time (minutes)	3.0	3.5
System dependability		
Average probability of delay-free trip	0.88	0.93

REFERENCES

1. D. L. Kershner, "An Assessment of Group Rapid Transit System Operating Characteristics," *Proceedings of the Fourth Intersociety Conference on Transportation*, Los Angeles, July 1976.
2. D. L. Kershner and W. J. Roesler, *Models for Assessing Trip Dependability in Automated Guideway Transit Networks*, APL/JHU CP 047/TPR 036, August 1976.

Author: *D. L. Kershner*

Support: *Urban Mass Transportation Administration, Contract DOT–UT–30010*

ST. MARYS RIVER COGLAD NAVIGATION SYSTEM

An APL-developed Coast Guard Loran Assist Device (COGLAD) was improved and used to provide continuous navigation guidance in field tests aboard Coast Guard vessels from January through July 1976. A short-baseline loran–C was used in these tests for the first time as an aid to piloting large vessels between Lake Superior and Lake Huron via the St. Marys River. The overall position accuracy of the system in a selected area of the river was 30 to 45 ft.

BACKGROUND

The St. Marys River forms part of the United States and Canadian border and links Lake Superior and Lake Huron. Throughout much of the 65 mi of river, large vessels (up to 1000 ft in length and 105 ft in beam) are confined to dredged channels no more than 300 ft in width. To facilitate movement of the large volume of traffic, the Coast Guard maintains an extensive array of buoys, day beacons, and visual ranges as well as a radio vessel reporting system. However, to extend the winter shipping season, additional piloting aids are needed to compensate for frequently poor visibility, buoys removed or pushed under the ice, and confusing radar returns because of ice ridges.

In 1967, APL developed a Loran Assist Device (LAD) for a military operation that required precision guidance of aircraft. Since then, APL has developed a number of newer, more sophisticated versions of the original LAD. In 1970, the Coast Guard funded APL to develop a civilian version that became known as COGLAD (Ref. 1). Two COGLAD systems were eventually built for the Coast Guard and have been used experimentally for positioning buoys in Lake Huron, ice patrol in the North Atlantic, and oceanographic research in the Gulf Stream. COGLAD was patented by APL in 1974, and the patent was signed over to the Government to ensure that the technology would remain available to all. One of the COGLAD systems (Ref. 2), specifically modified in late 1975, was used for testing aboard Coast Guard vessels on the St. Marys River from January through July 1976.

DISCUSSION

The St. Marys River loran minichain operated by the Coast Guard is identical functionally to a conventional loran–C chain except that it has shorter baselines (i.e., the transmitters are closer together) and uses lower-power transmitters. Four transmitters are used in a diamond configuration, two in Michigan and two in Ontario, Canada. The use of short baselines assures good signal strength within the coverage area and minimizes propagation and skywave distortion problems. The design goal stated by the Coast Guard was to determine a boat's cross-track position (i.e., left or right of channel) with an accuracy of ±25 ft 95% of the time.

Utilizing loran–C for precision guidance is basically a two-step process: data measurement and data transformation. Three or more loran transmitters and a suitable receiver provide the raw data for a position fix. Navigation with the raw data is awkward because the lines of position are hyperbolic curves and the units are microseconds of difference in time of arrival. Manual reduction of these data to a position fix (when loran charts are available) negates much of the true potential of loran–C, especially in speed and accuracy.

The data transformation step consists of using some form of processor to transform the raw data mathematically into a form usable for navigation and piloting. In the art of piloting, the most meaningful position information is position relative to a known point, an intermediate way point, or a final destination.

The entire St. Marys River from Whitefish Bay to De Tour Passage can be described as a series of 25 to 28 straight line segments where each segment is the center line of its respective channel. The intersection of the center lines of two adjacent channels has been defined as an intermediate way point. Each of the way points for the river has been numbered, and the loran coordinates have been surveyed. The loran coordinates are stored in the extended memory of the COGLAD system, and continuous navigation guidance relative to known points can be provided for the entire St. Marys River.

It was found that the most precise loran coordinates of the way points could be measured in the winter when the river is frozen. When a boat is stopped in the ice, neither current nor wind move the boat off station while loran coordinates are being measured.

A special display unit mounted on the bridge provides along-track distance to the way point in statute miles, cross-track distance relative to the center line of the channel in feet, along-track speed in miles per

hour, cross-track speed in feet per second, bearing angle to the next way point, time to the next way point in minutes, and the number of the way point. For evaluation purposes, an X–Y plotter and a digital printer are also part of the system. Figure 1 shows the COGLAD navigation system, and Fig. 2 is a system block diagram.

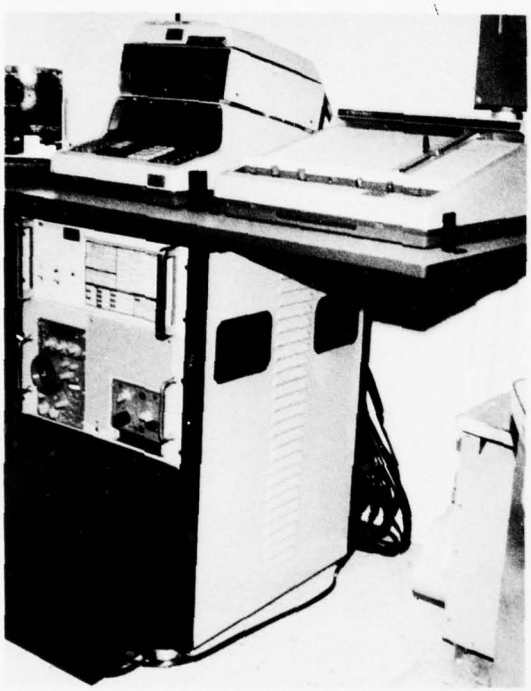

Fig. 1 COGLAD navigation system.

Prior to field testing, it was expected that the large ore carriers would cause local distortions in the loran grid and degrade accuracy during a passing situation. Numerous tests have been conducted and no such distortion has been observed to date. Distortions while vessels are passing through the Soo Locks are also much less than expected. Only under the International Bridge at Sault Ste. Marie were the signals observed to be significantly distorted. Other distortions in the loran grid observed in parts of the river were probably caused by power lines along the shore.

Figure 3 is a comparison of COGLAD and Autotape position data. Autotape is a line-of-sight radio ranging device that was used as a local reference. This track plot was made with the CGC *Naugatuck* downbound just south of Six Mile Point and steering on a visual range. The difference in cross-track distance

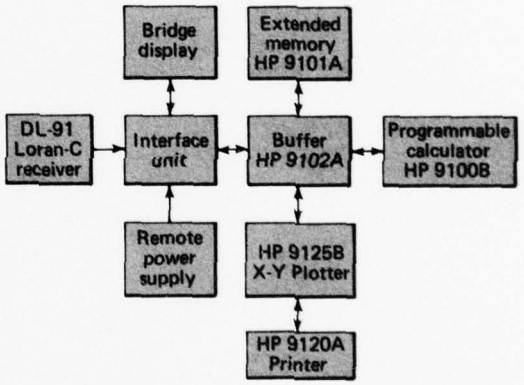

Fig. 2 Block diagram of COGLAD navigation system.

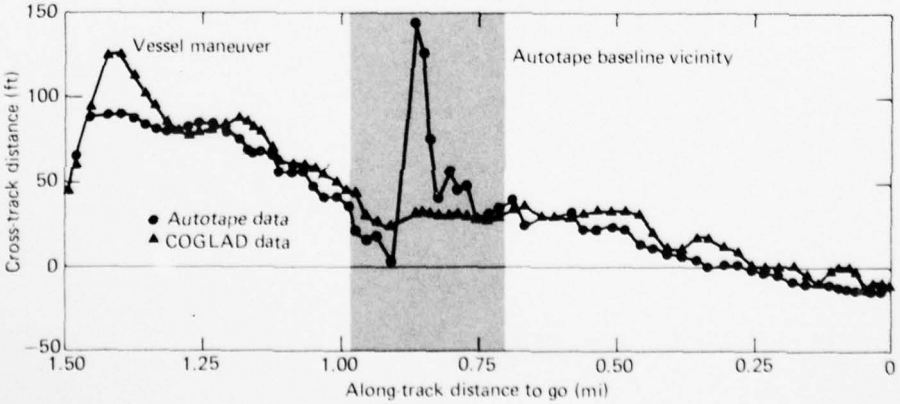

Fig. 3 Comparison of COGLAD and Autotape position data.

measured by the two systems is typically less than 15 ft. Except in areas of the river with known loran grid warpage, the overall system position accuracy was 30 to 45 ft 95% of the time.

REFERENCES

1. R. C. Moore, C. R. Edwards, R. K. Burek, and G. D. Wagner, *COGLAD: A Coast Guard Loran-C Assist Device*, APL/JHU CP 026, March 1973.
2. C. R. Edwards, R. C. Moore, and G. E. Baer, *St. Marys River COGLAD Navigation System Final Report*, APL/JHU CP 055, February 1977.

Authors: *C. R. Edwards, R. C. Moore, and G. E. Baer*

Support: *U.S. Coast Guard*

OCEAN RESEARCH

AD-A057 267 JOHNS HOPKINS UNIV LAUREL MD APPLIED PHYSICS LAB F/G 5/2
DEVELOPMENTS IN SCIENCE AND TECHNOLOGY.(U)
1976
UNCLASSIFIED APL/JHU/DST-4 N00017-72-C-4401
NL

2 OF 2
AD
A057 267

END
DATE
FILMED
9-78
DDC

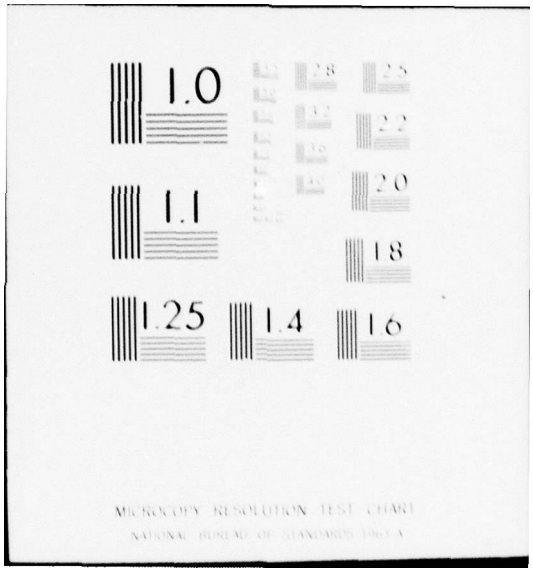
1.0
1.1
1.25
1.4
1.6
2.0
2.2
2.5
2.8
3.2
3.6
4.0
MICROCOPY RESOLUTION TEST CHART
NATIONAL BUREAU OF STANDARDS 1963-A

INTRODUCTION

An understanding of the physics of the ocean environment is essential to APL's mission in support of the Fleet. This includes, for example, electromagnetic and acoustic radiation propagation, absorption and scattering both within and at the surface of the ocean, hydrodynamic phenomena such as surface and internal waves, currents, etc., and the effects of physical variables such as water temperature, pressure, salinity, and density on ocean dynamic phenomena. Central to this effort is the development of sensing and data processing systems to detect and characterize signals propagated through or at the surface of the ocean. While analysis, simulation, and laboratory research are extremely useful, many phenomena of interest must be studied at sea. APL has accordingly developed a major capability to conduct large-scale scientific studies in the open ocean.

Much of the ocean research is not reported here for reasons of national security, but a small sample has been selected to illustrate different areas of interest. Theoretical studies are exemplified by a mathematical analysis of vertical flow generated by a moving submerged body under specified conditions. The design and operational evaluation of a more accurate, reliable, and durable towed thermistor chain to measure water temperature over a range of depths is illustrative of the extraordinary problems of developing instrumentation for scientific research at sea. The scattering of incident radiation—optical, radar, or sonar—from a rough surface is important both for direct observation of the ocean surface and because it may interfere with low-angle observations made above or below the surface. Understanding in this area is being enhanced both by development of more powerful theoretical analysis methods and by improved techniques for processing experimental data to yield two-dimensional, time-dependent surface wave spectra.

While APL's increasing expertise in ocean physics has to date been applied to Navy problems, it should be available in the future to enhance scientific understanding of the ocean environment and assist in its peaceful exploitation. Site surveys for optimum ocean thermal energy plant-ship locations is one example of many possible applications.

STEADY-STATE OSCILLATIONS IN A BUOYANT FLUID

Exact solutions have been found for the problem of fluid motion induced by small steady oscillations of various bodies immersed in a stratified fluid. We are able to show that as the buoyancy frequency is approached from above, the velocities become strongly vertical and approach strictly vertical limiting flows. These results may help in understanding the generation of surface disturbances by submerged bodies moving through stratified fluids such as the ocean.

BACKGROUND

The study of problems in the theory of stratified fluids is motivated by a need to understand the behavior of atmospheric and oceanographic flows in which the stratification and gravity introduce significant buoyant forces. When a fluid of variable density is acted on by gravity, the displacement of the heavier fluid by the lighter brings buoyant forces into play, and the movement of such a stratified fluid is also properly called a buoyant flow. Among such flows of practical interest are the induced movements caused by the displacement of submerged bodies in the ocean, which is a slightly stratified fluid.

Although buoyant flows have been widely investigated by hydrodynamicists for many years, only the simplest problems have been solved, and many phenomena remain poorly understood.

Recently we have solved exactly the problem for oscillatory translations and expansions of spheres and of long horizontal cylinders. As the frequency increases, the solutions approach those of nonbuoyant flow. On the other hand, as the buoyancy frequency is approached from above, the velocities become strongly vertical and approach strictly vertical limiting flows. These limiting flows suggest that the limiting vertical velocity above and below the body is independent of the vertical dimension and is determined solely by a boundary condition on the surface of the body.

DISCUSSION

Our results are best summarized in the figures. Figures 1 and 2 show how the flowfields change with

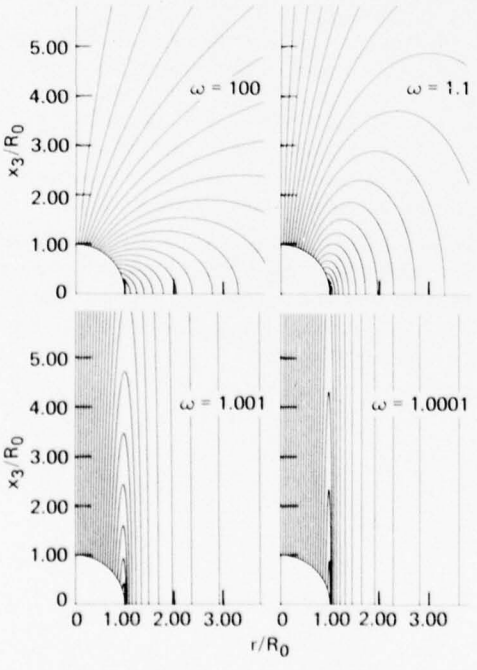

Fig. 1 Streamlines for a vertically oscillating sphere.

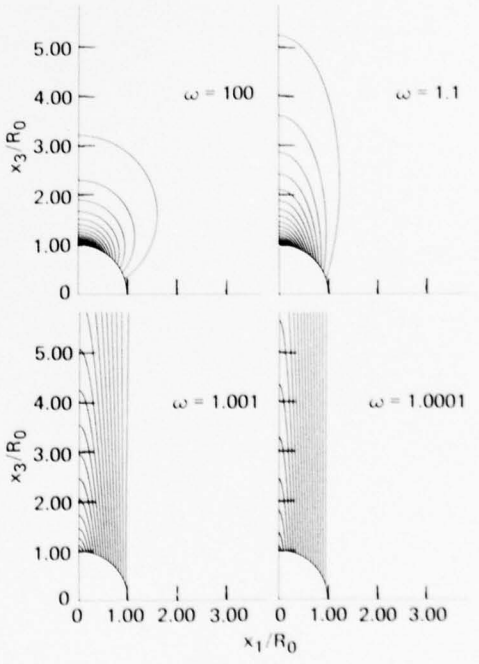

Fig. 2 Streamlines for a horizontally oscillating cylinder.

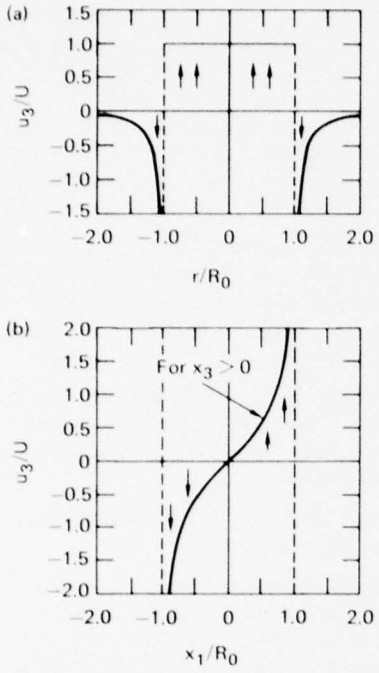

Fig. 3 Limiting velocities of (a) vertically oscillating sphere and (b) horizontally oscillating horizontal cylinder.

the frequency of oscillation; Fig. 3 shows the limiting velocities at the buoyancy frequency.

Because of space considerations, we give only the results for the vertically oscillating sphere and the horizontally oscillating cylinder. In the following, ω is the ratio of the oscillation frequency of the body to the buoyancy frequency of the fluid, R_0 is the radius of the sphere or cylinder, and x_3 is the vertical spatial coordinate.

The graphs of the flowfields have many features in common. For large values of the frequency (i.e., $\omega \geq 10$), the streamlines are nearly indistinguishable from those for nonbuoyant flow. For frequencies within 10% of the buoyancy frequency, the vertical tendency is apparent; as the buoyancy frequency is approached, this effect dominates the flow.

Figure 1 shows a slice through the stream surfaces for the vertical oscillation of a sphere. The cut is made by a plane through the x_3 axis. Figure 2 has two interpretations. It gives the streamlines in the plane containing the x_3 axis and the direction of motion for a horizontally oscillating sphere; it also gives the streamlines for a horizontal circular cylinder with the x_2 axis oscillating in the x_1 direction. The labels on these graphs are consistent with the second interpretation.

For each graph, the values of the stream function of the streamlines shown are taken on the surface for values of r/R_0 or x_1/R_0 ranging from 0.05 to 0.95 in steps of 0.05.

Figure 3 shows the limiting velocities in the examples as ω approaches 1^+. Figure 3a shows the limiting velocity produced by the vertically oscillating sphere. It is uniform above the sphere and has a return flow outside the vertical cylinder generated by the sphere. Figure 3b has two interpretations: the velocity above a horizontally oscillating sphere in the plane defined by its vertical axis and its direction of motion, and the velocity above a horizontal circular cylinder oscillating horizontally perpendicular to the axis of the cylinder. The velocities below the horizontally oscillating sphere and cylinder are the negatives of those above.

REFERENCES

1. D. W. Fox, "Transient Solutions for Stratified Fluid Flow," *J. Res. Nat. Bur. Stand.*, **80B**, No. 1, 1976, pp. 79–88.
2. D. W. Fox and V. G. Sigillito, "Steady State Oscillations in a Buoyant Fluid," *Z. Angew. Math. Phys.*, **27**, 1976, pp. 757–773.

Authors: ***D. W. Fox and V. G. Sigillito***

Support: ***NAVSEASYSCOM***

DEVELOPMENT OF A THERMISTOR CHAIN

A new thermistor chain for measurement of ocean temperature distributions has been developed by APL. It has been used successfully in tests and has achieved higher levels of accuracy, precision, and mechanical reliability than previous thermistor chains. An accuracy of 0.01°C and a precision of 0.001°C have been achieved.

BACKGROUND

The scientific study of underwater mixing processes in the ocean requires a special apparatus for measuring the water temperature at various depths and horizontal positions. One such system, called a thermistor chain, is a towed cable with thermistors to measure temperatures at different depths along the cable.

Research at APL on the dynamics of sea water mixing where there are thermal and salinity gradients required a thermistor chain with an accuracy of 0.01°C rms, a precision of 0.001°C rms, a temperature range of 20 to 30°C, and a response time constant ($1/e$) of 100 ms at a depth of 600 ft and a towing speed of 4 to 8 kt. These requirements could not be met by any previous thermistor chains.

In addition, thermistor chains typically have been subject to severe mechanical and electrical reliability problems because of the many wires required for the thermistors and the difficulty in preventing twisting and crushing of insulation during deployment and recovery.

DISCUSSION

The solution to the mechanical and electrical reliability problems was found in the use of special plastic fairings for the tow cable. Fathom Oceanology, Ltd., has pioneered in underwater tow cables consisting of a unique plastic fairing system, flexible polyurethane noses, and rigid ABS tails, segmented in short lengths for passage over sheaves and storage on winch drums. Our concept of the thermistor chain uses the Fathom nose and tail pieces as carriers for the thermistors and the thermistor cable, the assembly being free to rotate about the axis of the tension cable. The advantages of this system are:

1. The thermistors are always oriented forward by the hydrodynamic stability of the fairing and are not bothered by eddies or stagnant flow as they might be aft of a cable;
2. Rotation of the tension cable under the tow load does not damage the thermistor system because there is no interconnection of the two elements; and
3. The tail section of the fairings can be used as a carrier for the cables to service the thermistors and other instrumentation if appropriate slack is provided for passage over sheaves, etc.

Use of the fairing has the further advantage that the drag of the cable is reduced dramatically; the cable trails only 150 ft when it is deployed to 700 ft and towed at 4 kt.

Figure 1 shows the full thermistor chain deployed from the APL Research Vessel *Cape*.

Fathom Oceanology designed and built a special winch, storage drum, and fairings for APL. We then assembled the 750-ft cable with the nose and tail-fairing segments (each 4 in. long) and the 32 thermistor stations. Figure 2 is a cross section of the cable.

The tail pieces carry one cable bundle of 39 pairs of #30 Tefzel-insulated wire to service 32 thermistor stations (including spares) and, in a separate bundle, 36 pairs of wires for fluorometers and pressure transducers.

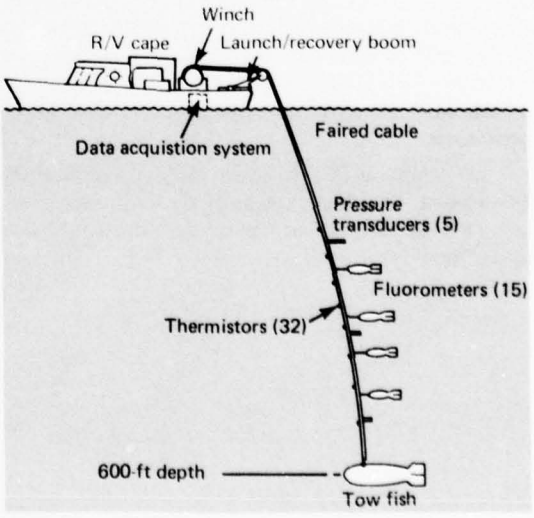

Fig. 1 Thermistor chain deployed from the APL Research Vessel *Cape*.

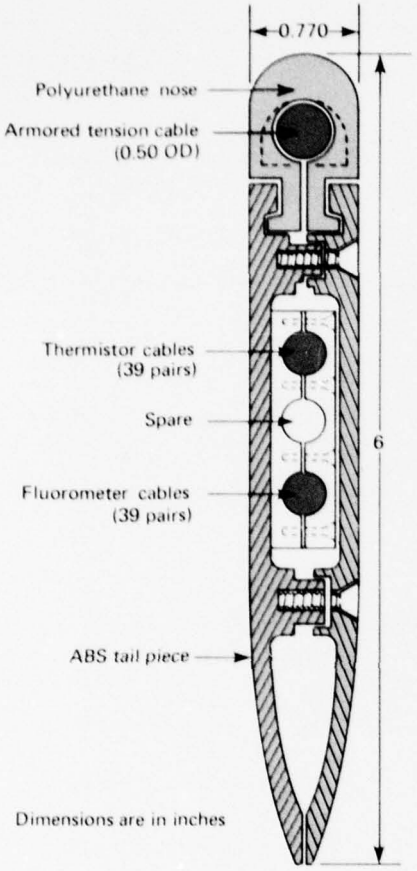

Fig. 2 Cross section of chain assembly.

The thermistors are cast into short (1.3 in. long) nose-piece segments (Fig. 3). The electronics to obtain accurate temperature data from the thermistors was designed and built by Sippican Corporation using techniques they developed for the expendable bathythermograph (XBT).

RESULTS

Preliminary sea trials began in November 1975. Some problems were encountered with "kiting" of the cable, especially at 8 kt. This means the cable tended to be towed off to one side rather than directly aft and is attributed to a slight asymmetry in the fairing assembly. Extreme kiting caused the cable to come out of the tow sheave and damage some

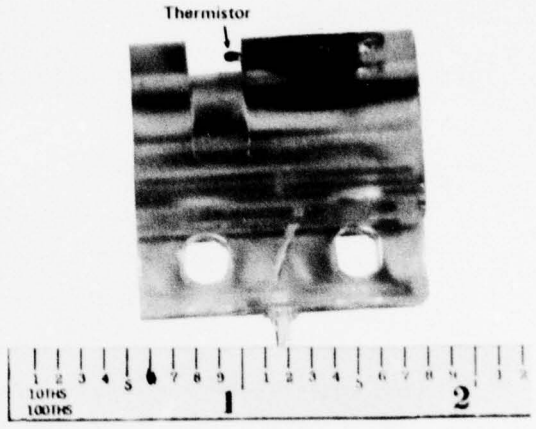

Fig. 3 Thermistor nose piece.

fairings. A special hanging sheave was built, and aluminum trim tabs were added to the fairings at 3-ft intervals. With these changes, towing at 8 kt was successful.

Operation Coral Trails began in January 1976 on the Underwater Tracking Range off the west coast of St. Croix, Virgin Islands. The chain was used for 15 days without substantial failures although frequent minor repairs to replace leaky connections were necessary.

Figure 4 is a typical computer plot of thermistor chain data. We believe the chain data are accurate to ± 0.01°C, as was desired. The typical thermistor had a time constant of 180 ms at 4 kt in sea water, which is slower than was desired. We have experimented with smaller thermistors (0.030-in. diameter vice 0.060-in.) and achieved a 50-ms response time. Thermistor T-12 of Fig. 4 is one of the faster thermistors.

ACKNOWLEDGMENTS

The success of this effort is due to the contributions of many individuals, especially K. Gardner and T. Slupski of Fathom Oceanology; C. Pierce and B. Tirrell of Sippican; and R. Strider, R. Miller, and R. Johnson of APL. The Program Manager for this work is Dr. F. S. Billig, of APL. A. C. Sadilek, C. J. Gundersdorf, and D. Speranza of APL shared responsibility for the development with the author.

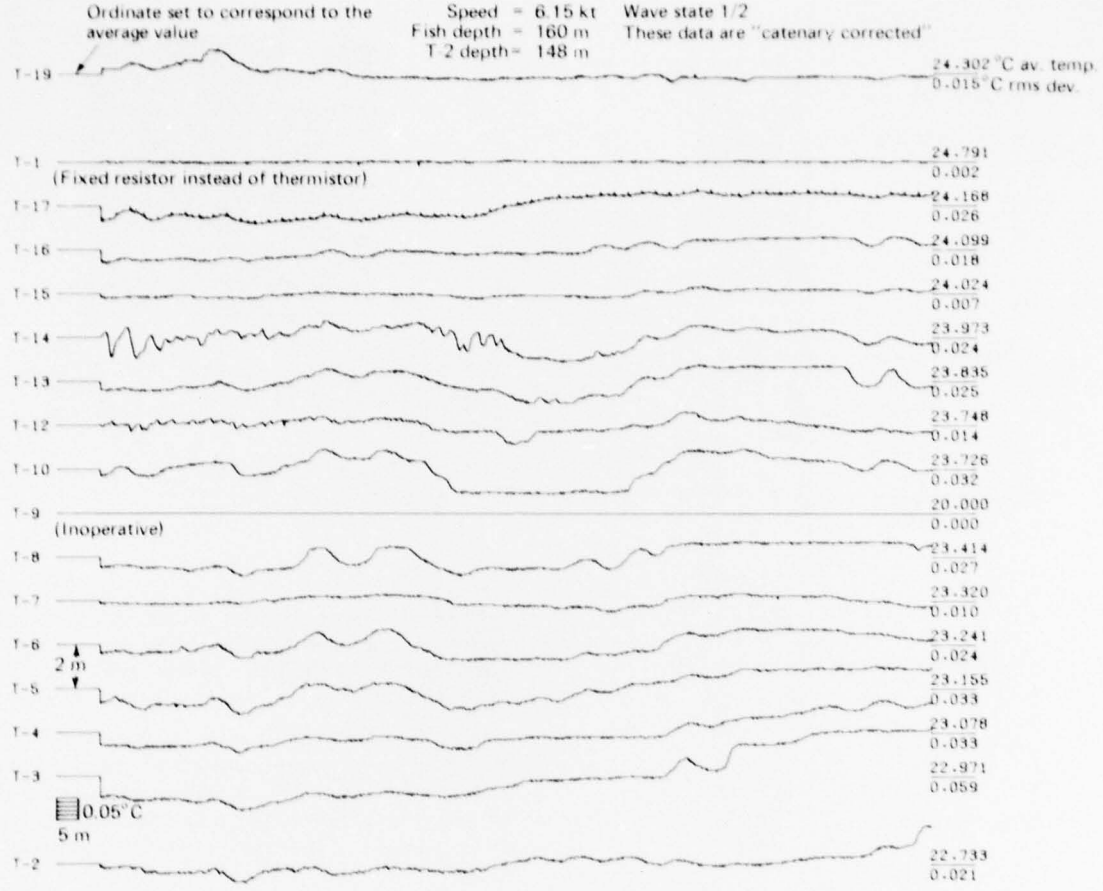

Fig. 4 Typical plot of thermistor output versus distance.

REFERENCE

1. F. F. Mobley, A. C. Sadilek, C. J. Gundersdorf, and D. Speranza, "A New Thermistor Chain for Underwater Temperature Measurement," presented at Oceans 76 Conference, sponsored by the Marine Technology Society and IEEE, September 1976.

Author: *F. F. Mobley*

Support: *Strategic Systems Projects Office, SP–202*

SCATTERING FROM ROUGH SURFACES

We have developed a variational principle that permits for the first time the application of this powerful method to the calculation of the scattering of radiation from a random rough surface. This is a significant advance because previous attempts at the straightforward extension of known variational methods for the calculation of the scattering from a fully specified surface have proven to be mathematically intractable. The new method can improve the accuracy of any approximation method for computing the scattered

field and has the added benefit of providing a built-in measure for quantitatively assessing such approximations. It has been applied to improve and assess the range of validity of the well-known perturbation approximation for the scattering of a horizontally polarized electromagnetic plane wave by a particular model of a random rough conducting surface.

BACKGROUND

The scattering of waves by random rough surfaces is of continued concern in technologies using radar, optical, and acoustical (sonar) scattering. While considerable progress has been made in recent years, analytical treatments continue to be approximate and fail to provide built-in measures of validity. As a result, it has frequently been impossible to assess an approximation or to assign a quantitative uncertainty to the result.

Variational principles are widely recognized as powerful tools for calculations in which the input quantity is not known precisely and must therefore be represented by some suitable approximation. These principles can improve the accuracy of nonvariational approximations because the error in the calculated quantity is proportional to the square of the error made in approximating the input quantity rather than its first power.

Previous studies (Ref. 1) have used variational methods to calculate scattering from complicated but fully specified surfaces. The input for these calculations is the surface field strength that could, in principle, be calculated exactly but must, in practice, be approximated. Previous attempts to extend these methods in a straightforward manner to the scattering from surfaces that are only statistically described have failed. Such extensions require the mathematically intractable evaluation of the statistical average over the distribution of surface heights of a quantity that depends on the surface field strength in a highly nonlinear fashion. In particular, the quantity to be averaged is the product of two surface integrals, each having the surface field strength as a linear factor in the integrand, divided by a double surface integral with the surface field strength appearing twice.

Recently, we have developed a new variational principle for the random rough surface scattering problem (Ref. 2). Instead of requiring the average of the complicated quotient of integrals, this principle has the virtue that the scattered field is expressed as the product of the individual averages of the two integrals in the numerator divided by the average of the double surface integral in the denominator—a far easier calculation. It has the further virtue of providing a built-in measure of the accuracy of the scattered field intensity in terms of the averaged integrals. Clearly, the new approach should prove very useful for the calculation of scattering from rough surfaces. We have used it to assess and improve the accuracy of the first-order perturbation calculation of scattering from a model of a random rough surface.

DISCUSSION

Considerable progress has been made in recent years toward obtaining a theoretical description of the scattering of waves by statistically rough surfaces, but analytical treatments continue to be approximate. As in the case of smooth surfaces, an integral equation relates the field at an arbitrary point to the field and/or its derivatives on the surface. In general, two kinds of approximations are involved: (a) the field and/or its derivatives at the surface, and (b) the statistical (roughness) properties of the surface. Here (Ref. 2), we regard the statistics of the surface as given and develop an expression for the scattered amplitude that is insensitive to small errors made in approximating the surface field. The method is illustrated for a scalar field whose normal derivative vanishes on the boundary.

The initial step is to note that for fixed (nonstatistical) surfaces, one can write a variational principle for the scattered amplitude, T, in the form

$$T = \frac{N_1 N_2}{D}, \tag{1}$$

where N_1, N_2, and D are surface integrals whose integrands depend on the fields. If the exact surface fields are used and the amplitude of the incident plane wave is $-i$, then $T = N_2$. Thus, the closeness of N_1/D to unity (for incident amplitude $-i$) is a measure of the quality of any approximate surface field. Straightforward application of Eq. 1 to statistical surfaces would require evaluation of averages of the form $\langle N_1 N_2 / D \rangle$, which would be formidable. Fortunately, we have been able to circumvent this difficulty by demonstrating that the expression

$$\langle N_1 \rangle \langle N_2 \rangle / \langle D \rangle \tag{2}$$

provides a variational principle for the ensemble average T, and that, when the amplitude of the incident wave is $-i$, the closeness of $\langle N_1 \rangle / \langle D \rangle$ to unity is a quantitative measure of accuracy.

The scattering cross section, frequently of central importance in scattering from rough surfaces, is proportional to the absolute square of the scattered amplitude. We have shown that

$$\langle |T|^2 \rangle = \frac{\langle |N_1|^2 \rangle \langle |N_2|^2 \rangle}{\langle |D|^2 \rangle} \qquad (3)$$

is a valid variational expression for $\langle |T|^2 \rangle$, and that $\langle |N_1|^2 \rangle / \langle |D|^2 \rangle$ provides a measure of accuracy. Evaluation of the ensemble averages in Eq. 3 are straightforward, although nontrivial, and its application to improve the first-order perturbative approach to a model problem is discussed below.

We have tested the method by applying it to a particular model for a random rough surface (Ref. 3) very similar to one for which the scattering problem had previously been investigated by exact numerical and nonvariational approximation methods (Ref. 4). The model, which has the virtue of comparative simplicity, consists of an infinite conducting plane with a random array of nonoverlapping, parallel, hemicylindrical, conducting bosses of equal radius, a, projecting upward (Fig. 1). The improvement achievable for a single boss by the variational method is illustrated in Fig. 2, which compares, for an incident angle of 45° and the parameter $ka = 0.4$ (k is the wave number), the dependence on the scattering angle of the approximate normalized cross section, computed both variationally and nonvariationally, with the exact result. Comparable improvements are achieved in the parameter range $0 < ka \lesssim 1$, but results deteriorate rapidly beyond this range.

Figure 3 illustrates how the variational method can be used to generate a quantitative measure for assessing the validity of whatever approximation is used in the variational process for the initial representation of the surface field strength. The plotted quantity, $\langle |N_1|^2 \rangle / \langle |D|^2 \rangle$, would have the value 1 if the true value were used for the surface field strength. Its deviation from 1 can therefore be regarded as a

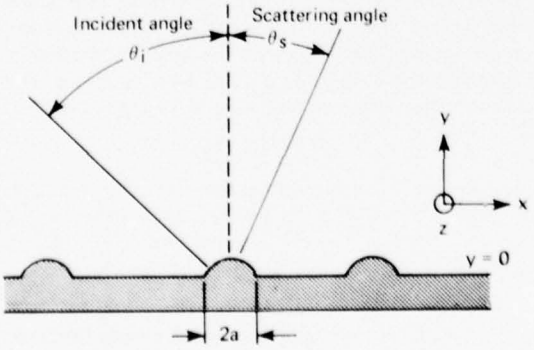

Fig. 1 Scattering configuration.

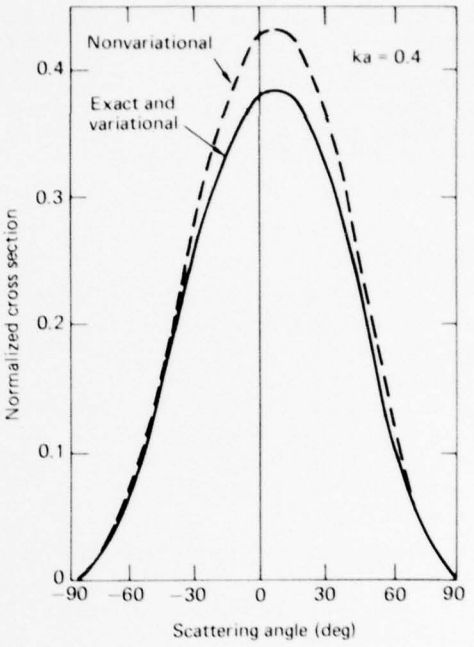

Fig. 2 Normalized cross section versus scattering angle for a single scatterer for an incident angle of 45°.

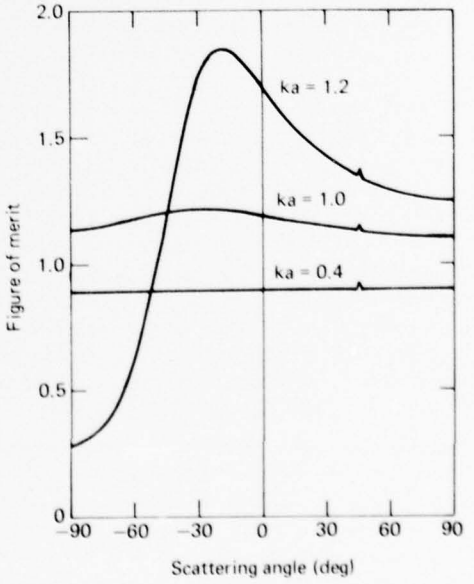

Fig. 3 Figure of merit $< |N_1|^2 > / < |D|^2 >$ versus scattering angle for a single scatterer for an incident angle of 45°.

figure of merit for the perturbation approximation, our starting point for the variational calculation. The rapid deterioration of this approximation for $ka > 1$ is evident; this causes the variational approximation to fail likewise. For a random array of 1000 bosses, the variational result for the normalized cross section per scatterer, σ_s, divided by $(ka)^4$ is shown in Fig. 4

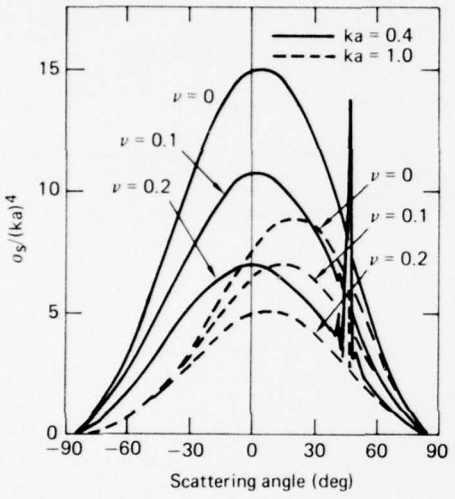

Fig. 4 Normalized cross section per scatterer divided by $(ka)^4$ versus scattering angle for an incident angle of 45° and 1000 bosses.

for an incident angle of 45° and $ka = 0.4$ and 1, for several values of the parameter, v, which denotes the fraction of the plane covered by bosses. The pronounced specular peak is caused by the coherent scattering from the tops of all the (equally high) bosses. The decrease with increasing values of v in the cross section in all directions other than specular is caused by increasing destructive interference attributable to the no-overlap condition.

It is evident from these results that the variational method may be very useful for practical scattering problems. Some of these will be addressed in the future.

REFERENCES

1. P. M. Morse and H. Feshback, *Methods of Theoretical Physics*, McGraw-Hill, New York, 1953, p. 1134 ff.
2. R. W. Hart and R. A. Farrell, "A Variational Principle for Scattering from Rough Surfaces" (to be published in *IEEE Trans. Antennas Propag.*).
3. E. P. Gray, R. W. Hart, and R. A. Farrell, "A New Variational Approach to Scattering by Random Media," *Proceedings of Open Symposium on Propagation in Non-Ionized Media*, La Boule (France), 1977, pp. 111–115 (URSI Commission F).
4. V. Twersky, "On Scattering and Reflection of Electromagnetic Waves by Rough Surfaces," *IRE Trans. Antennas Propag.*, **AP–5**, 1957, pp. 81–90.

Authors: *R. W. Hart, E. P. Gray, and R. A. Farrell*

Support: *NAVSEASYSCOM*

TWO-DIMENSIONAL WAVE SPECTRA FROM OCEAN PHOTOGRAPHS USING AN OPTICAL FOURIER ANALYSIS TECHNIQUE

Equipment has been developed to allow rapid processing of sea-surface photographs to obtain fine-time-scale, two-dimensional wave spectra using an optical Fourier analysis technique.

BACKGROUND

A description of the sea surface in terms of the spectral distribution of wave heights is needed for a variety of applications. Remote microwave sensing of the sea surface by backscatter and radiometry methods for descriptions of sea state, radar altimetry, and radar sea clutter requires an understanding of the wind wave spectrum and the energy balance between short and long waves. To first order, time averaged microwave signals contain information on only the short-wave region, i.e., the capillary region. This information can only be related to the energy-containing

long-wave part of the wind wave spectrum if the dynamical relationships between the two ranges of wave numbers are understood.

In 1975, the Joint North Sea Wave Project (JONSWAP) investigated the short-wave/long-wave interaction and energy transfer process for fetch-limited seas. The primary goal of the sea photography portion of the JONSWAP program was to investigate the temporal behavior of the two-dimensional short-wave spectrum and correlate this behavior with long-wave action measured by other sources. The optical Fourier analysis technique, first described by Barber (Ref. 1) and refined by Stilwell (Ref. 2), is being used to extract the two-dimensional wave spectrum in the 3 to 30 cm wavelength region from the sea photographs.

The technique involves illuminating the film negative of the sea surface with collimated, monochromatic light from a laser, focusing the resulting diffraction pattern via a lens, and measuring the light amplitude in the back focal plane of the lens. The distribution in light intensity can be directly related to the spectrum of wave slopes since the transfer function from the front to the back focal plane of any lens is functionally identical to a Fourier transform. Thus, the optical technique performs the complex mathematical procedure in an analogous manner.

Sea photographs taken from a tower were recorded on a fine time scale at four frames per second for 25-minutes periods under a variety of sea conditions. To the authors' knowledge, this is the first time such a data set has been available to study the spectral modulation. Special equipment for handling film and recording data was required to process the rolls of film rapidly. The present program was undertaken to develop this equipment and begin the wave-analysis process.

DISCUSSION

The first part of the effort was to devise a system to handle and process the thousands of sea photographs rapidly. The second was to devise a method for recording semiquantitatively the resulting wave slope spectra along with a way of presenting these data for analysis of the time-dependent spectral behavior.

The basic optical spectrum analyzer system is shown in Fig. 1. The system was designed to handle large rolls of 35-mm film. Control logic and circuitry advance the film from frame to frame and accurately index each frame at the same location with respect to the laser beam. Accurate indexing of the film is most important when the sea is photographed at an oblique angle since the scale factor on the film changes throughout the frame. The laser spot may be positioned in the frame by means of micrometers that translate the film carriage assembly relative to the laser axis. The film may be advanced continuously or by single frames; counters record the scene frame numbers.

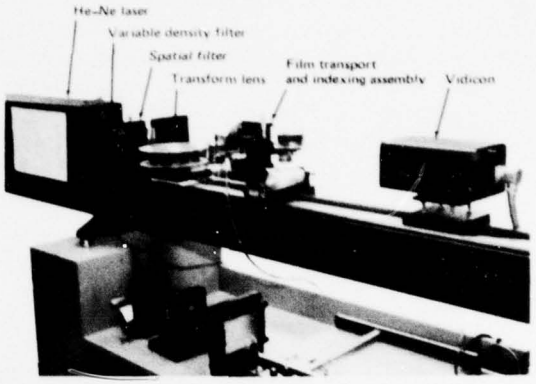

Fig. 1 Optical bench setup used in optical Fourier analysis of sea-surface photographs. Vidicon is located in transform plane when closed-circuit television system is used for detection, display, and recording.

Two data display and recording systems have been developed for the preliminary data analysis. The first uses a closed-circuit television to detect and display the two-dimensional spectrum. A vidicon camera is located in the transform plane, i.e., the back focal plane of the transform lens (see Fig. 1). The video signal is contoured, color coded, and displayed on a television monitor. The monitor is photographed by either a 16-mm cine camera for slow-motion movies of the spectral modulations or by a 35-mm still camera. Figure 2 is a black and white reproduction of the color coded spectrum as it appears on the monitor.

The number of photographs to be taken of any spectrum is selectable via thumb wheels on the camera control box of the control circuitry. When the required photographs have been taken, the film is advanced automatically and indexed to the next one. Thus, slow-motion, real-time, or single-frame movies of the wave spectra may be produced. The movies have been most useful in illustrating the temporal behavior of the complete two-dimensional spectrum. This is the first time such a presentation has been attempted. The cine-type presentation also illustrates

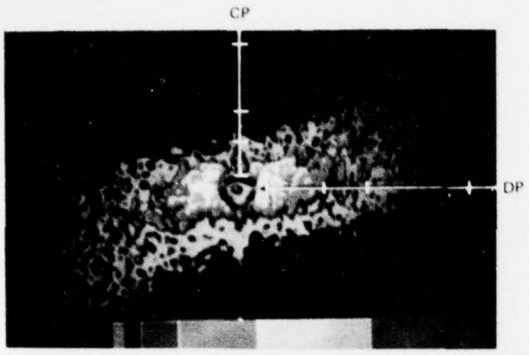

Fig. 2 Color display of two-dimensional slope spectrum of sea surface. Number indicates frame number. Circular contours at wave numbers about zero are caused by a 40-dB attenuator spot placed on vidicon tube face to protect tube. Color ranges are relative to video system noise level. Ticks on depression plane (DP) and cross plane (CP) axes are at 30, 10, 6, and 3 cm wavelengths on the sea surface.

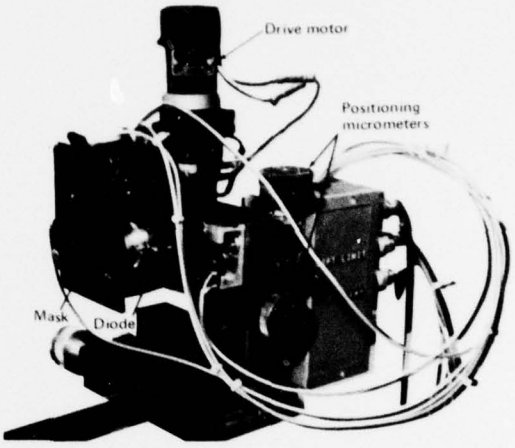

Fig. 3 Traveling diode system used to measure spectral values at specific wave numbers along a given direction.

how difficult it is to interpret time series data for specific wavenumbers in a single direction.

The traveling diode system (Fig. 3) was designed to gather quantitative data at specific wavenumbers along a given direction. An opaque mask is placed in the transform plane; a diode mounted on a carriage travels along the line of the holes corresponding to specific wavenumbers and reads the light intensity. A separate system controls data recording so that the readings are taken only when the diode is centered over a hole in the mask. The diode carriage is driven continuously from one side of the spectrum to the other; two values are read at each wavenumber. When the traverse is complete, the film is automatically advanced and indexed to the next frame, and the diode traverses in the opposite direction. The sequence is repeated for as many frames as desired; the number can be set in the control circuitry.

The combination of the full two-dimensional spectral photographs in single or cine form along with the spectral values at specified wavenumbers represents a unique data set for the study of the fine-time-scale behavior of the wind wave spectra. Although the sea photographs processed to date have been for the study of the temporal changes in wave spectra at a given point on the sea surface, the optical Fourier technique and the rapid processing equipment are also applicable to the study of spatial changes in the sea surface due to underwater disturbances.

REFERENCES

1. N. F. Barber, "A Diffraction Analysis of a Photograph of the Sea," *Nature*, **164**, 1949, pp. 485–486.
2. D. Stilwell, "Directional Energy Spectra of Sea Surface Photographs," *J. Geophys. Res.*, **74**, No. 8, 1969, pp. 1974–1986.

Authors: *T. G. Konrad and J. R. Rowland*

Support: *NSF Grant OCE75-21524*

FUNDAMENTAL RESEARCH

INTRODUCTION

Leadership in the application of technology to programs in the national interest requires a diverse and strongly rooted base in the underlying basic sciences of physics, chemistry, and mathematics. In recognizing this relationship, APL has consistently supported basic science programs in areas that are broadly relevant to the technologies employed in national defense, energy, transportation, computer applications, and biomedicine. Much of this effort has been concentrated in the Research Center.

The orientation of most of this work is motivated by a desire to understand the basic physical laws underlying the topic under investigation. This approach continues the Hopkins tradition of research from which the Laboratory sprung. It provides continuing areas of contact with the academic and medical divisions of the University and a link with the international academic community in science, and constitutes a reserve of new ideas and directions for technological innovation. Furthermore, it acts as a resource for those specific problems where application of current technology or current engineering practice is inadequate and where a broader approach is needed.

Current research interests include projects in the general areas of materials sciences, biology, chemistry, physics, and mathematics. Some especially noteworthy advances made in these areas appear as individual accomplishment reports, which follow. An example of the work in materials research is the report on the theoretical study on amorphous magnetism. Magnetism in amorphous materials has only recently been recognized as providing unique magnetic structures not present in conventional polycrystalline materials. Studies in this area are still in an early stage of development; however, some direct applications of the properties of these materials have been made. The report on the spectroscopic investigation of metal porphins is an example of fundamental research into the structure of materials of biological interest. The metal porphins play an essential role in biologically active systems as the active sites for oxygen exchange in respiration and photosynthesis. Recently, they have been suggested as potential materials for solar energy conversion.

Two other reports deal with fundamental research in the area of chemistry. One reports on the discovery of the new rare gas monohalide molecule, XeCl, using APL's extensive expertise in the microwave spectroscopy of matrix-trapped molecules. These molecules are of scientific interest because the chemical bonding and structure of the inert gas compounds violate the classical

principle of inertness of closed shell atoms, and of technological interest because partially tunable ultraviolet lasers can be constructed, based on emission from excited states of these inert gas monohalide molecules. The other report in the area of chemistry describes the progress in constructing a theory of diffusion in quantum mechanical systems, a matter of considerable importance in describing energy transport in gases and in some solids. The final report in this section in the area of mathematical physics describes an important new invariance in the Padé approximants to the electronic energy of atoms and molecules. While the initial motivation for this work stemmed from a problem in theoretical molecular physics, the development should be of value in many complex systems where optical approximate solutions to a dynamical problem are important.

Reports on other IR&D-funded work are found in other sections of this book, where appropriate. These include the work of Hart, Farrell, and Gray on a variational treatment of scattering from rough surfaces applied to the ocean, and that of Fox and Sigillito on the mathematics of internal wave generation in the ocean. Other topics include the work of Adrian on laboratory experiments relevant to the identification of interstellar molecules, that of Parker on water purification using laser-excited oxygen, that of Feldman and Blum on thin-film solar cells, and the work of O'Brien and Ehrlich on the solution of heat transfer in finned heat exchangers. The initial motivation for each of these reports was interest in the basic physics or mathematics. Their inclusion in specific-interest sections of this volume reflects the synergistic relationship that connects basic studies and practical applications.

Finally, these accomplishment articles should be viewed in the context of broader continuing programs in the areas of materials sciences, chemical structure and kinetics, and the other categories cited previously. Each area includes other projects not explicitly described in this volume. Some examples follow. The general program of studying the transport properties and energy level structures of materials using a variety of experimental methods, notably several branches of spectroscopy, includes projects related to the study of organic charge-transfer salts, chemically induced dynamic nuclear polarization in free-radical reactions, electrode reactions at solids including the study of photoelectrolysis for solar energy conversion, and studies of electrocorrosion. Other general programs involve *ab initio* molecular structure calculations and calculations of hyperfine structure splittings in molecules.

MAGNETISM IN DISORDERED SOLIDS

Novel magnetic structures, recently discovered in disordered solids, have raised fundamental questions concerning magnetism in disordered solids and have already led to new materials that could find potential applications in magnetic devices. A theoretical research program has been undertaken to elucidate magnetic phenomena in disordered solids.

BACKGROUND

Two basic requirements need to be satisfied for the existence of ferromagnetism in a solid: the presence of an uncompensated spin, and therefore magnet moment, on an atom; and the exchange interaction between spins on neighboring atoms. Thus, it is evident that ferromagnetism, like many other properties of solids, does not depend on the periodic or regular arrangement of atoms in a crystalline solid. However, it was only 15 years ago that the existence of ferromagnetism in a structurally disordered solid was predicted theoretically. Since then, various aspects of disordered magnetic systems have been studied. Experimentally, many unusual magnetic structures have been discovered in disordered solids that do not appear in crystalline solids. Extensive research in this field is now in progress, ranging from the most fundamental investigations of physical phenomena to the most practical applications of novel materials and innovative concepts.

The work presented here was motivated by experimental results on systems containing a large concentration of ferromagnetic metallic impurities in a disordered diamagnetic host. An example of such a system is randomly distributed iron atoms in a thin film of amorphous germanium. These alloys exhibit many interesting properties that should help us to understand phenomena as varied as hopping conduction, insulator-metal transition, and magnetic interactions in disordered solids. The investigation of the latter property has been emphasized in the present study.

DISCUSSION

A theoretical model has been constructed to demonstrate the magnetic phenomena in structurally and compositionally disordered solids (Ref. 1). In its present form, the model consists of a site-disordered alloy, A_xB_{1-x}, with concentration x of magnetic atoms, A, randomly distributed in a nonmagnetic lattice of B atoms with concentration $1 - x$. The lattice is assumed to be structurally disordered, which induces fluctuations in the ferromagnetic exchange interactions between magnetic atoms. Thus, besides the temperature and the coordination number of the lattice, the relevant parameters for the discussion of thermodynamic quantities are the concentration of the magnetic atoms, x, and the measure of fluctuations, Δ. The crystalline ferromagnet results in the limits $x = 1$ and $\Delta = 0$ and serves as a useful check on the calculations performed.

In binary alloys, A_xB_{1-x}, one would observe the onset of ferromagnetism for a critical concentration, x_0, of magnetic atoms. Since the conventional molecular field approximation does not predict a critical concentration, it would not be appropriate for discussion of the properties of A_xB_{1-x} over the entire range of x. We have therefore considered a cluster model and have investigated it within the Bethe-Peierls-Weiss approximation. The resulting free energy is averaged over all the configurations of the disordered system, and a self-consistent condition on magnetization is used to yield expressions for thermodynamic quantities of interest. The procedure allows a systematic investigation of the effect of fluctuations on various thermodynamic variables.

It is shown that the critical concentration, x_0, is not influenced by the presence of fluctuations. This is a reasonable result since it is the presence of a magnetic bond that is important, not its strength. The value of x_0 ($= 1/3$) is found to be in fair agreement with the experimental value (0.4 ± 0.02) recently deduced from the Curie temperature versus concentration measurements on iron atoms randomly substituted in amorphous germanium. For $x > x_0$, the fluctuations depress the values of the Curie temperature, the high temperature magnetic susceptibility (Fig. 1), and the magnetization (Fig. 2) relative to the corresponding values for the average crystal. For small values of Δ, explicit expressions for the amount of decrease in these quantities are obtained. However, the critical indices for magnetization as well as susceptibility are found to be unaffected by fluctuations. The detailed calculations are given in Ref. 1.

Although most amorphous solids containing a substantial proportion of magnetic atoms are ordered ferromagnetically, more complex magnetic structures can and do occur. The complexity of the magnetic structure is determined by the crystalline field anisotropy and relative strengths and signs of various

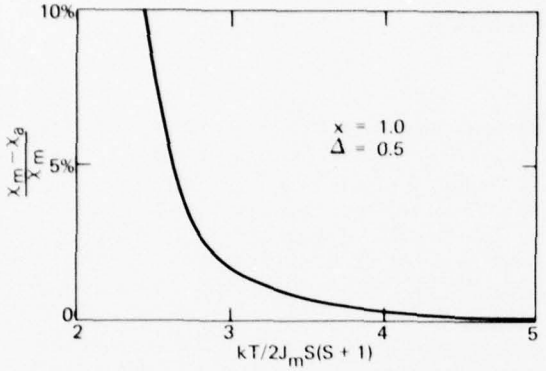

Fig. 1 Relative susceptibility versus reduced temperature for a structurally disordered ferromagnet. χ_m and J_m are the susceptibility and the exchange constant, respectively, of the mean crystal while χ_a is the susceptibility of the disordered solid and S is the spin.

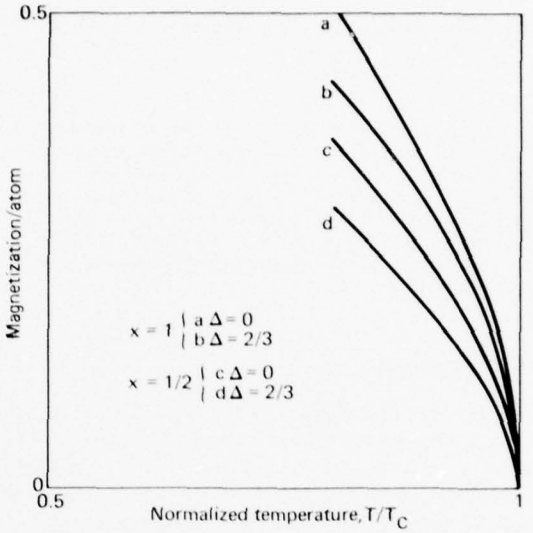

Fig. 2 Magnetization versus normalized temperature for different values of x and Δ in the vicinity of the Curie temperature, T_c. For each case, the temperature is normalized with respect to the corresponding T_c.

magnetic interactions. One such complex magnetic structure, termed "spin glass," possesses neither short- nor long-range magnetic order but does exhibit anomalies in its thermodynamic behavior. It is expected that a study of spin glasses will answer questions concerning the fundamental nature of exchange interactions and will aid in exploring the possible uses of disordered magnetic solids in magnetic devices.

The above formulation has been modified to discuss the static properties of spin glasses. In our treatment, the presence of a finite number of nearest neighbors increases the value of the spin glass transition temperature compared to the molecular field result. Furthermore, in contrast to the molecular field approximation, the magnetic susceptibility approaches the transition temperature from below with a finite positive slope, in agreement with the experimental results. The detailed results have been published (Ref. 2).

REFERENCES

1. K. Moorjani and S. K. Ghatak, "Critical Behavior of a Structurally and Chemically Disordered Ferromagnet," *J. Phys. C* **10**, 1977, pp. 1027–1038.
2. S. K. Ghatak and K. Moorjani, "Spin Glasses: Beyond the Molecular Field Approximation," *J. Phys. C*, **9**, 1976, pp. L293–L295.

Author: *K. Moorjani*

Support: *NAVSEASYSCOM, SEA-0253Y*

SINGLE-SITE SPECTRA OF ZINC PORPHIN

Single-site spectra of zinc porphin in triphenylene have been recorded at low temperature using a tunable dye laser. There were three principal site species, each of which had slightly different fluorescence and absorption spectra. Because the spectra of each site were recorded separately, the confusion in previous studies caused by the spectra of multiple-site species was eliminated.

BACKGROUND

Porphyrin molecules are of great interest and importance because they perform vital functions in a number of biological molecules. An iron porphyrin complex forms the central or prosthetic group of the hemoglobin molecule that transports oxygen in blood and also of the various cytochromes that act as catalysts in the respiratory cycle. A magnesium porphyrin is contained in the chlorophyll molecule.

Optical spectroscopic studies of a number of metalloporphins have been made at APL using triphenylene as a host for the guest porphin molecules (Refs. 1 and 2). The use of this host material results in sharp-line optical spectra at low temperature. In single crystal specimens, the guest molecules are spatially oriented, allowing polarization of the spectra to be observed. However, the potential advantages of these specimens were not fully exploited in previous studies because of limitations imposed by the occurrence of multiple inequivalent metalloporphin site species in the host matrix. Since the spectra from all the inequivalent site species were recorded simultaneously, they were exceedingly complex and, in some cases, resulted in overlapping lines from different site species. Hence, definitive spectral assignments were difficult or impossible in many cases. Similar problems also occur in the use of Shpol'skii matrices to study spectra.

The objective of this study was to use narrow-line selective excitation of fluorescence as a technique to obtain single-site absorption and fluorescence spectra of zinc porphin in triphenylene. This allowed the spectrum intrinsic to each site species to be recorded separately, thereby eliminating interference from spectra of different sites.

DISCUSSION

Briefly, the technique of site-selection spectroscopy involves the use of high-resolution selective excitation to record the spectra from molecules in a single type of site. Single-site fluorescence spectra are obtained by exciting a single sharp absorption line. The corresponding single-site absorption spectrum is obtained by recording the intensity of a single sharp fluorescence line that has been spectrally isolated with the spectrograph while scanning the excitation source through the region of the absorption spectrum. This yields the excitation spectrum of the fluorescence line that is equivalent to the absorption spectrum of the same site species from which the fluorescence line originates.

A scanning dye laser with a 0.1-nm bandwidth was used as a light source. A pulsed nitrogen laser with a 10-ns pulse width and 100-kW peak power was used to pump the dye laser at a rate of 50 pps. A photomultiplier tube and boxcar integrator were used to acquire the average peak intensity of the pulsed fluorescence signal.

Figure 1a shows the fluorescence spectrum of zinc porphin in *tri*phenylene at 4.2 K using broadband excitation. Three strong lines associated with the 0–0 transitions of three principal site species are observed at 567.8, 568.7, and 570.1 nm. Figures 1b, 1c, and 1d show fluorescence spectra of zinc porphin in triphenylene at 4.2 K, using narrowband excitation at 570.1 568.7, and 567.8 nm, respectively. The three lower spectra are distinct from one another, and their sum gives the spectrum of Fig. 1a.

Figure 2 shows a portion of the narrowband excitation spectrum of the 570.1-nm site obtained by detecting fluorescence at 614.1 nm. Similar excitation spectra were obtained for the 568.7– and 567.8-nm sites.

In this manner, the absorption and fluorescence spectra of a single type of zinc porphin molecule have been obtained. Difficulties associated with multiple-site spectra have been largely eliminated, allowing more definitive assignments and interpretation of the spectra. The data in this study provide fairly detailed information on the ground-state vibrational energy levels and the lowest excited singlet vibronic levels with observable transitions between these electronic states. This is the first spectroscopic study of a porphyrin molecule doped into a crystalline matrix in which the spectra of inequivalent porphyrin site species were recorded separately.

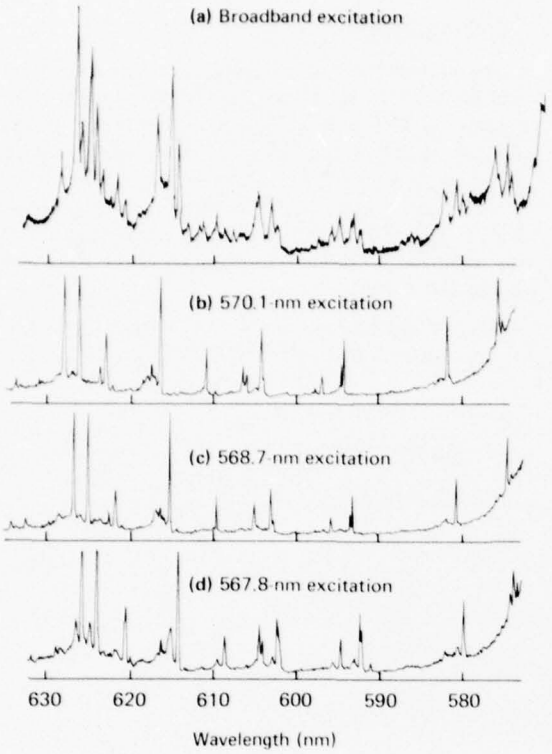

Fig. 1 Fluorescence spectra of zinc porphin in triphenylene at 4.2 K.

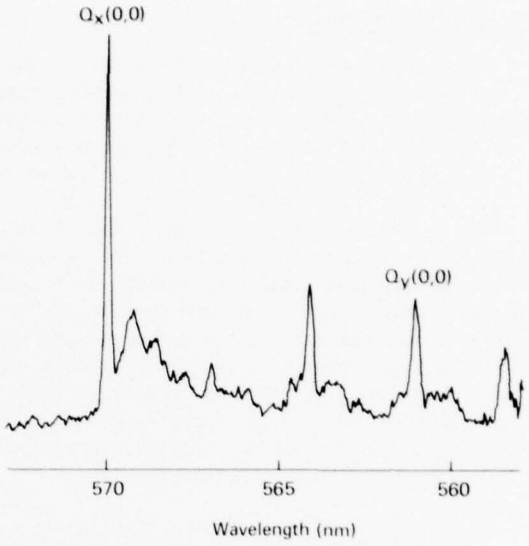

Fig. 2 Excitation spectra (558.0 to 573.0 nm) at 4.2 K for the 570.1–nm site species; detection at 614.1 nm.

REFERENCES

1. B. F. Kim, J. Bohandy, and C. K. Jen, "Low Temperature Optical Spectra of Zn Porphin in Triphenylene," *J. Chem. Phys.*, **59**, 1973, pp. 213–224.

2. J. Bohandy and B. F. Kim, "Optical Spectra of Ni Porphin, Pd Porphin, and Free Base Porphin in Single Crystal Triphenylene," *Spectrochim. Acta Part A*, **32**, 1976, pp. 1083–1088.

Authors: *B. F. Kim and J. Bohandy*

Support: *U.S. Public Health Service Grant GM–21897, National Institute of General Medical Science*

ESR IDENTIFICATION OF CHEMICALLY BOUND XENON MONOCHLORIDE

Electron spin resonance (ESR) spectroscopy has shown that, contrary to theoretical predictions, chemically bound xenon monochloride (XeCl) is formed when chlorine is photodissociated in an argon matrix containing 1% of xenon. The spectrum contained observable hyperfine structure (hfs) splittings resulting from the interaction of the magnetic moment of the unpaired electron with both Cl and Xe nuclei. The magnitude of these hfs splittings provides information about the distribution of the unpaired electron charge density in the molecule, a quantity that is closely related to the nature of the chemical bonding in the molecule.

BACKGROUND

Interest in the electronic structure and chemical bonding of the rare gas monohalides is generally high because they violate the principle that closed-shell atoms do not form compounds. It has been stimulated further by the discovery that emission from an excited state of these molecules can yield high-energy ultraviolet laser action. In work done to date at other laboratories, theory predicts that all these molecules have nonbonding ground states, whereas experiments (most notably electron spin resonance studies) have indicated that XeF and KrF have bound ground states. This bonding problem has fundamental interest and significance for laser emission because the ground state bonding involves an interaction between the basic ground state and the excited charge-transfer state responsible for the ultraviolet emission.

These states may be denoted, respectively, as $\psi(\mathrm{Rg}\ldots\mathrm{X})$ and $\psi(\mathrm{Rg}^{+}\ldots\mathrm{X}^{-})$, where Rg denotes the rare gas and X the halogen. The quantum theory of bonding shows that admixture of the $\psi(\mathrm{Rg}^{+}\ldots\mathrm{X}^{-})$ state into the ground state, formally described by the wave function $\psi(\mathrm{RgX}) = \sqrt{1-\varepsilon^2}\,\psi(\mathrm{Rg}\ldots\mathrm{X}) + \varepsilon\psi(\mathrm{Rg}^{+}\ldots\mathrm{X}^{-})$, must lower the energy of the ground state and may lead to bonding. Quantum theory also requires that the ground and excited states be related, the excited state wave function being $\psi(\mathrm{RgX}^{*}) = -\varepsilon\psi(\mathrm{Rg}\ldots\mathrm{X}) + \sqrt{1-\varepsilon^2}\,\psi(\mathrm{Rg}^{+}\ldots\mathrm{X}^{-})$. Therefore an ESR or other experiment on the ground state that determines the charge distribution parameter, ε, will simultaneously determine the charge distribution in the excited state.

An important point is that the lower the energy of the $\psi(\mathrm{Rg}^{+}\ldots\mathrm{X}^{-})$ state, the greater its contribution to ground state bonding. Factors affecting this energy are the rare gas ionization potential, the electron affinity of the halogen, and the ionic radii of the Rg^{+} and X^{-} ions. For example, in comparing XeCl and KrF, one finds that the Xe ionization potential (12.1 eV) is substantially lower than that of Kr (14.0 eV), while the Cl and F electron affinities are roughly equal (−3.5 eV). This leads to the conclusion that the energy of the state $\psi(\mathrm{Xe}^{+}\ldots\mathrm{Cl}^{-})$ will be somewhat lower than that of the state $\psi(\mathrm{Kr}^{+}\ldots\mathrm{F}^{-})$ even though interionic coulomb energy favors the latter state slightly because the Kr^{+} and F^{-} ionic radii are smaller than those of Xe^{+} and Cl^{-}. This suggests that XeCl should be at least as strongly bound in the ground state as KrF. Accordingly, it was decided to attempt to prepare XeCl using procedures previously used for XeF and KrF (Ref. 1) and to detect by ESR spectroscopy any XeCl formed.

DISCUSSION

The ESR spectrum of the product of the ultraviolet photolysis of an $\mathrm{Ar{:}Xe{:}Cl_2} = 98{:}1{:}1$ sample on a sapphire rod at 4 K is shown in Fig. 1 (Ref. 2). No ESR spectrum was observed after photolysis of either an $\mathrm{Ar{:}Cl_2} = 98{:}2$ matrix or an $\mathrm{Ar{:}Kr{:}Cl_2} = 98{:}1{:}1$ matrix, indicating that the observed spectrum is very likely XeCl and that KrCl is not formed by this photolytic reaction, probably because it is not chemically bound.

The ESR spectrum in Fig. 1 results from transitions of the magnetic moment of the XeCl unpaired elec-

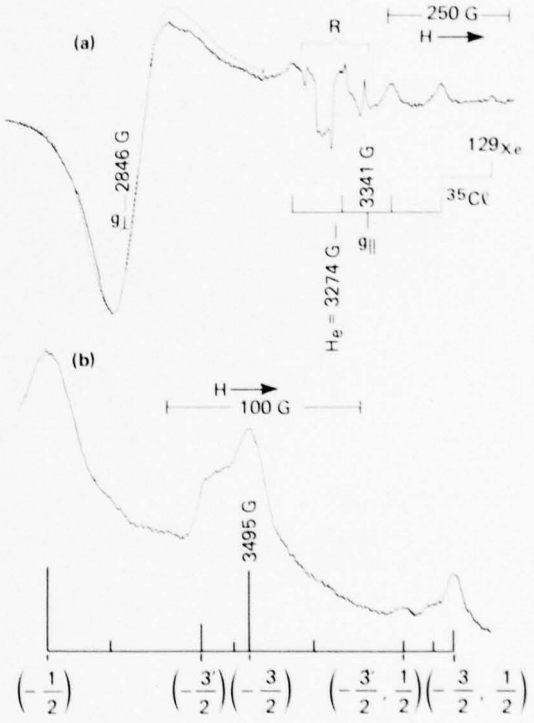

Fig. 1 ESR spectrum.

(a) —ESR spectrum of the photolysis products of an $\mathrm{Ar{:}Xe{:}Cl_2} = 98{:}1{:}1$ sample at 4.2 K. The sharp weak lines in the region denoted by R• are traces of radical impurities. H_e denotes the resonant field of a free electron spin. – – –Computed spectrum in the perpendicular region for the parameters given in the text.

(b) Expanded trace of the two highest field lines of the complete spectrum in (a). The stick spectrum at the bottom is computed from the ^{35}Cl and ^{129}Xe hfs constants given in the text, where the numbers in parentheses indicate the magnetic quantum numbers of the strong hfs lines. The first number is M_{Cl}, with the ^{37}Cl isotope indicated by a prime, and the second number, if present, is M_{Xe} of ^{129}Xe. The weak lines, not denoted by numbers, are ^{131}Xe hfs lines.

tron between states where it is parallel and antiparallel to the external magnetic field. The transitions occur when the transition frequency, which is a function of magnetic field strength, matches the frequency of the stimulating microwave source at about 9100 MHz. The spectrum has two branches, $g_{\parallel}$ and $g_{\perp}$, because the magnetic moment of the unpaired electron (denoted $g\mu_{\beta}S$, where μ_{β} is the Bohr magneton and S is the electron spin) contains contributions from both the spin and the orbital motion of the electron and is substantially different for directions parallel and perpendicular to the molecular axis.

In the present case where the radicals are randomly oriented in the polycrystalline matrix, the $g_{\parallel}$ and $g_{\perp}$ regions correspond to radicals whose molecular axes are parallel and perpendicular to the field, respectively. The corresponding values are $g_{\parallel} = 1.962$ and $g_{\perp} = 2.302$. The g shifts (i.e., $\Delta g = g - g_e$, where $g_e = 2.0023$ is the free spin g value) are similar to but larger than those of XeF. This is the expected effect of the increased halogen spin-orbit interaction and/or the decreased chemical bonding on going from XeF to XeCl (Ref. 2).

The structure of the spectrum in the parallel region is due to magnetic hfs interactions between the electron magnetic moment and a number of magnetic nuclei in the XeCl molecule. The four strongest lines, associated with the 53% abundant, $I = 0$, Xe isotopes (^{132}Xe, ^{134}Xe, etc.), are a Cl hfs quartet [$|A_{\parallel}(^{35}\mathrm{Cl})/h| = 288$ MHz, where $A_{\parallel}$ is the hfs constant]. The weak highest field line is due to hfs splitting of the high field member of the Cl quartet by the 26% abundant, $I = 1/2$, ^{129}Xe isotope [$|A_{\parallel}(^{129}\mathrm{Xe})/h| = 582$ MHz]. This assignment is confirmed by an expanded trace of the two highest field lines (Fig. 1b). These lines have identical structure due to hfs splittings from both the 75% abundant ^{35}Cl and the 25% abundant ^{37}Cl, proving that both lines have the same Cl hfs splitting, and their relative intensities are consistent with assignment of the highest field line as part of a ^{129}Xe doublet.

No structure is discernible in the perpendicular region of the spectrum; however, trial-and-error comparisons of observed and computed line shapes in this region gave the following estimates of the perpendicular hfs constants: $A_{\perp}(^{35}\mathrm{Cl})/h \simeq 0$ MHz; $|A_{\perp}(^{129}\mathrm{Xe})/h| \simeq 280$ MHz. As shown in Fig. 1a, this assignment gave good agreement between the observed and computed lines.

The Xe hfs splittings are much smaller in XeCl than in XeF (Ref. 2). This is consistent with the expected weaker bonding and a correspondingly smaller transfer of unpaired electron density from the halogen to Xe in XeCl as compared with XeF.

The method of preparation combined with the hfs data prove that the observed species is XeCl. The Xe hfs argues strongly for chemical bonding in XeCl, which may be defined roughly as nonzero ε in the XeCl wave function: $\psi_{\mathrm{XeCl}} = N\,[\sqrt{1-\varepsilon^2}\,\psi(\mathrm{Xe}\ldots\mathrm{Cl}) + \varepsilon\psi(\mathrm{Xe}^{+}\ldots\mathrm{Cl}^{-})]$. For $\varepsilon = 0$, the Xe hfs is due solely to overlapping of the Xe $5s$ and $5pz$ orbitals with the Cl $3pz$ unpaired electron orbital. Calculations show that even at a separation, R, of 0.32 nm, which is considerably less than the R of 0.42 nm estimated from the nearest true van der Waals molecule ArXe, the overlap cannot account for the observed Xe hfs. A more detailed argument (Ref. 2) shows that the observed perpendicular g shift ($\Delta g_{\perp}$) also requires chemical bonding in XeCl.

REFERENCES

1. B. S. Ault and L. Andrews, "Absorption and Emission Spectra of Argon Matrix Isolated XeF and KrF," *J. Chem. Phys.*, **64**, 1 April 1976, pp. 3075–3076.
2. F. J. Adrian and V. A. Bowers, "ESR Spectrum of XeCl in Argon at 4.2 K," *J. Chem. Phys.*, **65**, 15 November 1976, p. 4316.

Authors: F. J. Adrian and V. A. Bowers

Support: Indirectly Funded R&D

DIFFUSION OF EXCITED MOLECULES

In a pure gas, molecules in different internal (quantum) states behave like the chemically distinct molecules in a gas mixture. In particular, like molecules in different internal states can diffuse relative to each other. In addition, collisions that change the internal states of two like molecules are comparable to reactive collisions in a gas mixture. In both cases, the "reactions" tend to suppress the diffusion. In the work described here, we developed a theoretical description of these processes.

BACKGROUND

Even in a pure gas (containing only one chemical species), molecules in a given internal quantum state can diffuse relative to their partners in other states. This process can occur in a laser, for example, and may adversely affect its performance; that is, the molecules pumped into an excited state can diffuse to the walls and be quenched. The diffusion of quantum states is similar to the relative diffusion of different chemical species in a multicomponent gas. The latter process is a familiar phenomenon in flames.

The kinetic theory of gases has been successful in explaining the relative diffusion of molecular species. Specifically, the diffusion coefficients may be calculated accurately from details of the molecular collisions that take place in the gas. The same theory fails to explain internal state diffusion. The difficulty is in properly accounting for a fundamental quantum mechanical constraint on molecular collisions. One earlier attempt to describe nuclear spin diffusion did not properly account for this constraint and failed by a factor of two to predict the experimental results. In the work described here, we set the foundations of a corresponding kinetic theory of internal state diffusion.

DISCUSSION

When two molecules of the same chemical species, initially in states *a* and *b*, undergo a collision in which the final states are also *a* and *b*, it is impossible to tell whether or not the states were exchanged (Fig. 1). An accurate kinetic theory of quantum state diffusion must be consistent with this fact. However, it is of little importance in theories of species diffusion, where colliding molecules are distinguishable by their different chemical identities.

The first step toward an accurate theory of internal state diffusion was to build the exchange requirements into the fundamental equation of kinetic theory

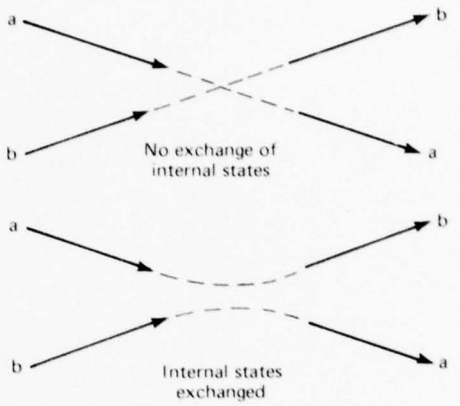

Fig. 1 Two indistinguishable collisions between molecules of the same chemical species in different internal states, *a* and *b*.

(Ref. 1). Known as the Boltzmann equation, it determines the probability distribution of internal states (and molecular velocities) in a gas but becomes very complicated when it explicitly recognizes and accounts for all the internal states.

The second step was the simplification of the Boltzmann equation (Ref. 2). The equation was simplified exactly when it was written in a form that did not vary with rotations of coordinate axes.

The third step was "solving" the Boltzmann equation (Ref. 3). When it is solved, the results resemble the usual hydrodynamic equations for balance of mass, energy, and momentum but have the important additional feature that the thermal conductivity, the diffusion coefficients, and the viscosities are given in terms of molecular collision cross sections. We obtained two mass-balance equations controlling the diffusion of internal states. One was in the form of the familiar Fick's law of hydrodynamics, in which the flux of internal states is "proportional" to their gradients. The proportionality constants that arose in this solution were analogous to the multicomponent diffusion coefficients of a gas mixture (Ref. 4). The second solution was similar to the inverse of Fick's law, known as the Stefan-Maxwell equation (Ref. 3). The different set of diffusion coefficients that arose here had the advantage of being independent of the populations of the internal states.

Both diffusion equations contained additional terms describing the creation and destruction of internal

states by molecular collisions. The terms are analogous to the chemical reaction terms in the traditional Fick's law and Stefan-Maxwell equations. The distinguishing feature of our "reaction" terms is that they are consistent with the exchange requirements for molecular collisions.

This work establishes a theoretical basis for internal state diffusion. We are currently applying it to practical experimental systems. Our theory gives correct results for the simple case of nuclear spin diffusion.

REFERENCES

1. L. W. Hunter, *J. Chem. Phys.*, **63**, 1975, p. 2010.
2. L. W. Hunter, *J. Chem. Phys.*, **63**, 1975, p. 345.
3. L. Monchick and L. W. Hunter, *J. Chem. Phys.*, **66**, 1 May 1977.
4. L. Monchick, K. S. Yun, and E. A. Mason, *J. Chem. Phys.*, **39**, 1963, p. 654.
5. L. Monchick, S. I. Sandler, and E. A. Mason, *J. Chem. Phys.*, **49**, 1968, p. 1178.

Authors: *L. W. Hunter and L. Monchick*

Support: *NAVSEASYSCOM*

SPECIAL INVARIANCE PROPERTIES OF PADÉ APPROXIMANTS

A special invariance property has been proven to exist for a certain sequence of Padé approximants useful for the representation of solutions to complex physical problems. Its application to the electronic structure of atoms and molecules produces a calculated energy result that reflects the true properties of the system rather than the arbitrary vagaries inherent in the method of calculation.

BACKGROUND

It is often necessary to determine the electronic energy of atoms and molecules by theoretical methods. When a perturbative expansion of the energy is used, the problem arises of determining which of several possibilities is the most suitable representation of the energy. This study solves that problem since it specifies an appropriate representation of the energy in terms of a particular class of Padé approximants possessing a unique invariance property.

DISCUSSION

Theoretical models of complex physical systems seldom lead to mathematical solutions in closed form. However, in many cases, useful approximate solutions can be obtained using a perturbative approach in which a related but solvable problem forms the basis of a lowest-order result. The solvable problem is then perturbed in a way that should make the results converge to the solutions of interest.

A solvable problem related to the electronic structure of atoms and molecules is the independent particle model. Rayleigh-Schrödinger perturbation theory provides a convenient method for describing the corrections to this model. Thus, if $\mathcal{H}$ is the exact Hamiltonian and H_0 is the Hamiltonian corresponding to the independent particle model, the perturbative operator, H_1, is defined as $H_1 = \mathcal{H} - H_0$. The operator, $H_0 + \lambda H_1$, is then equal to the independent particle model when λ is zero, and it approaches the exact problem as λ approaches unity. The energy for these systems is written as a power series in the variable λ. In all practical applications, the power series is truncated after a finite number of terms and evaluated for $\lambda = 1$ to obtain an approximation to the true energy.

Considerable freedom exists in the choice of H_0; for example, one might modify a given H_0 to produce a change of scale and a shift of origin in the zero-order energy spectrum, provided that H_1 is suitably modified so that $\mathcal{H}$ is still recovered at $\lambda = 1$. However, although $\mathcal{H}$ is independent of the scale and shift parameters, the truncated power series for the energy contains an unwanted residual dependence on these arbitrary and irrelevant parameters. This suggests that the power series may not be a suitable form to represent the energy.

Around the turn of the century, Padé (Ref. 1) noted that a truncated power series was a special case of the class of representations, $P(L-m,m)$, in which the function is written as the ratio of a polynomial of order $L-m$ to one of order m. Of course, the original power series corresponds to the case where m equals zero. For each of these representations, the independent variable is λ and the coefficients in the

numerator and denominator polynomials are determined so that the correction terms are of order λ^{L+1} or greater.

Padé demonstrated that the coefficients in the various polynomial representations are related (Ref. 1). Thus, if the first L terms in the power series are known, one can easily determine the representations $P(L-m,m)$, where $m = 0,1,\ldots,L$. Since each of these representations corresponds to the same order of accuracy with respect to λ, a question arises as to which value of m ought to be used. Although Padé recognized the freedom available in representing a result to a given order by these approximants, general rules for selecting "appropriate" values of m unfortunately do not exist. The rules must be dictated by the nature of the physical quantity (function) being approximated.

Application of the Padé approximants to the perturbative problem involving the arbitrary scale and shift of the unperturbed Hamiltonian leads to an apparent difficulty: one must select suitable values for the scale and shift parameters and a suitable value for m, even though the exact result is independent of these parameters. Fortunately, we are able to resolve this quandary by demonstrating that only the $P(N+1,N)$ approximants share a property of the exact result by being independent of the scale and shift parameters (Ref. 2). This invariance property recommends the $P(N+1,N)$ approximants as being appropriate representations of the energy.

The first suggestion that an appropriate representation could be selected on the basis of the behavior of the various approximants under arbitrary changes of scale and/or origin in the zero-order operator became apparent to us during numerical studies. As noted above, the exact Hamiltonian is recovered at $\lambda = 1$ so that these changes should not affect the exact energy. However, truncation at a finite order can produce an apparent dependence of the energy on these changes. In fact, we show by numerical analysis of the 41-term series for the H^- ion that the only entries that do not depend on these changes belong to the class of $P(N+1,N)$ approximants for all the available values of N. We also give an analytic proof that this invariance is a direct consequence of the transformation relations among the coefficients in the unmodified Hamiltonian and those in the shifted and scaled Hamiltonian. Moreover, the invariance is totally independent of the actual values of the coefficients.

In addition to the analytic proof, we consider the rather arbitrary case in which the unscaled coefficients correspond to the Taylor series expansion $[\lambda\, ln(1+\lambda)]$. The coefficients in the corresponding "scaled-energy" series are obtained by using the previously mentioned transformations. We then generate the Padé tables for both the "unscaled" and "scaled" energies at $\lambda = 1$. The results are summarized in Fig. 1 for a scale factor of 2. Only for the $P(N+1,N)$ approximants do we find that the energies are independent of the arbitrary scaling.

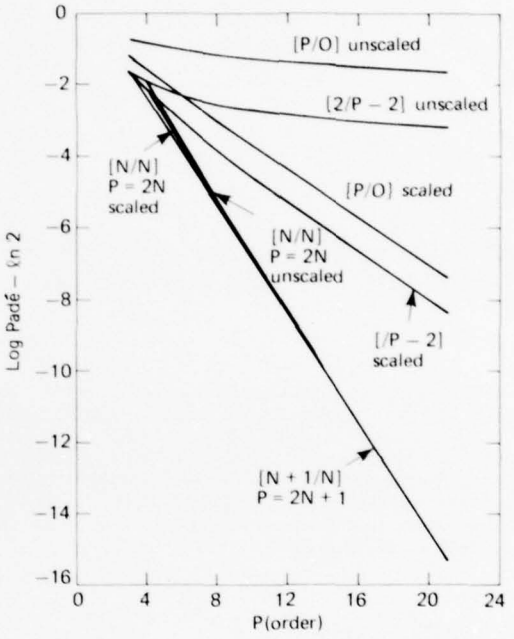

Fig. 1 Logarithm of the difference between *ln* 2 and various Padé approximants to the series representation of $\lambda\, ln(1+\lambda)$, for $\lambda = 1$, as a function of order. The results correspond to a scale factor of 2.

The significance of the general result is that the use of the $P(N+1,N)$ approximant eliminates a certain arbitrariness in the splitting of a problem into unperturbed and perturbed parts. This suggests that the $P(N+1,N)$ approximant may be a particularly appropriate representation of approximate solutions to complex physical problems.

REFERENCES

1. H. Padé, *Ann. Sci. Ec. Norm. Sup. (Paris) Suppl.*, 9, 1892, p. 3.
2. S. Wilson, D. M. Silver, and R. A. Farrell, "Special Invariance Properties of the [N+1,N] Padé Approximant to the Rayleigh-Schrödinger Perturbation Expansion" (to be published in *Proc. R. Soc. London*).

Authors: *S. Wilson, D. M. Silver, and R. A. Farrell*

Support: *NAVSEASYSCOM*

JHU EVENING COLLEGE CENTER AT APL

THE APL GRADUATE EDUCATION CENTER

During its thirty-four years of existence, APL has used various methods to help its staff members maintain and improve skills needed to carry out their technical assignments in the most effective manner. These methods include financial support for pertinent programs at educational institutions and specialized short courses taught both inside and outside the Laboratory.

In 1964, in order to make some of APL's in-house courses available to all qualified persons regardless of whether he or she was employed by the Laboratory, the Evening College of The Johns Hopkins University and APL cooperated to establish a Graduate Center at APL oriented to the educational needs of employed scientists and engineers. Classes meet in the R. E. Gibson Library (Fig. 1).

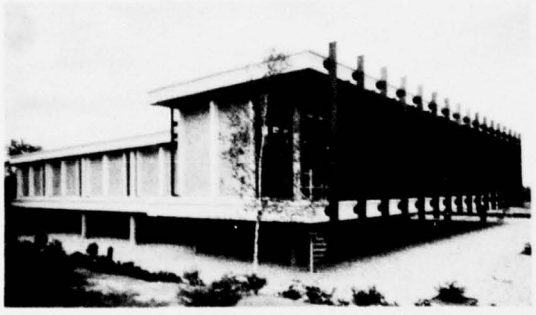

Fig. 1 The R. E. Gibson Library where Graduate Center classes meet.

The Center, under the academic sponsorship of the Evening College and with faculty members drawn primarily from APL's Senior Staff, offers a variety of courses in scientific and engineering areas and has proven to be a substantial asset to the technical community. Current programs lead to master of science degrees in Applied Physics, Computer Science, Electrical Engineering, Numerical Science, and Space Technology.

During Fiscal Year 1976, class registrations for APL Center programs were as follows: Fall 1975, 696; Spring 1976, 626; Summer 1976, 176; and Fall 1976, 748.

Because some students take more than one course, the number of individual students is slightly less than the number of class registrations. For example, in Fall 1976, a total of 552 individuals made up the 748 class registrations shown. Of these individuals, 485 (88%) were *not* APL staff members. It is evident that the Center is an important resource in the educational community. These inidviduals were employed as follows:

Private industry	232
Government institutions	167
Educational institutions	47
Not employed or did not reply	39

Eighty-six persons completed their programs and received master's degrees in 1976. The total number of APL Center students who have received master's degrees is 663. Of this number, 129 were APL staff members and 534 were not. These 663 individuals constitute 71% of all those who received master of science degrees in technical areas from the JHU Evening College during that time. The areas of specialization and the number of recipients in each are:

Numerical Science	267
Electrical Engineering	249
Computer Science	96
Applied Physics	27
Space Technology	24

When the Center began its operation, all courses were taken from the existing JHU curriculum. In Fiscal Year 1976, however, only 16% of the offerings were derived from the curriculum. In fact, the majority (62%) were originated and taught by APL staff members. Another 16% were created expressly for the Center by JHU faculty members of the Baltimore campus, and 6% were originated by Center instructors who are primarily employed by other organizations.

In our continuing effort to maintain the leadership that the APL Center has attained, we are constantly analyzing curricula and then making revisions. In Fiscal Year 1976, APL Center instructors originated and taught for the first time three courses: Computer Communication Networks, Introduction to Switching Theory, and Computer System Engineering Management. Five new courses are planned for Fiscal Year 1977.

Figure 2 discloses that records were set in Fiscal Year 1976 for class roll totals, number of individuals enrolled, number of outside participants, number of participants from private industry, number of participants from government facilities, and number of candidates for master's degrees offered at APL.

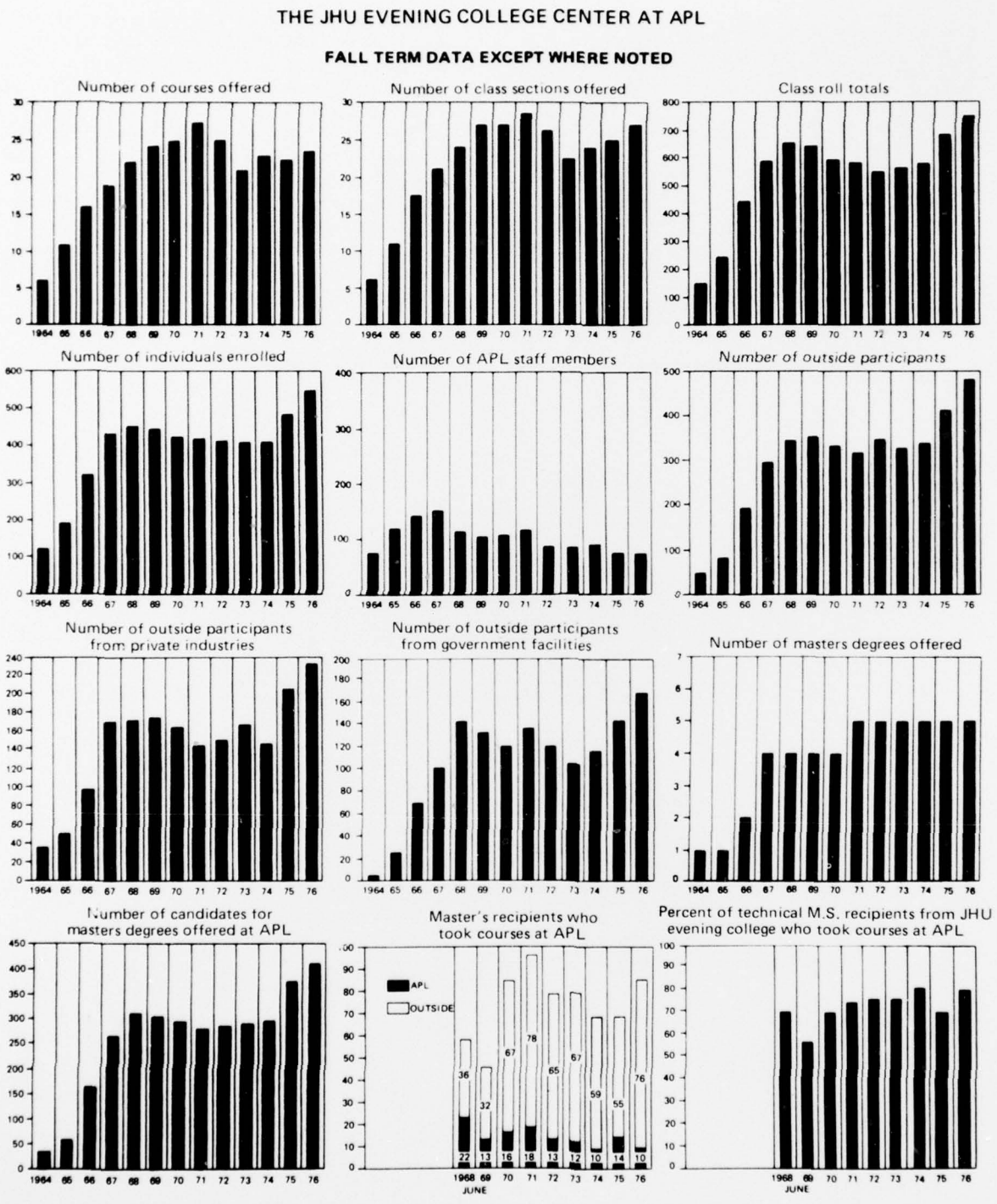

Fig. 2 Data on the APL Graduate Education Center.

Fig. 3 A typical class in session.

The physical facilities are modern and the audio visual aids are excellent, but the primary strength of the Center is its faculty. (Figure 3 shows a typical class.) Some full-time faculty members from the Baltimore campus instruct in this program, but 70% of the Center's faculty are members of he APL Senior Staff and 15% are members of similar staffs of other scientific or engineering organizations. The students appreciate and appear to benefit from studying under academically qualified instructors who are actively involved with the subjects they teach and who understand the needs of part-time students who work in research and development organizations.

Author: P. B. Edwards

PATENTS

PATENTS ACTIVITIES

The APL Patents Office has the responsibility for assuring compliance with contract and grant requirements relative to patent and data rights, as imposed by the various governmental agencies that sponsor work at the Laboratory. In addition to preparing formal disclosures of inventions for the appropriate sponsors, the Patents Office prepares and prosecutes patent applications on behalf of both the University and the Department of the Navy.

The following lists indicate the invention disclosures submitted to sponsors, the patent applications prepared and filed in the United States Patent Office, and the previously filed applications that were successfully prosecuted to issuance as patents, during Fiscal Year 1976.

INVENTION DISCLOSURES

Method for Water Purification by Laser Irradiation
J. G. Parker

Fluorometer
B. F. Hochheimer and G. S. Keys

Radar Evaluation Data Collector
R. W. Pickering, H. E. Plants, and C. L. Roe

Microwave 180° Hybrid or Magic Tee
G. J. Laughlin

Metal Reinforced Pseudo-Isotropic Filament Disc Rotor
D. W. Rabenhorst and K. E. Darnell

Single-Axis Disturbance Compensation System
R. E. Fischell, A. C. Sadilek, F. F. Mobley, and G. H. Fountain

Pin/Socket Microelectronic Interconnections
F. R. Muccino

Powered Manipulator
W. Seamone and J. H. Loveless

Kevlar Dewar
W. M. Chambers

MAGNEBOB
W. R. Powell

Liquid Gradiometer
W. R. Powell

Digital Beamsteering for a Parametric Scanning Sonar
J. W. Follin, Jr., and R. E. Miller

Wave Motion Sensor
G. B. Bush, I. Katz, and R. A. Kropfli

Solder Station Apparatus
R. T. Wilson

Circuitry for High Speed Television Display of Data
L. L. Warnke and J. R. Dozsa

Security Hasp Assembly
J. J. Breivogel, Sr.

Data Input Interface Device for Bus-Type Computer System
P. J. Grunberger

Tripod Base Joint
K. L. Nichols

Circuit for Digital Cursor Display
R. C. Moore

Magnetic Card to Magnetic Tape Converter
R. K. Higgins

NRZ Peak Detector
P. Klose

Method for Making Discrete Ring Rotary Energy Storage Structures
D. W. Rabenhorst

Dual Mode Laser
J. W. Leight and T. O. Poehler

Thin Surface Barrier Diode
K. Reinitz

Radar Environment Simulator
J. T. Miller, Jr.

Method for Aircraft Beacon Tracking
E. L. Brickner

A Method for Automatically Transferring Data to a Large Computing System Through Its Time Sharing Network
K. W. Colby

Tubular Self-Potting Connector
F. F. Mobley

Output Summing Network
E. A. Beck

Zero-Leakage High-Pressure Seal
T. R. Small and W. O. Wilkinson

Elastic Internal Gimbal for Flywheels
D. W. Rabenhorst

IBM Compatible Input-Output Channel for a Nova Mini Computer
J. S. Lombardo

Method for Crystallization of Highly Conductive Radical-Cation-Radical-Anion Organic Salts
J. W. Leight

Low-Cost Blast Test Vehicle
W. F. Williams and M. L. Yost

Method for Obtaining Improved Magnetometer Readings
L. W. Hart

Electric-Magnetic Gradiometer for Improved In-Air Readings
L. W. Hart

Solar Panel Deployment Mechanism
L. E. Stillman and T. B. Coughlin

Tunable Laser Mount
J. W. Leight

Priority-Controlled A/D Converter
B. E. Raff

Security Locking Mechanism
J. J. Breivogel

Anti-Submarine Graphical Resource Allocation Model (ASGRAM)
R. H. Kidwell, J. A. Yingling, M. Block, T. P. Modelski, and L. R. Gieszl

Solid-State TWT Modulator
M. J. Feil

Navigation System Data Processor
D. L. Mitchell, R. K. Burek, R. H. Bauer, M. O. Marshall, M. C. Osborne, and K. Lew

Radio Frequency Receiver for Satellite Navigation System
J. R. Norton

War At Sea Graphical Analysis Model (WASGRAM)
T. P. Modelski and J. Wang

Apparatus for Phase-Modulated Detection
P. H. Gilbert

Roll Attitude and Rate Sensor
M. L. Hill

Low Axial Force Servo Valve Spool
W. Seamone

Cable Clamp
R. A. Mattey and G. A. Starstrom

SO_2 Fuel Cell
L. W. Hunter

High Voltage Sawtooth Generator
J. H. Kuck

Portable Microthruster Test System
S. J. Kowal

Deployable Ground Plane
L. Schwerdtfeger, L. E. Stillman, and W. E. Frain

Dissolved Hydrogen Sensor
J. H. Panesci, S. J. Seymour, and M. L. Snow

Error Correction Encoder and Decoder
P. J. Luke, J. L. Machamer, and W. A. Becraft

Monitoring Apparatus for Resonant Circuit Intracranial Pressure Implants
G. R. Seylar

High Resolution Radar Control System
B. E. Raff

Computer-Stabilized Director Sight
S. E. Bonwit and S. Tsakos

Large Angle-of-Attack Missile Control System for Aerodynamically Controlled Missile
D. J. Yost and A. Arrow

Three Dimensional Laser Doppler Velocimeter (3-D LDV)
O. J. Deters and C. B. Bargeron

Integral Rocket Ramjet Port Cover Activating Switch
R. T. Cusick and W. J. Fleagle

Reversible Clock for Use in Missiles
J. E. Hanson

Pin Isolator for Dual-In-Line Packaged (DIP) Circuits
J. G. Rozema

A System for Continuous Detection of Possible Carcinogens in Water Supply Samples
J. G. Parker and R. vonBriesen

Skin Friction Balance Mechanism
R. C. Orth, P. J. Waltrup, H. B. Land, and F. S. Billig

Signal Processing Method for Superconducting Total Field Magnetic Sensors
C. H. Sinex

Seizure Monitor
W. R. Powell

Force-Sensing Cervical Dilator
J. G. Chubbuck and H. R. Bittner

Passive Infrared Ranging Means for Gun Fire Control
R. A. Rollin

Laser Beam Switch
R. H. Lapp

Microcircuit Soldering Method
F. R. Muccino

Ionic Air Speed Indicator
M. L. Hill and T. R. Whyte

Ionic Conduction Angular Rate Sensor
M. L. Hill

Ionic Conduction Air Flow Sensor
M. L. Hill

Digital Clock Alternate Power Circuit
R. C. Moore

Micropuncture Pressure Measurement Probe
J. G. Chubbuck and H. R. Bittner

Hydrogen Maser Receiver
A. G. Bates and J. R. Norton

Gauze Sensor
J. H. Panesci and M. L. Snow

Focused-Blast Warhead with Liner
C. R. Brown

Method and Apparatus for High Sensitivity Tensile Modulus Testing
S. N. Foner and B. H. Nall

Direct Digital Control for an Air Mass Flow Control System
J. H. Zouck and R. T. Cusick

Guidance Control for Recovery of Remotely Piloted Vehicles
M. L. Hill

Method for Particle Velocity Detection in Standing Sound Waves
B. H. Nall

Arrayed Absorption Detector
J. H. Higbie

Radar Video Converter
J. Phipps, R. C. Thurber, and R. Prengaman

Moving Wire Technique
R. M. Fristrom, L. W. Hunter, C. Grunfelder, and H. Schacke

Neuromuscular Evaluation System
H. R. Bittner

Muscle Puller
H. R. Bittner

Primate Cage Trainer
J. G. Chubbuck and H. R. Bittner

Head Restraint Mechanism
J. G. Chubbuck and R. E. Digman

Community Annual Storage Energy System (CASES)
W. R. Powell

TV Tracker/Image Processor
F. W. Schenkel, W. C. Trimble, J. R. Dozsa, and J. R. Albertine

Apparatus and Method for Measuring the Value of Electrical Components
J. H. Zouck

Ammonia Chemical Heat Pump for Utilization of Geothermal Energy
R. J. Taylor

Mask and Substrate Holder
H. K. Charles, Jr., and H. J. LaBelle

PATENT APPLICATIONS

Universal Binary Code Converter
D. L. Sharp and E. A. Frekko

Woven Filament Rotor Structures
D. W. Rabenhorst

Convoluted Rotor Structures
D. W. Rabenhorst

Time and Frequency Control Unit
A. G. Bates and T. L. McGovern

Carrier-Modulation Coherency Monitoring System
E. F. Osborne

Simplified Time Code Reader with Digital PDM Decoder
J. M. DuBrul

Filament Rotor Having Elastic Sheaths Covering the Filamentary Elements of the Structure
D. W. Rabenhorst

Monotrack Radar Recording/Playback System
R. E. Miller

Composition of Matter for Practice of Simultaneous Angiography of the Separate Retinal and Choroidal Circulations
B. F. Hochheimer and R. W. Flower

Filament Connected Rim Rotor
D. W. Rabenhorst

An X–Y Range-Bearing Converter
E. J. McDevitt

Fractional Binary to Decimal Converter
R. W. Fowler

Antenna Scan System for Helicopter Wire Detection
R. H. Lapp

Intracranial Pressure Monitor
J. G. Chubbuck

Digital Radar Signal Processor
R. P. Colbert, G. Dimitriou, M. E. Jones, and J. I. Haberman

Rechargeable Body Tissue Stimulator
R. E. Fischell

Line Scan Radar Antenna Using a Single Motor
R. H. Lapp

Radar Sector Scan Reversal Apparatus
R. H. Lapp and J. D. Schneider

Error Correction Encoder and Decoder
P. J. Luke, J. L. Machamer, and W. A. Becraft

Random Scanning Receiver
J. F. Gulick, Jr., and D. R. Marlow

Method and Apparatus for Terrain Avoidance
M. L. Hill

Presettable Rate Multiplier
P. G. Casner, Jr., and E. J. McDevitt

ISSUED PATENTS

No. 3,893,447
Simultaneous Angiography of the Separate Retinal and Choroidal Circulations
B. F. Hochheimer and R. W. Flower

No. 3,897,918
Interferometric Rolling Missile Body Decoupling Guidance System
J. F. Gulick, Jr., and J. E. Hanson

No. 3,905,033
Single Composite Pulse Moving Target Indicator Radar System
T. A. Moore and F. R. Castella

No. 3,908,933
Guided Missile
W. H. Goss, H. H. Porter, R. B. Roberts, M. A. Tuve, J. W. Beams, and H. Selvidge

No. 3,913,109
Antenna Erection Mechanism
C. F. Owen

No. 3,916,320
Loran Receiver Signal Canceller
R. G. Roll and H. H. Elliott, Jr.

No. 3,921,498
Fin Clip and Connector Mount
S. Kongelbeck

No. 3,928,801
Method and Apparatus for Sensing Rate of Angular Displacement
M. L. Hill

No. 3,934,131
Output Controller for Initiating Delayed or Conditional Commands via a General Purpose Computer
J. A. Perschy

No. 3,934,250
Helicopter Blind Landing and Hover System
O. M. Martin, Jr.

No. 3,937,388
Method for Sealing Packages
D. D. Zimmerman

No. 3,938,150
Microwave Amplifier Tube Coherency Test Set
C. C. Phillips, W. H. Zinger, R. F. Platte, M. M. Jesurun, and D. H. Matthias

No. 3,939,411
Instantaneous Frequency Measurement System
W. G. James

No. 3,946,382
Search Radar Adaptive Video Processor
A. Kossiakoff and J. R. Austin

No. 3,947,849
Loran Receiver-Navigator
L. F. Fehlner, T. W. Jerardi, and R. G. Roll

No. 3,951,659
Method for Resist Coating of a Glass Substrate
J. L. Abita and J. G. Bebee

No. 3,953,674
Telemetry Synchronizer
C. T. Pardoe

No. 3,964,341
Multi-Ring Filament Rotor
D. W. Rabenhorst

No. 3,974,457
Time and Frequency Control Unit
A. G. Bates and T. L. McGovern

No. 3,978,796
Focused Blast-Fragment Warhead
E. E. Hackman

No. 3,982,447
Convoluted Rotor Structures
D. W. Rabenhorst

PUBLICATIONS

PUBLICATIONS IN PROFESSIONAL JOURNALS
1 July 1975 - 30 September 1976

F. J. Adrian and V. A. Bowers, "g-Tensor and Spin Doubling Constant in the $^2\Sigma$ Molecules CN and C_2H," *Chem. Phys. Lett.*, **41**, No. 3, 1 August 1976, pp. 517–520.

———, and H. M. Vyas and J. K. S. Wan (Queen's University, Ontario, Canada), "Magnetic Field and Concentration Dependence of CIDNP in Some Quinone Photolyses: Further Evidence for an Overhauser Mechanism," *J. Chem. Phys.*, **65**, No. 4, 15 August 1976, pp. 1454–1461.

T. P. Armstrong (University of Kansas) and S. M. Krimigis (APL), "Interplanetary Acceleration of Relativistic Electrons Observed with IMP 7," *J. Geophys. Res.*, **81**, No. 4, 1 February 1976, pp. 677–682.

———, ———, D. Hovestadt and B. Klecker (Max-Planck Institute for Extraterrestrial Physics), and G. Gloeckler (University of Maryland), "Observations of Temporal and Spatial Variations in the Fe/O Charge Composition of the Solar Particle Event of July 4, 1976," *Solar Phys.*, **49**, No. 2, August 1976, p. 395.

———, ———, and L. J. Lanzerotti (Bell Laboratories), "A Reinterpretation of the Reported Energetic Particle Fluxes in the Vicinity of Mercury," *J. Geophys. Res.*, **80**, No. 28, 1 October 1975, pp. 4015–4017.

R. J. Bartlett (The Johns Hopkins University) and D. M. Silver (APL), "Many-Body Perturbation Theory Applied to Electron Pair Correlation Energies. II. Closed-Shell Second-Row Diatomic Hydrides," *J. Chem. Phys.*, **64**, No. 11, June 1976, pp. 45–78.

——— and ———, "Some Aspects of Diagrammatic Perturbation Theory," *Int. J. Quantum Phys.*, **9**, December 1975, pp. 183–198.

N. A. Blum and C. Feldman, "The Crystallization of Amorphous Germanium Films," *J. Non-Cryst. Solids*, **22**, 1976, pp. 29–35.

J. F. Bird, "An Elemental Phenomenon of Vision-Suprafusion Transients: General Theory, Retinal-Cortical Manifestations, Potential Application," *J. Theor. Biol.*, **55**, No. 2, December 1975, pp. 553–557.

———, G. H. Mowbray, and R. W. Flower, "Visual Cortex Responses to Abrupt Changes in the Periodicity of Rapidly Intermittent Light," *Electroencephalogr. Clin. Neurophysiol.*, **39**, No. 4, October 1975, pp. 305–312.

J. Bohandy and B. F. Kim, "Optical Spectra of Ni Porphin, Pd Porphin and Free Base Porphin in Single Crystal Triphenylene," *Spectrochim. Acta*, **32A**, 1976, pp. 1083–1088.

N. J. Brown (University of California, Berkeley) and D. M. Silver (APL), "Reactive and Inelastic Scattering of $H_2 + D_2$ Using a London-Type Potential Energy Surface," *J. Chem. Phys.*, **65**, No. 1, 1 July 1976, pp. 311–325.

F. R. Castella, "Probability of Detection for ICW Radars," *IEEE Trans. Aerosp. Electron. Syst.*, **AES-12**, No. 1, January 1976, pp. 68–71.

H. K. Charles, Jr. (APL) and R. I. Joseph (The Johns Hopkins University), "Exchange Model of Antiferromagnetism," *Phys. Rev. B*, **12**, No. 9, 1 November 1975, pp. 3918–3932.

E. P. Cunningham, "False Alarm Rate for Rank Quantizer When Input Range Samples Are Not Independent," *IEEE Trans. Aerosp. Electron. Syst.*, **AES-12**, No. 1, January 1976, pp. 65–67.

M. Davidson, S. F. Haase, J. L. Machamer, and L. H. Wallman, "High Density Magnetic Recording Using Digital Block Codes of Low Disparity," *IEEE Trans. Magn.*, September 1976, pp. 584–586.

J. P. Doering and W. K. Peterson (The Johns Hopkins University), and C. O. Bostrom and T. A. Potemra (APL), "High Resolution Daytime Photoelectron Energy Spectra from EA-E," *Geophys. Res. Lett.*, **3**, March 1976, p. 129.

G. L. Dugger, H. L. Olsen, W. B. Shippen, E. J. Francis, and W. H. Avery, "Floating Ocean Thermal Power Plants and Potential Products," *J. Hydronaut.*, **9**, No. 4, October 1975, pp. 129–141.

L. W. Ehrlich (APL) and M. M. Gupta (University of Western Australia), "Some Difference Schemes for the Biharmonic Equation," *SIAM J. Numer. Anal.*, **12**, No. 5, October 1975, pp. 773–790.

R. A. Farrell and R. L. McCally, "On Corneal Transparency and Its Loss with Swelling," *J. Opt. Soc. Am.*, **66**, No. 4, April 1976, p. 342.

——— and ———, "On the Interpretation of Depth Dependent Light Scattering Measurements in Normal Corneas," *Acta Ophthalmol.*, **54**, 1976, pp. 261–270.

R. W. Flower and B. F. Hochheimer, "Indocyanine Green Dye Fluorescence and Infrared Absorption Choroidal Angiography Performed Simultaneously with Fluorescein Angiography," *Johns Hopkins Med. J.*, **138**, No. 2, February 1976, pp. 33–42.

M. H. Friedman, "Self-Consistent Analysis of Arterial Uptake of Cholesterol from Perfusing Serum," *Cir. Res.*, **38**, No. 3, March 1976, pp. 215–216.

———, "The Effect of Membrane Heterogeneity on the Predictability of Fluxes with Application to the Cornea," *J. Theor. Biol.*, **61**, 1976, pp. 307–328.

———, "Transport Through a Growing Boundary Layer to a Permeable Wall," *Am. Inst. Chem. Eng. J.*, **22**, No. 2, March 1976, pp. 407–409.

——— and L. W. Ehrlich, "Effect of Spatial Variations in Shear on Diffusion at the Wall of an Arterial Branch," *Cir. Res.*, **37**, October 1975, pp. 446–454.

R. M. Fristrom and C. Grunfelder, "Moving Wire Technique Studies of Ablation, Ignition and Extinction of Polymer Flames," *Fire Mater.*, **1**, 1976, pp. 48–51.

———, ———, and L. W. Hunter, "Exploratory Studies in Polymer Ablation, Ignition and Extinction by the Moving Wire Technique," *Combust. Flame*, **27**, 1976, pp. 33–49.

S. K. Ghatak (C.N.R.S., Grenoble, France) and K. Moorjani (APL), "Spin Glasses: Beyond the Molecular Field Approximation," *J. Phys. C*, **9**, 1976, pp. L293–L295.

J. Goldhirsh, "Prediction Methods for Rain Attenuation Statistics at Variable Path Angles and Carrier Frequencies between 13 and 100 GHz," *IEEE Trans. Antennas Propag.*, **AP–23,** No. 6, November 1975, pp. 786–791.

M. C. Green, "Gain of a Linear Array for Spatially Dependent Signal Coherence," *J. Acoust. Soc. Am.*, **60,** No. 1, July 1976, pp. 129–132.

S. Greene (Goddard Institute for Space Studies) and L. Monchick (APL), "Validity of Approximate Methods in Molecular Scattering: Thermal HCl–He Collisions," *J. Chem. Phys.*, **63,** No. 10, 15 November 1975, pp. 4198–4205.

E. J. Hoffman, R. C. Moore, and T. L. McGovern, "Designing a Magnetic Bubble Data Recorder. Part 1—The Component Level," *Comput. Des.*, March 1976, pp. 77–85.

———, ———, and ———, "Designing a Magnetic Bubble Data Recorder. Part 2—The System Level," *Comput. Des.*, March/April 1976, p. 99.

L. W. Hunter, C. Grunfelder, and R. M. Fristrom, "The Effect of CF_3Br on a $CO–H_2–O_2–Ar$ Diffusion Flame," *Halogenated Fire Suppressants*, ACS Symposium Series, No. 16.

T. Iijima and T. A. Potemra, "The Amplitude Distribution of Field-Aligned Currents at Northern High Latitudes Observed by Triad," *J. Geophys. Res.*, **81,** No. 13, May 1976, p. 2165.

E. P. Irzinski, "The Input Admittance of a TEM Excited Annular Slot Antenna," *IEEE Trans. Antennas Propag.*, **AP–23,** No. 6, November 1975, pp. 829–834.

E. P. Keath, E. C. Roelof, and C. O. Bostrom (APL), and D. J. Williams (NOAA, Boulder), "Fluxes of $\geq$50 keV Protons and $\geq$30 keV Electrons at $\sim$35 R_e. 2. Morphology and Flow Patterns in the Magnetotail," *J. Geophys. Res.*, **81,** No. 13, May 1976, p. 2315.

B. F. Kim, "Low-Angle Light-Scattering Apparatus," *Rev. Sci. Instrum.*, **47,** No. 9, September 1976, pp. 1039–1043.

J. F. Kincaid, "Communications: The Driving Force Behind the Accelerating Rate of Change," *Ann. Clin. Lab. Sci.*, **6,** No. 4, July–August 1976, pp. 283–290.

S. M. Krimigis and J. W. Kohl (APL), and T. P. Armstrong (University of Kansas), "The Magnetospheric Contribution to the Quiet-Time Low Energy Nucleon Spectrum in the Vicinity of Earth," *Geophys. Res. Lett.*, **2,** No. 10, October 1975, pp. 457–460.

——— and E. T. Sarris (APL), and T. P. Armstrong (University of Kansas), "Observations of Jovian Electronic Events in the Vicinity of Earth," *Geophys. Res. Lett.*, **2,** No. 12, December 1975, pp. 561–564.

G. J. Laughlin, "A New Impedance-Matched Wide-Band Balun and Magic Tee," *IEEE Trans. Microwave Theory Tech.*, **MTT–24,** No. 3, March 1976, pp. 135–141.

J. W. Love (Santa Barbara City College), K. B. Lewis (Franklin Square Hospital), and R. E. Fischell (APL), "The Johns Hopkins Rechargeable Pacemaker, Historical Aspects," *J. Am. Med. Assoc.*, **234,** No. 1, 6 October 1975, pp. 64–66.

J. H. Manley, "Embedded Computer Systems—Personnel Development," *Abridged Proceedings from the AIAA Software Management Conference, First Series*, 1976.

———, "Training Requirement for Defense System Software Managers," *Conference Proceedings: Managing the Development of Weapon System Software*, Air Command and Staff College, Maxwell AFB, AL, 1976.

R. L. McCally and R. A. Farrell, "The Depth Dependence of Light Scattering from the Normal Rabbit Cornea," *Exp. Eye Res.*, **23,** 1976, pp. 69–81.

R. A. Meyer (APL), V. B. Mountcastle (The Johns Hopkins University), and R. E. Walker (APL), "A Laser Stimulator for the Study of Cutaneous Thermal and Pain Sensations," *IEEE Trans. Biomed. Eng.*, **23,** No. 1, December 1975, pp. 54–60.

——— and R. E. Walker (APL), and V. B. Mountcastle, Jr. (The Johns Hopkins University), "A Laser Stimulator for the Study of Cutaneous Thermal and Pain Sensations," *IEEE Trans. Biomed. Eng.*, **BME–23,** No. 1, January 1976, pp. 54–60.

F. F. Mobley, G. H. Fountain, and A. C. Sadilek (APL), and P. W. Worden and R. Van Patten (Stanford University), "Electromagnetic Suspension for the TIP–II Satellite," *IEEE Trans. Magn.*, **MAG–11,** No. 6, November 1975, pp. 1712–1716.

K. Moorjani (APL) and S. K. Ghatak (C.N.R.S., Grenoble, France), "Bethe-Peierls-Weiss Approximation in Disordered Ferromagnets," *AIP Conference Proceedings*, **29,** May 1976, p. 152.

J. T. Nolte, A. S. Krieger, A. F. Timothy (American Science and Engineering, Inc.), R. E. Gold, E. C. Roelof (APL), G. Vaiana (Center for Astrophysics), A. J. Lazarus, J. D. Sullivan (Massachusetts Institute of Technology), and P. S. McIntosh (National Oceanic and Atmospheric Administration), "Coronal Holes as Sources of Solar Wind," *Solar Phys.*, **46,** 1976, pp. 303–322.

J. B. Oakes, "Clinical Engineering—The Problems and the Promise," *Science*, **190,** 17 October 1975, pp. 239–242.

V. O'Brien, L. W. Ehrlich, and M. H. Friedman, "Unsteady Flow in a Branch," *J. Fluid Mech.*, **75,** Part 2, 1976, pp. 315–336.

D. H. Orth and A. Patz (the Wilmer Ophthalmological Institute), and R. W. Flower (APL), "Potential Clinical Applications of Indocyanine Green Choroidal Angiography—Preliminary Report," *Eye, Ear, Nose, Throat Mon.*, January 1976.

J. G. Parker, "Laser Radiation Reduces Coliform Counts in Water," *Water Sewage Works*, **123,** No. 5, May 1976, p. 52.

T. O. Poehler (APL), and D. O. Cowan and A. N. Block (The Johns Hopkins University), "Chemical Purity and the Electrical Conductivity of Tetrathiofulvalinium," *Org. Chem.*, **40,** No. 24, November 1975, pp. 35–47.

———, ———, and ———, "The Organic Metallic State," *J. Mol. Cryst. Liq. Cryst.*, **32,** March 1976, pp. 223–225.

———, T. Kistenmacher, T. E. Phillips, D. O. Cowan, and A. N. Block (The Johns Hopkins University), "Crystal Structure and Diffuse X-Ray Scattering of the 1:2 Salt of TMTTF and TCNQ, a Non-Stoichiometric Quasi One-Dimensional Organic Conductor," *Acta Crystallogr. Sect. B*, **32,** No. 2, February 1976, pp. 539–547.

J. D. Randall, "Comment on 'Explicit Numerical Method for Solution of Heat-Transfer Problems'," *Am. Inst. Aeronaut. Astronaut. J.*, **14**, No. 1, January 1976, pp. 127–128.

———, "Finite Difference Solution of the Inverse Heat Conduction Problem and Ablation," *Proceedings of the 1976 Heat Transfer & Fluid Mechanics Institute*, Stanford University Press, 1976.

E. C. Roelof, "Solar Particle Emission," *Physics of Solar Planetary Environments*, **1**, Proceedings of the International Symposium on Solar-Terrestrial Physics, American Geophysical Union, Washington, DC, 1976, pp. 214–231.

———, E. P. Keath, and C. O. Bostrom (APL), and D. J. Williams (NOAA, Boulder), "Fluxes of ≥ 50 keV Protons and ≥ 30 keV Electrons at ~ 35 R_e. 1. Velocity Anisotropies and Plasma Flow in the Magnetotail," *J. Geophys. Res.*, **81**, No. 13, May 1976, p. 2304.

J. R. Rowland, "Clean Air Convective Behavior Revealed by Radar Chaff," *J. Appl. Meteorol.*, **15**, No. 5, May 1976, p. 521.

E. T. Sarris and S. M. Krimigis (APL), and T. P. Armstrong (University of Kansas), "Observations of Magnetospheric Bursts of High Energy Protons and Electrons at ~ 35 R_e with IMP-7," *J. Geophys. Res.*, **81**, No. 13, May 1976, p. 2341.

———, ———, T. Iijima (University of Tokyo), C. O. Bostrom (APL), and T. P. Armstrong (University of Kansas), "Location of the Source of Magnetospheric Energetic Particle Bursts by Multispacecraft Observations," *Geophys. Res. Lett.*, **3**, No. 8, August 1976, pp. 437–440.

———, ———, and T. P. Armstrong (University of Kansas), "Observations of a High-Energy Ion Shock Spike in Interplanetary Space," *Geophys. Res. Lett.*, 3 March 1976, p. 133.

J. A. Schetz (Virginia Polytechnic Institute and State University), and F. S. Billig and S. Favin (APL), "Simplified Analysis of Supersonic Base Flows Including Injection and Combustion," *Am. Inst. Aeronaut. Astronaut. J.*, **14**, No. 1, January 1976, pp. 7–8.

———, and S. Favin and F. S. Billig (APL), "Analytical Comparison of the Performance of Different Base-Burning Modes," *Am. Inst. Aeronaut. Astronaut. J.*, **14**, No. 9, September 1976, pp. 1337–1338.

V. G. Sigillito, "A Priori Inequalities and Approximate Solution of the First Boundary Value Problem for $\Delta^2 u = f$," *SIAM J. Num. Anal.*, **13**, No. 2, April 1976, p. 251.

———, "A Priori Inequalities and the Dirichlet Problem for a Pseudo-Paraboloid Equation," *SIAM J. Math. Anal.*, **7**, No. 2, April 1976, p. 222.

D. M. Silver (APL) and R. J. Bartlett (The Johns Hopkins University), "Modified Potentials in Many-Body Perturbation Theory," *Phys. Rev. A.*, **13**, No. 1, January 1976, pp. 1–12.

M. Sugiura (Goddard Space Flight Center) and T. A. Potemra (APL), "Net Field-Aligned Currents Observed by TRIAD," *J. Geophys. Res.*, **81**, No. 13, May 1976, p. 2155.

R. T. Tsunoda and R. I. Presnell (Stanford Research Institute), and T. A. Potemra (APL), "The Spatial Relationship Between the Evening Radar Aurora and Field-Aligned Currents," *J. Geophys. Res.*, **81**, No. 22, 1 August 1976, pp. 3791–3802.

G. W. Turner, H. K. Charles, Jr., and C. Feldman, "Switching in Amorphous Boron Films Under Single-Pulse Conditions," *J. Appl. Phys.*, **47**, No. 8, August 1976, pp. 3618–3624.

R. Turner and R. A. Murphy, "The Far Infrared Helium Laser," *Infrared Phys.*, **16**, March 1976, pp. 197–200.

——— and T. O. Poehler, "Electrically Initiated Pulsed Chemical DF–CO_2 and DF Lasers," *J. Appl. Phys.*, **47**, No. 7, July 1976, pp. 3038–3041.

A. A. Westenberg and N. deHaas, "Rate of the Reaction $O + SO_2 + M \rightarrow SO_3 + M^*$," *J. Chem. Phys.*, **63**, No. 12, 15 December 1975, pp. 5411–5415.

S. Wilson (The University, Bristol, England, and APL), "The Group Function Model. A Set of Orthogonality Conditions," *J. Chem. Phys.*, **64**, No. 4, 15 February 1976, pp. 1692–1696.

AUTHOR INDEX

AUTHOR INDEX